December 1997 • NREL/SR-520-23266

New Approaches for High-Efficiency Solar Cells

Final Report

S.M. Bedair and N.A. El-Masry
North Carolina State University
Raleigh, North Carolina

National Renewable Energy Laboratory
1617 Cole Boulevard
Golden, Colorado 80401-3393
A national laboratory of
the U.S. Department of Energy
Managed by Midwest Research Institute
for the U.S. Department of Energy
under Contract No. DE-AC36-83CH10093

NREL/SR-520-23266 • UC Category: 1260

New Approaches for High-Efficiency Solar Cells

Final Report

S.M. Bedair and N.A. El-Masry
North Carolina State University
Raleigh, North Carolina

NREL technical monitor: R. McConnell

National Renewable Energy Laboratory
1617 Cole Boulevard
Golden, Colorado 80401-3393
A national laboratory of
the U.S. Department of Energy
Managed by Midwest Research Institute
for the U.S. Department of Energy
under Contract No. DE-AC36-83CH10093

Prepared under Subcontract No. XDA-3-12114-5
December 1997

Available to DOE and DOE contractors from:
Office of Scientific and Technical Information (OSTI)
P.O. Box 62
Oak Ridge, TN 37831
Prices available by calling (423) 576-8401

Available to the public from:
National Technical Information Service (NTIS)
U.S. Department of Commerce
5285 Port Royal Road
Springfield, VA 22161
(703) 487-4650

Printed on paper containing at least 50% wastepaper, including 20% postconsumer waste

TABLE OF CONTENTS

I. Summary

This report summarizes the activities carried out in this subcontract. These activities cover, first the atomic layer epitaxy (ALE) growth of GaAs, AlGaAs and InGaP at fairly low growth temperatures. This was followed by using ALE to achieve high levels of doping both n-type and p-type required for tunnel junctions (Tj) in the cascade solar cell structures. Then we studied the properties of AlGaAs/InGaP and AlGaAs/GaAs tunnel junctions and their performances at different growth conditions. This is followed by the use of these tunnel junctions in stacked solar cell structures. The effect of these tunnel junctions on the performance of stacked solar cells was studied at different temperatures and different solar fluences. Finally, we studied the effect of different types of back surface fields (BSF), both p/n and n/p GaInP solar cell structures, and their potential for window layer applications. Parts of these activities were carried in close cooperations with Dr. Mike Timmons of the Research Triangle Institute.

II. Graduate Students and their Thesis high lights:

Three graduate students Ph.D. theses were supported by this subcontract. Copies of there theses are available upon request.

1) Donggeun Jung - Ph.D. (1993)

The thesis has both experimental and modeling parts.

I. Experimental

- Growth of GaAs by ALE in a prototype reactor
- C-doping of AlGaAs to 10^{20} / cm^3
- Low temperature growth of InGaP by ALE in the range 400-500 °C
- Se doping of InGaP ~ $9x10^{19}$ / cm^3
- Properties of tunnel junctions in the AlGaAs/InGaP material systems.
- Effect of Annealing on the tunnel junction properties.

ii. Modeling

- Band line-up of the AlGaAs/InGaP heterointerfaces
- Modeling of T.j. I-V characteristics
- Effect of depletion layer thickness on peak current in T.j.
- Dopants diffusion in annealed T.j.

2) Jamal Eldallal - Ph.D. (1994)

Thesis contains three major parts.

I. ALE Development in a Semiproduction Reactor

- Conditions for monolayer / ALE cycle
- Low background carrier concentrations
- n^+ - type doping using silane ~ 10^{19} / cm^3
- High growth rate of 2 μm / h in multi-wafer reactor (3 wafer, 2" diameter)
- p-type carbon doping ~ 10^{20} / cm^3 in AlGaAs

ii. p^+ - AlGaAs/n^+ - GaAs Tunnel Junction

- I-V characteristics
- Dependence of peak currents on growth conditions

iii. GaAs/AlGaAs Tandem Cells and their performances

- Temperature effects
- High solar concentration effects

3) Nadia Rafat - Ph.D. (1995)

The thesis contains experimental and modeling activities.

I. Experimental

- Growth and characterization of $GaInP_2$, top cell lattice matched to GaAs substrate
- Study the effect of BSF on p/n and n/p structures
- Compare the performances of abrupt $GaInP_2$, graded $GaInP_2$ and AlGaAs BSF layers

ii. Modeling

- Bandgap calculations to study the bandgap line up in $Ga_{0.5}In_{0.5}P$ / $Ga_xIn_{1-x}P$ material systems
- Study the effect of strain and doping levels on this bandgap line up
- Study band line up for window layers including different material systems such as $In_xGa_{1-x}P$ and GaP thin films

III. Technical Contents

Activities were carried along the following six research directions.

1) Atomic Layer Epitaxy of Device Quality AlGaAs and AlAs

Atomic layer epitaxy (ALE) of device quality AlGaAs and AlAs has been demonstrated on a modified commercial metalorganic vapor phase epitaxial (MOVPE) reactor with a rotating susceptor. Growth rates up to 2 μm / h were achieved in this reactor AlAs had a much narrower plateau of saturated growth as compared to GaAs and $Al_{0.3}Ga_{0.7}As$, which many be due to the higher Al-CH_3 bond energy. This growth rate is comparable to that of MOCVD, however, the thickness is controlled to the monolayer level.

2) Selenium Doping of GaInP by Atomic Layer Epitaxy

Selenium doping of GaInP was performed using atomic layer epitaxy. The dependence of the n-type carrier concentration of Se-doped GaInP on growth temperature was quite different from that of Se-doped GaAs. Reducing growth temperature was found to be a crucial factor in achieving high n-type doping levels in as-grown Se-doped GaInP. Carrier concentrations in the high 10^{19} / cm^3 was achieved.

3) $Al_{0.3}Ga_{0.7}As$/GaAs Heterojunction Tunnel Diode for Tandem Solar Cell Applications

A p^+ - $Al_{0.3}Ga_{0.7}As/n^+$ - GaAs heterojunction tunnel diode was fabricated using an Atomic Layer Epitaxy (ALE) growth technique. Background carbon doping of ~ 10^{20} cm^{-3} was achieved in the p-side of the diode by optimizing growth conditions such as the V/III ratio, exposure times to reactant gases, and growth temperature. In the n - side of the diode, GaAs was doped with silane and doping concentrations as high as $7x10^{18}$ cm^{-3} were also achieved. The dopants are chosen to satisfy the high levels and low diffusion requirements. ALE grown p^+ - $Al_{0.3}Ga_{0.7}As$ / n^+ - GaAs heterojunction tunnel diodes showed high peak current density of 40 A / cm^2 and a high peak-to-valley ratio of 10. The diode can be used to interconnect the high and low band-gap cells in the AlGaAs/GaAs cascade solar cell structure. The reactor used in this investigation is a commercial MOCVD system which has been specially modified for dual operation of ALE and MOCVD growth modes.

4) Effect of Strain and Heavy Doping on $Ga_xIn_{1-x}P/Ga_{0.51}In_{0.49}P$ Band Structure for BSF and Window Layer Applications

We have carried out bandgap calculations to study the bandgap line-up in the $Ga_{0.5}In_{0.5}P/Ga_xIn_{1-x}P$ material system. The goal is to determine ΔE_c and ΔE_v and thus the potential applications of Ga_xIn_{1-x} P ($x>0.5$) both as a BSF window layer, for p/n and n/p structures. In these calculations the following factors were considered:

I) effect of strain
ii) effect of heavy doping.

Strain effects were studied using both Van de Walle's and Hrivnak's models. Effective mass data were obtained using the Krijn approach. These calculations were first applied to the strained GaInAs ternary alloy and results compared favorably to the available experimental data for this

system.

5) Back Surface Fields for n/p and p/n GaInP Solar Cells

We have grown n/p/p^+ $GaInP_2$ top cells, lattice matched to GaAs for multijunction tandem solar cells. We have studied the effect of different types of back surface field (BSF) layers on the cell parameters of each cell. These layers are namely, abrupt strained $GaInP_2$, graded strained $GaInP_2$, disordered $GaInP_2$ and AlGaAs layers. The measurements were done under 1-sun AMO spectrum. The results show that the abrupt strained $GaInP_2$ BSF outperforms the disordered $GaInP_2$ BSF. Likely related to material quality, the AlGaAs layer clearly produce the least efficient BSF. It has been found that the abrupt strained $Ga_xIn_{1-x}P$ BSF with x=0.56 gives better results than the case with x=0.63 for the p/n/n^+ structure.

6) AlGaAs/GaInP Heterojunction Tunnel Diode for Cascade Solar Cell Application

A p^+ - AlGaAs/n^+ - GaInP heterojunction tunnel diode with bandgap $E_g \approx 1.9$ eV was fabricated by atomic layer epitaxy growth. Doping levels of $1x10^{20}$ cm^{-3} and $5x10^{19}$ cm^{-3} were achieved in the *p* and *n* side of the diode using carbon and selenium, respectively. The diode can be used to interconnect the high and low band-gap cells in the AlGaAs/GaAs cascade solar cell structure. For forward current of 20 A/cm^2, which is the expected current density at 1000 suns operation, there is only ~ 20 mV voltage drop across the tunnel junction. When annealed at 650 and 750 °C to simulate the growth of the top cell, the diode was still suitable for 1000 suns operation. This is the first reported tunnel diode fabricated in high band-gap material systems that can be used as the connecting junction in the cascade solar cell structure operating at 1000 suns.

7) Properties of Highly Strained GaP and GaP/GaAs/GaP Quantum Wells Grown on GaAs Substrates by Atomic Layer Epitaxy

Atomic layer epitaxy (ALE) has been employed for the growth of highly strained (3.6%) GaP films and GaP/GaAs/GaP single quantum wells on (100) GaAs substrates at 500 °C. Misfit dislocation formation in GaP was observed by Scanning Transmission Electron Microscopy (STEM) and chemical delineation of dislocations. The onset of dislocations in the GaP layers was also determined by the onset of degradation in electrical properties (breakdown voltage and reverse current) of GaP/GaAs Schottky diodes and in low temperature photoluminescence (FWHM and intensity) of GaP/GaAs/GaP single quantum wells. All techniques experimentally indicate a critical layer thickness (CLT) greater than 60 Å. This value is several times larger than the theoretical value ($h_c < 20$ Å) predicted by the force balance model. This result may be related to the low growth temperature and the two dimensional (2-D) nature of the ALE growth process.

Atomic Layer Epitaxy of Device Quality AlGaAs and AlAs

N. Hayafuji
Mitsubishi Electric Corporation, Optoelectronic & Microwave Devices Laboratory, 4-1, Mizuhara, Itami, Hyogo 664, Japan
G. M. Eldallal, A. Dip, P. C. Colter, and S. M. Bedair
North Carolina State University, Department of Electrical and Computer Engineering, Raleigh, North Carolina 27695-7911, U. S. A.

ABSTRACT

Atomic Layer Epitaxy (ALE) of device quality AlGaAs and AlAs has been demonstrated on a modified commercial metalorganic vapor phase epitaxial (MOVPE) reactor with a rotating susceptor. AlAs had a much narrower plateau of saturated growth as compared to GaAs and $Al_{0.3}Ga_{0.7}As$, which would be due to the higher Al-CH_3 bond energy. At 650°C the ALE region of AlAs is confined to a 10% input flux ratio, though tiny this is the highest temperature reported for self-limited growth of AlAs. Purely ALE grown p^+-$Al_{0.3}Ga_{0.7}As/n^+$-GaAs heterojunction tunnel diodes showed high peak current density of 44mA/cm^2 and high peak-to-valley ratio of 10, which were obtained from a half of 2-inch diameter wafer. The diodes were successfully applied to interconnect the high and low bandgap cells in a AlGaAs/GaAs tandem solar cells without any degradation of electrical performance.

1. Introduction

Current interest in advancing the state of the art in semiconductor technology has led to several novel devices. Dramatic reductions in device dimensions for improvements in speed and packing densities have placed stronger demands on the epitaxial methods. Quantum devices, such as quantum well lasers, resonant tunneling diodes (RTD's) and transistors (RTT's) have operating characteristics which are strongly dependent upon monolayer thickness variations. Atomic Layer Epitaxy (ALE) holds great potential as a growth technique capable of providing control on the atomic scale over thickness and

uniformity for tomorrow's ultra-thin semiconductor films. ALE also offers the potential for high yields over large area substrates in a consistent, reproducible fashion with minimal periodic system re-calibration. Other appealing features of ALE includes selective area growth [1], built-in high p-type doping [2] and well-behaved side-wall deposition [3] not possible by the conventional means.

Recent reports of various GaAs/AlGaAs devices [4,5] have used ALE to grow only the GaAs layers for part of the device structure, where as the AlGaAs layers were grown at higher growth temperatures mainly by metalorganic vapor phase epitaxy (MOVPE). This is chiefly due to the difficulties in growing AlGaAs layers with low background carbon levels by ALE while maintaining self-limited growth at the optimum growth conditions. This paper first reports on the method and growth conditions used to overcome those shortcomings of the ALE method and some preliminary device characteristics achieved using the purely ALE grown AlGaAs/GaAs layers.

2. Experimental

The design of the ALE system used in this study is based upon one developed previously in our laboratory [6]. The modified commercial MOVPE reactor was used. The chamber is subdivided into six equally spaced compartments by the quartz partitions which separate the reactant gases and shear off a part of the boundary layer above the substrate [7]. A growth cycle is composed of an exposure to the column III reactant gas stream, purge/dilution by H_2, an exposure to the column V reactant gas stream, and purge/dilution by H_2. This sequence is carried out by rotating the substrate holder. The distance between the substrate and the quartz partitions is finely controlled for improved confinement of reactant gases and boundary layer sheering. In addition, the inclination of the gas inlet jets is well adjusted to minimize mixing near the center of rotation.

The metalorganic sources used were trimethlgallium (TMGa) and trimethylaluminum (TMAl). Pure arsine was used as the arsenic source. A 1000 ppm silane source (n-type) and

carbon (p-type) from the metalorganic sources were used as the dopants. All experiments were conducted at a system pressure of 30 torr.

3. Results and Discussion

3.1 ALE of AlAs and $Al_{0.3}Ga_{0.7}As$

Figure 1 shows growth curves for AlAs at 550°C and 650°C using the exposure times of 0.42 sec and 1.11 sec for each reactant gas, which correspond to the holder's rotation speeds of 24 rpm and 9 rpm. The saturated growth of AlAs at one monolayer/cycle was achieved over the input flux range for all cases studied. It should be noted that AlAs has a much narrower plateau of saturated growth as compared to GaAs. At 650°C the ALE region of AlAs is confined to a 10% input flux variation, though tiny this is the highest temperature reported for saturated growth of AlAs. The self-limited behavior of the AlAs is quite narrow. It would be expected that the higher Al-CH_3 bond energies would result in a lower desorption of CH_3 thus increasing the self-limited plateau for similar conditions as in the GaAs case. Typically, a TMAl radical has a higher decomposition energy than a TMGa radical [8]. For the TMAl case, the loss of the first methyl to form $Al(CH_3)_2$ requires 65.2 kcal/mol [9] compared to TMGa which requires 59.5 kcal/mol to form $Ga(CH_3)_2$ [10]. The loss of the second methyl to form $AlCH_3$ requires 39.9 kcal/mol [11] compared to TMGa which requires 35.4 kcal/mol to form $GaCH_3$ [10]. The bond energy of the final methyl in $AlCH_3$ can be estimated using the average energy for complete decomposition to atomic Al of 68.3 kcal/mol [12] and the published values for removal of the first two methyls provided above. This yields a value of 99.9 kcal/mol to form Al from $AlCH_3$ as compared to $GaCH_3$ to form Ga which requires 77.6 kcal/mol [10].

Another factor contributing a reduction to the regions of saturated growth may be attributable to flux variations of the column III reactant gas. It is observed that under conditions that permit conventional MOVPE growth to occur (column III and V gas mixing), a 20-40% variation in layer thickness is observed across the substrate where virtually none

would be observed for ALE growth. This suggests that the saturated growth regions are further reduced due to large input reactant flux variations. The sharp contrast in layer uniformity between ALE and MOVPE modes of operation truly demonstrates the power and flexibility of the ALE growth technique.

The regions of saturated growth for both AlAs and GaAs are found to overlap over the same temperature ranges, exposure times and column III reactant input fluxes. This fact indicates that we can actually get the self-limiting growth of the $Al_{0.3}Ga_{0.7}As$ as shown in fig. 2. The region of saturated growth of fig. 2 appears more related to the AlAs growth curve than that of GaAs. This implies that the reaction(s) taking place which result in saturated growth have a higher sensitivity to the TMAl than the TMGa. The electrical property of the layers was evaluated by Van der Pauw Hall measurement. The variation of background carbon doping levels for AlGaAs and AlAs was found to increase with increasing total flux of TMGa and TMAl. The source of the higher carbon incorporation observed for AlGaAs may be due to the difficulties in breaking the stronger Al-C bond. Background doping levels from low 10^{17} cm^{-3} to mid 10^{19} cm^{-3} were found to be possible by changing the conditions under which saturated growth is obtained, such as temperature, exposure time or V/III ratio. Background doping levels are controllable over a much wider range by more dramatic changes to the V/III ratio or exposure times to the column III flux, without loss of saturated growth. The n-type doping experiment was also carried out at 650°C with a total column III input flux of about 0.055 µmoles/cycle. These conditions gave a background carbon doping level of about $2x10^{17}$ cm^{-3}. For example, Si doping levels from mid 10^{17} cm^{-3} to mid 10^{18} cm^{-3} were obtained for the $Al_{0.3}Ga_{0.7}As$ layer.

3.2 AlGaAs/GaAs Quantum Wells

The epitaxial layers also demonstrated good optical properties. Intense photoluminescence (PL) emissions from ALE-grown $Al_{0.3}Ga_{0.7}As$/GaAs/$Al_{0.3}Ga_{0.7}As$ (1500/50/1500Å) quantum wells (QW's) were obtained at room temperature (RT) and 77K. The deviation in the peak emissions of the 50Å QW's taken at several locations along the

substrate's radial (x) and tangential (y) directions are shown in fig. 3. The same data were obtained reproduciblly for the QW's grown over a one month period (about 25-30 runs apart) using the same column III dose. The average shift\ in peak energies was 2.9 meV corresponding to a 0.4 monolayer change in thickness of the QW (±1.4% variation). This result is comparable to or slightly better than reported for MOVPE grown 40Å QW where the average thickness variation is about ±2.4% [13]. This serves to reiterate an important benefit of ALE growth, namely desensitization to short and long term system transients or variations due to mass flow controllers, reactant sources, thermal gradients, etc. An important advantage of this feature is that periodic system re-calibration is reduced or eliminated thus increasing productivity.

3.3 Tunnel diode and tandem solar cell

As mentioned in 3.1 and 3.2, the ALE has the feasible controllability of n and p-type doping for AlGaAs and excellent interface quality of AlGaAs/GaAs. These are very fitted for the internal connection between the solar cells which requires a low resistance but transparent structure. Consequently, the ALE growth of tandem solar cell with tunnel junction was tried. First, the tunnel diode structure was grown by ALE at 650°C. It consisted of 300Å thick n^+-GaAs layer ($n=7x10^{18}cm^{-3}$), 300Å thick p^+-$Al_{0.3}Ga_{0.7}As$ layer ($p=8x10^{19}cm^{-3}$) and 0.7μm thick p^+-GaAs contacting layer ($p=5x10^{18}cm^{-3}$) on a half of 2 inch diameter n-GaAs (100) substrate. After growth, mesas with an area of 200 x 200μm^2 were etched using H_2O_2-H_3PO_4-H_2O (1:2:5) solution. Then, AuGe/Ni/Au and Au were deposited as the front and back electrodes, respectively. Figure 4 shows the typical current density-voltage cheracteristics of the tunnel diode. High peak-to-valley ratio of 10 was obtained in a whole wafer. In addition, the sheet resistance was found to be sufficiently low ($2.2x10^{-3}$ Ωcm^2). If used for a tandem solar cell having a current density of 20 mA/cm^2 at 1 sun-AM 1.5 condition, there will be only 44 mV voltage drop across the tunnel junction at 1000 suns. Next, the above tunnel junction was used to connect a GaAs bottom cell with an $Al_{0.3}Ga_{0.7}As$ top cell, to form a cascade solar cell structure. Figure 5 show the cross-

sectional schematic of the cell structure. The size was 4x4mm^2. Figure 6 shows a typical current-voltage characteristics of the cell measured at 10 suns-AM 1.5 condition. The open circuit voltage of 1.945 V, the short circuit current of 2.465 mA and fill factor of 0.812 were obtained. The energy coversion efficiency was estimated as 11.5 %. The reason of a little low value of the efficiency is thought to be due to the uncertainty of the light intensity of the solar simulator. Apart from this question, the other characteristics were reasonable and there was no plateau on the curve. These results indicate that the tunnel juncution does not result in any appreciable deterioration in solar cell performance.

4. Summary

ALE growth of AlAs, $Al_{0.3}Ga_{0.7}As$ was achieved over a wide range of growth conditions on large area substrates in a specially modified MOVPE reactor. AlAs had a much narrower plateau of saturated growth as compared to GaAs and $Al_{0.3}Ga_{0.7}As$, which would be due to the higher Al-CH_3 bond energy. At 650°C the ALE region of AlAs is confined to a 10% input flux ratio, though tiny this is the highest temperature reported for self-limited growth of AlAs. Photoluminescence results of $Al_{0.3}Ga_{0.7}As$/GaAs quantum wells showed the material to be high quality and good uniformity (less than 1 monolayer thickness variation). Purely ALE grown p^+-$Al_{0.3}Ga_{0.7}As$/n^+-GaAs heterojunction tunnel diodes showed high peak current density of 44mA/cm^2 and high peak-to-valley ratio of 10, which were obtained from a half of 2-inch diameter wafer. The diodes were successfully applied to interconnect the high and low bandgap cells in a AlGaAs/GaAs tandem solar cells without any degradation of electrical performance.

Acknowledgment

The authors acknowledge support from ONR/SDIO, the National Renewable Energy Laboratory, and the National Science Foundation for their support which made this work possible.

REFERENCES

[1] A. Usui and H. Sunakawa, Jpn. J. Appl. Phys. **25** (1986) L212.

[2] K. G. Reid, H. M. Urdianyk and S. M. Bedair, Appl. Phys. Lett. **59** (1991) 2397.

[3] S. M. Bedair, B. T. McDermott, Y. Ide, N. H. Karam, H. Hashemi, M. Timmons, M. A. Tischler, J. C. L. Tarn and N. El-Masry, J. Cryst. Growth **93** (1988) 182.

[4] S. P. DenBaars, C. A. Beylar, A. Hariz and P. D. Dapkus, Appl. Phys. Lett. **51** (1987) 1530.

[5] R. Bhat, J. R. Hayes, E. Colas and R. Esagui, IEEE Electron Device Lett. **9** (1988) 442.

[6] S. M. Bedair, M. A. Tischler, T. Katsumaya and N. A. El-Masry, Appl. Phys. Lett. **47** (1985) 51.

[7] P. C. Colter, S. A. Hussien, A. Dip, M. U. Ergogan, W. M. Duncan and S. M. Bedair, Appl. Phys. Lett. **59** (1991) 12.

[8] "Chemical Kinetics", C. H. Bamford and C. F. H. Tipper eds., Elsevier Publishing (1972) 253.

[9] H. A. Skinner, Adv. Organomet. Chem. **2** (1964) 49.

[10] M. G. Jacko and S. J. W. Price, Can. J. Chem. **41** (1963) 1560.

[11] M. Tirtowidjojo and R. Pollard, J. Crystal Growth **77** (1986) 200.

[12] W. V. Steele, Chem. Soc. Ann. Rep. **71A** (1974) 103.

[13] S. Ochi, N. Hayafuji, Y. Kajikawa, K. Mizuguchi and T. Murotani, J. Crystal Growth **77** (1986) 553.

LIST OF FIGURE CAPTIONS

Figure 1 AlAs growth rate versus TMAl flow rate.
[(◆) TMAl exposed for 0.42 sec at 550°C, (■) TMAl exposed for 1.11 sec at 550 °C, (O) TMAl exposed for 1.11 sec at 650°C.]

Figure 2 $Al_{0.3}Ga_{0.7}As$ growth rate versus total flow rate of TMAl and TMGa.
[(●) TMAl and TMGa exposed for 0.42 sec at 550°C, (■) TMAl and TMGa exposed for 0.42 sec at 650 °C, (◆) TMAl and TMGa exposed for 1.11 sec at 650°C, (O) TMAl and TMGa exposed for 2.22 sec at 650°C.]

Figure 3 PL emission scans for a 50Å QW conducted at RT.
[(□) scanned in radial (X) direction, (■) scanned in tangential (Y) direction.]

Figure 4 Typical current density-voltage characteristics of n^+-GaAs/p^+-$Al_{0.3}Ga_{0.7}As$ tunnel diode grown by ALE at 650°C.

Figure 5 Cross-sectional schematic drawing of AlGaAs/GaAs tandem solar cell structure grown by ALE.

Figure6 Typical current-voltage characteristics of the cell measured at 10 suns-AM 1.5 condition. Open circuit voltage, short circuit current and fill factor are 1.945 V, 2.465 mA and 0.812, respectively.

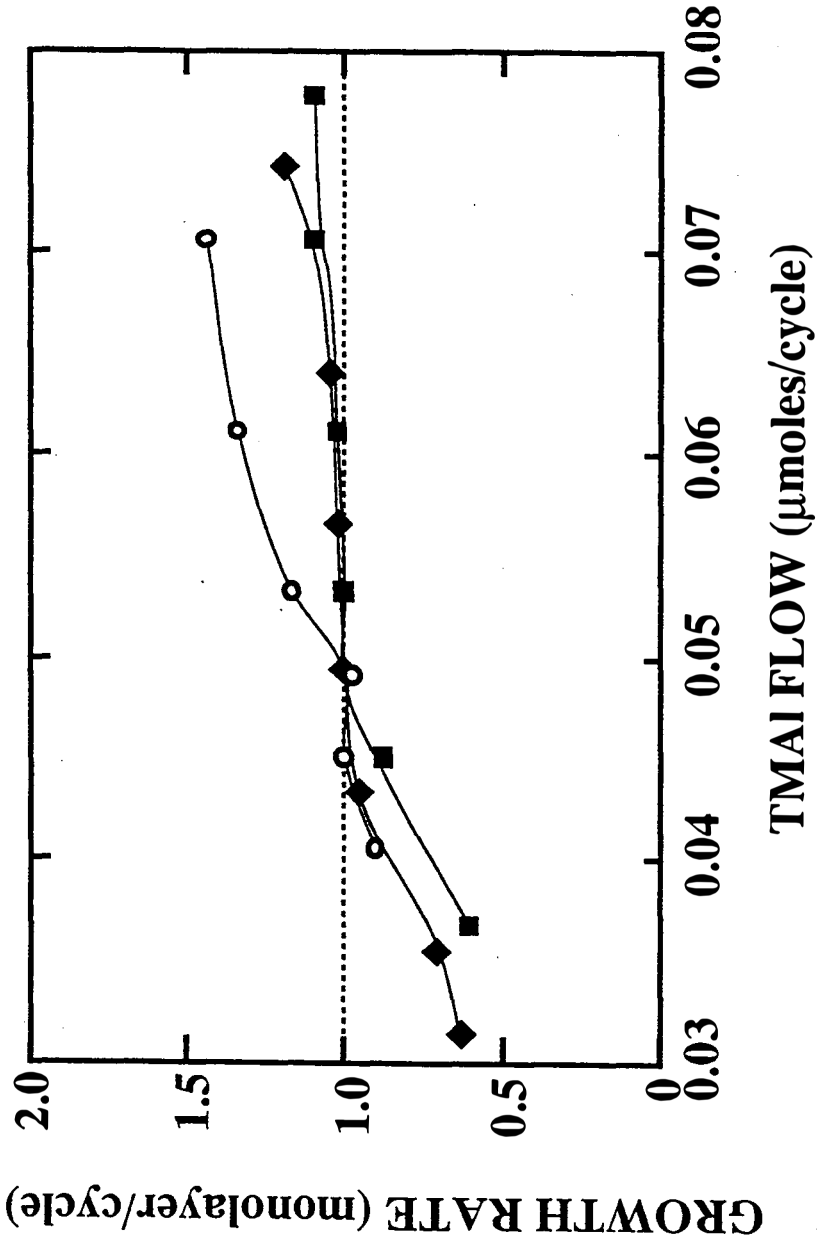

Figure 1

N. Hayafuji et al.

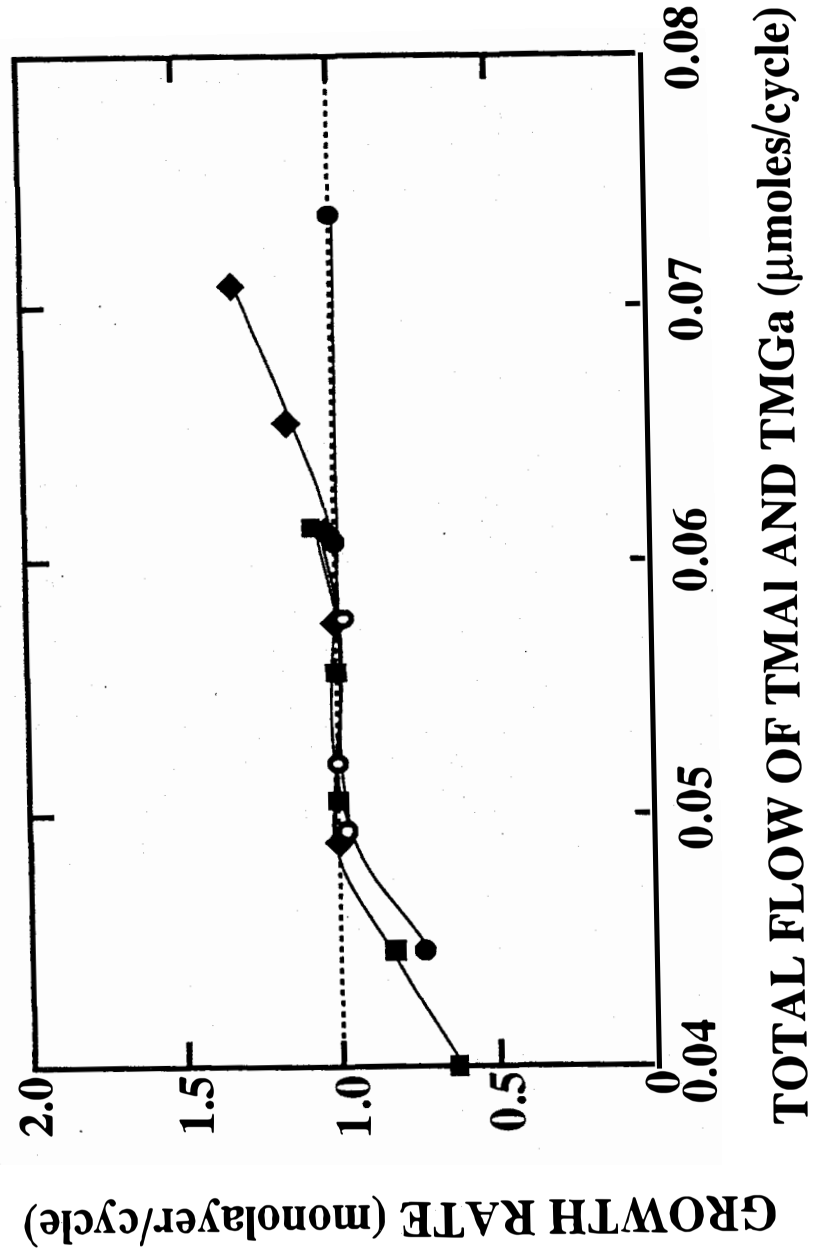
GROWTH RATE (monolayer/cycle)
2.0
1.5
1.0
0.5
0
0.04
0.05
0.06
0.07
0.08
TOTAL FLOW OF TMAl AND TMGa (μmoles/cycle)

Figure 2

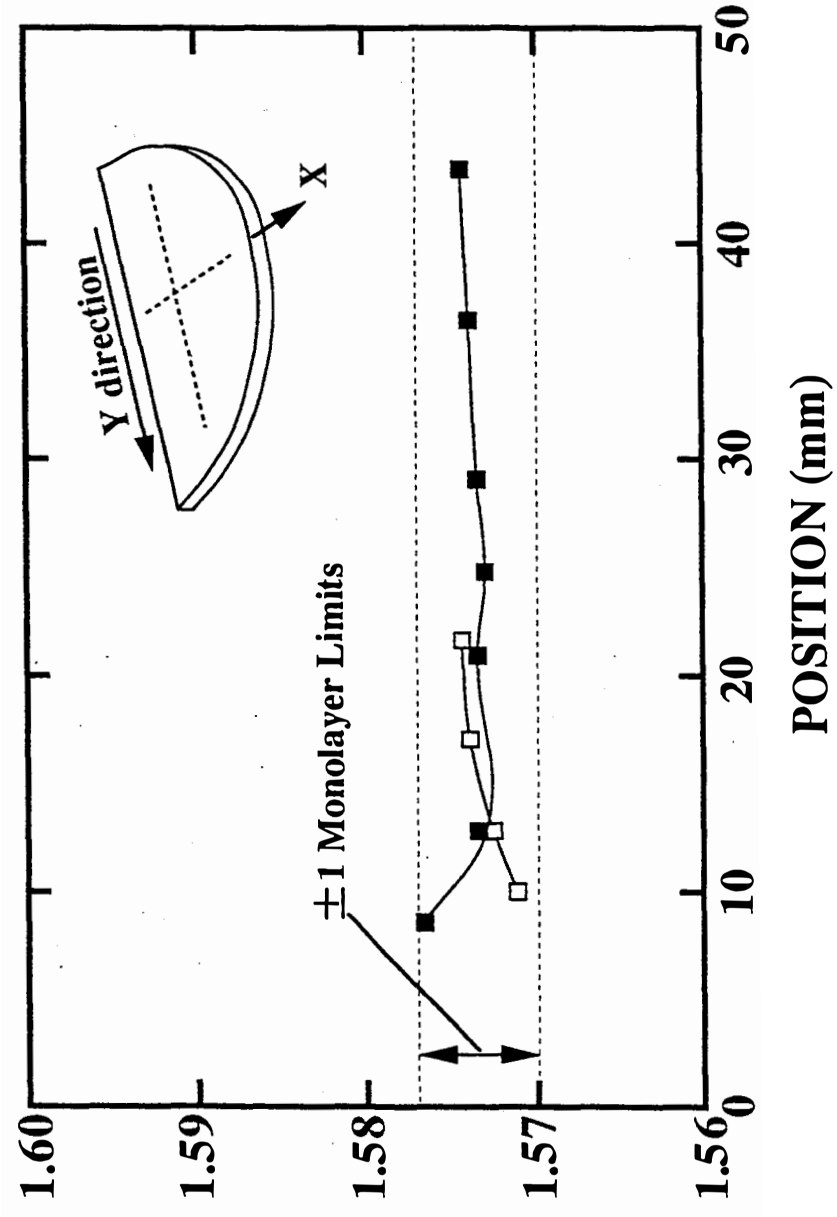
PL EMISSION ENERGY (eV)
1.60
1.59
1.58
1.57
1.56
0
10
20
30
40
50
POSITION (mm)
±1 Monolayer Limits
Y direction
X

Figure 3

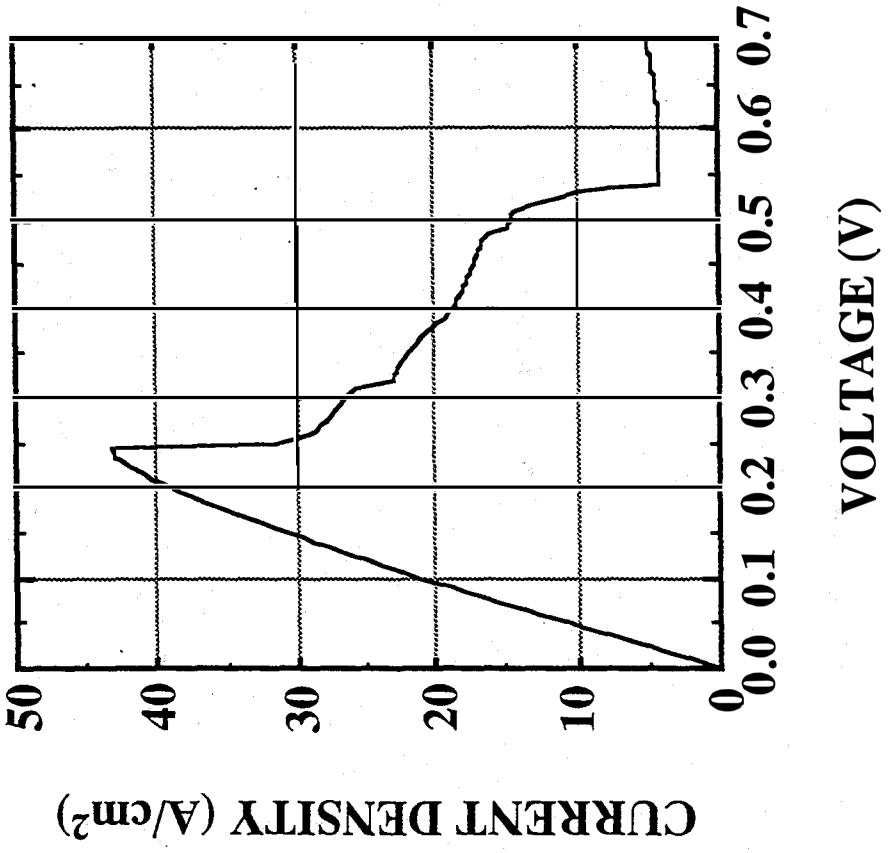
CURRENT DENSITY (A/cm²)
50
40
30
20
10
0
0.0 0.1 0.2 0.3 0.4 0.5 0.6 0.7
VOLTAGE (V)

Figure 4

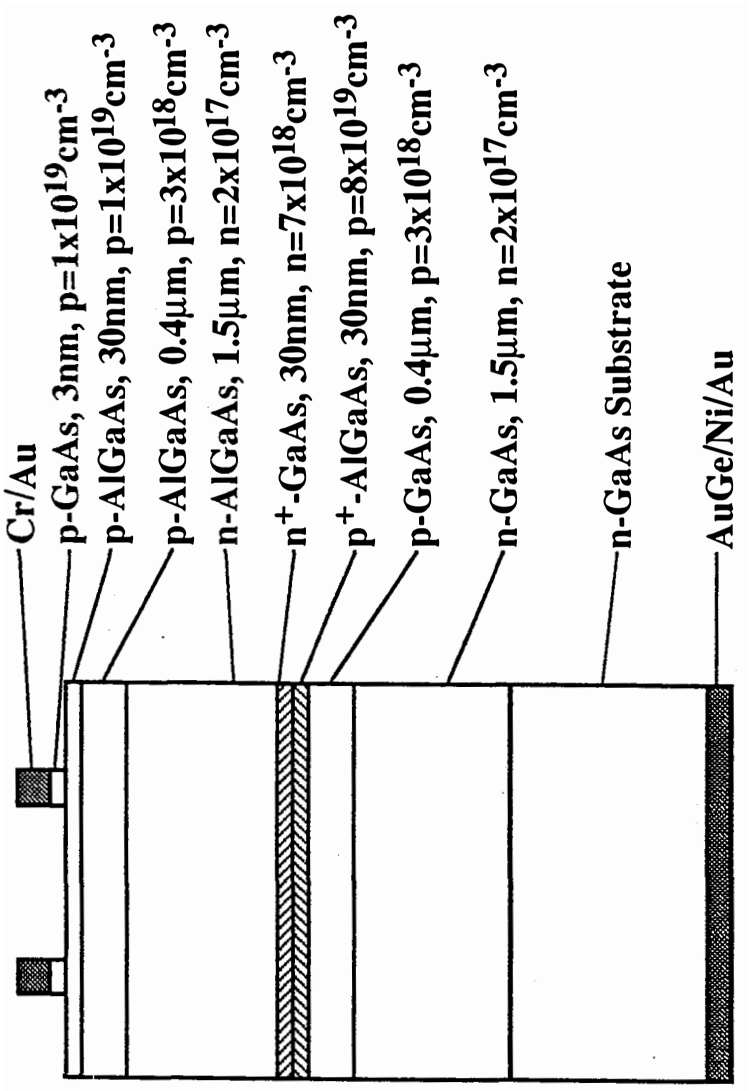

Figure 5

N. Hayafuji et al.

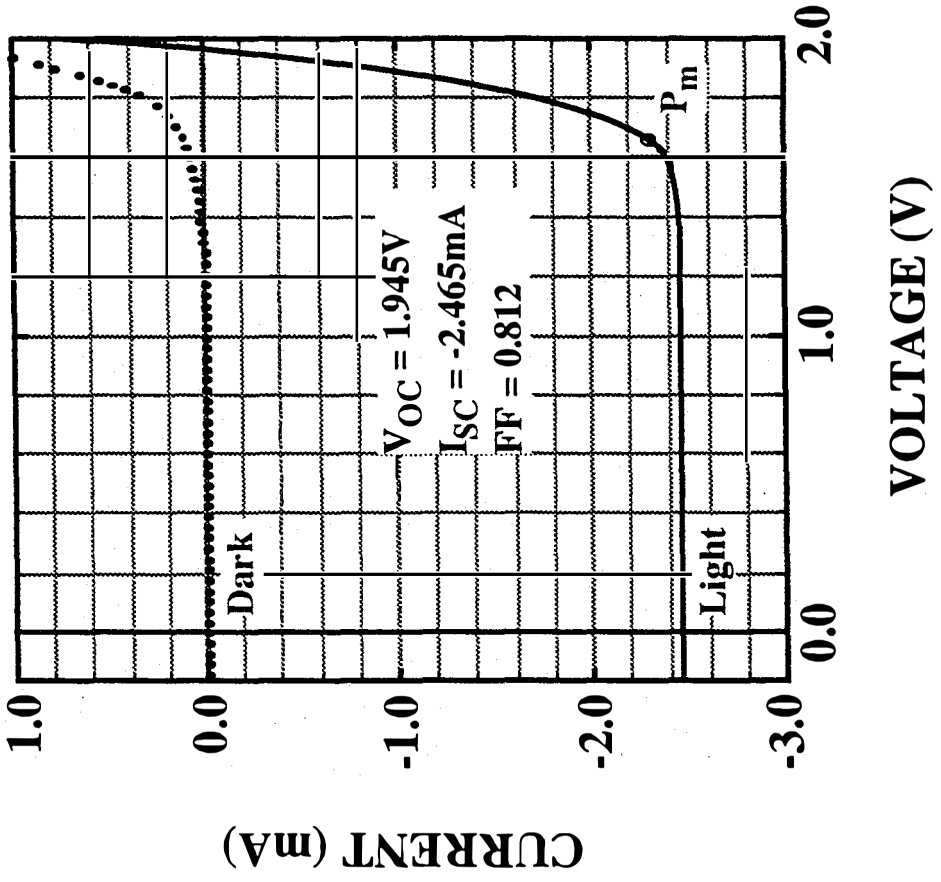
CURRENT (mA)
1.0
0.0
-1.0
-2.0
-3.0
0.0
1.0
2.0
VOLTAGE (V)
Dark
Light
V_{OC} = 1.945V
I_{SC} = -2.465mA
FF = 0.812
P_m

Figure 6

Journal of Electronic Materials, Vol. 24, No. 2, 1995

Selenium Doping of GaInP by Atomic Layer Epitaxy

D. JUNG*

Department of Physics, North Carolina State University, Raleigh, NC 27695-8202

M. LEONARD, N.E. EL-MASRY, and S.M. BEDAIR

Department of Electrical and Computer Engineering, North Carolina State University, Raleigh, NC 27695-7911

Selenium doping of GaInP was performed using atomic layer epitaxy. The dependence of the n-type carrier concentration of Se-doped GaInP on growth temperature was quite different from that of Se-doped GaAs. Reducing growth temperature was found to be a crucial factor in achieving high n-type doping levels in as-grown Se-doped GaInP.

Key words: Atomic layer epitaxy (ALE), GaAs, GaInP, selenium (Se)

INTRODUCTION

Recently, there has been great interest in the $Ga_xIn_{1-x}P$ alloy with a lattice constant at $x \approx 0.51$ close to that of GaAs. Because of its wide bandgap (~1.9 eV), $Ga_xIn_{1-x}P$ with $x \approx 0.51$ (hereafter referred to as GaInP) is a promising material for visible light emitting diodes (LEDs)[1] and visible lasers.[2] GaInP/GaAs heterostructures may also be a good alternative to AlGaAs/GaAs heterostructures in heterojunction bipolar transistors (HBTs) and in high electron mobility transistors (HEMTs) due to their large valence band discontinuity and the much smaller density of DX centers in the n-type GaInP layers.[3,4] While most of the donors in AlGaAs with aluminum composition close to the direct-to-indirect transition composition act as deep donors, deep level densities less than 1×10^{13} and 1×10^{14} cm^{-3} are reported in molecular beam epitaxially (MBE) grown Si-doped GaInP with $n \sim 1 \times 10^{17}$ cm^{-3},[5] and in metalorganic vapor phase epitaxially (MOVPE) grown Se-doped GaInP with $n \approx 2\text{–}4 \times 10^{17}$ cm^{-3}.[6] GaInP was also used in cascade solar cells for the active layer[7] and for the high bandgap connecting junction.[8] Carrier concentrations of n-type GaInP layers in the active layer and the connecting tunnel junction were about 10^{18} cm^{-3} and 10^{19} cm^{-3}, respectively. For device applications, control of doping levels in n-type GaInP is necessary. Selenium (Se) is a common n-type dopant species in III-V compounds due to its low activation energy[9] and high solubility.[10] Since selenium has a high vapor pressure at elevated temperatures, for the effective Se incorporation into the epitaxial layers, it is necessary to reduce the growth temperatures.[11] Atomic layer epitaxy (ALE) can be a good choice because it permits lower temperature growth of several III-V compounds, including GaInP[12,13] than MBE or MOVPE. Low temperature growth is possible even outside of the self-limiting regime, providing the ALE application with

(Received May 25, 1994; revised October 14, 1994)

* Present address: Laser Diode Laboratory, Samsung Advanced Institute of Technology, P.O. Box 111, Suwon 440-600, South Korea

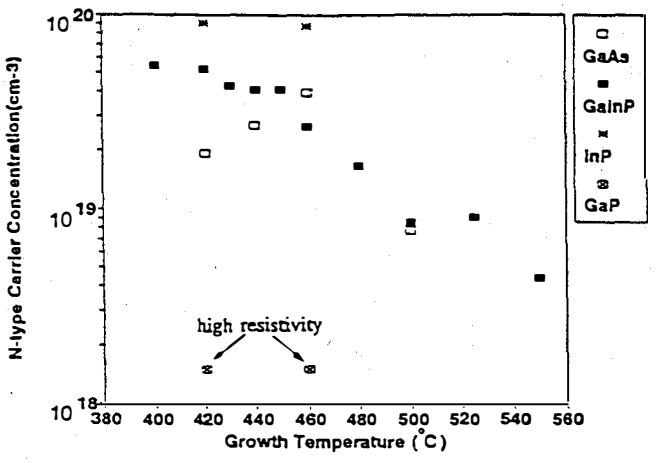

a

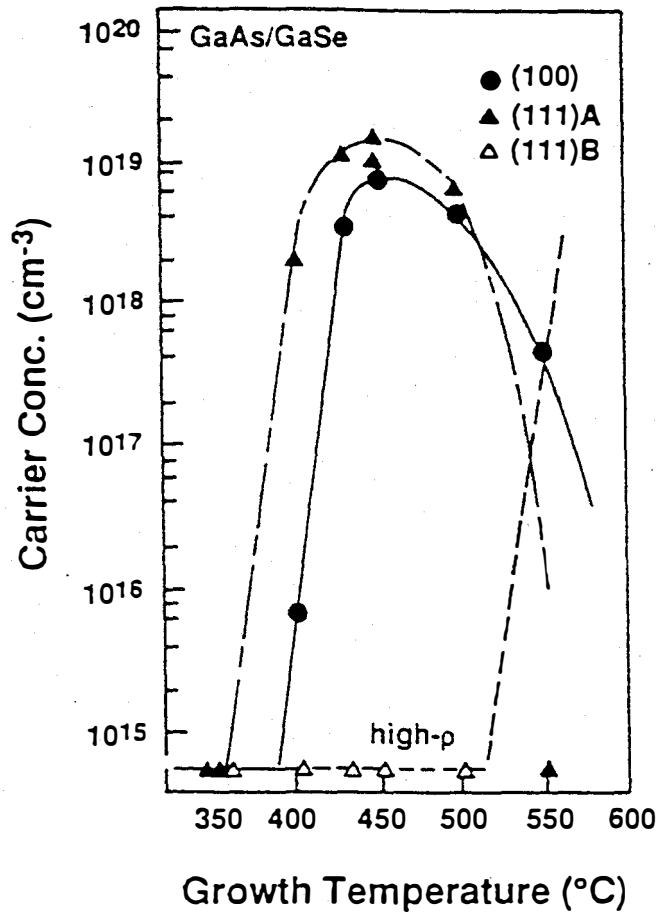

b

Fig. 1. (a) Dependence of n-type carrier concentrations on growth temperatures in Se-doped GaInP, GaAs, InP, and GaP. Although carrier concentrations of GaP samples grown at 460 and 420°C were too low to be put on the same scale with those of GaInP, GaAs, and InP samples, they were included for the ease of comparison, and (b) variation of n-type carrier concentrations of Se-doped GaAs with growth temperatures.[11]

more flexibility.

In this paper, we report the ALE growth of Se-doped GaInP. The dependence of the n-type carrier concentration of Se-doped GaInP on growth temperature was studied and compared with that of GaAs. Variation of the n-type carrier concentration of Se-doped GaInP with the Se source flow rate was also studied.

EXPERIMENTS

Atomic layer epitaxial growth of GaInP was performed in a modified atmosphere pressure MOVPE system described earlier.[14] The growth system can also perform conventional MOVPE growth. The group III precursors were trimethylgallium (TMGa) and trimethylindium (TMIn). These group III sources were introduced on the column III side of the reactor. AsH_3 (100%) and PH_3 (100%) were the group V source materials and were introduced on the column V side of the reactor. H_2Se (45 ppm in H_2) was used as the n-type dopant source and introduced on the column V side mixed with PH_3. Chromium-doped semi-insulating GaAs (100) substrates were used. Before being loaded into the reactor, the substrates were cleaned by organic solvents and etched with H_2SO_4:H_2O_2:H_2O = 7:1:1 solution. Before the growth of GaInP, the sample was heated to 650°C and kept at 650°C under AsH_3 flux on the column V side for 5 min to remove the native oxide, then cooled to the growth temperature. After the temperature was stabilized, AsH_3 was turned off, PH_3 was turned on; and after ~20 s, the ALE growth was started. The ALE growth consisted of the simultaneous exposure of the substrate to TMGa and TMIn fluxes followed by rotation to the PH_3 side to complete one cycle. The composition of $Ga_xIn_{1-x}P$ was controlled by the TMGa/(TMGa + TMIn) molar ratio in the column III stream and determined from x-ray diffraction. The growth temperature was varied from 400 to 550 C. The exposure time to TMGa and TMIn fluxes was 0.2 s. However, it was necessary to keep the sample under PH_3 flux for 3 s due to the low decomposition rate of PH_3 at the temperatures used in this experiment.[15] In our growth system, since PH_3 and H_2Se were mixed before they were introduced into the reactor, it was impossible to expose the sample separately to PH_3 and H_2Se fluxes. Although samples with better quality were obtained with longer exposure to PH_3 in the case of undoped GaInP, an exposure time of 3 s was used for Se-doped GaInP. Longer exposure of the sample to the mixture of PH_3 and H_2Se resulted in the degradation of the surface morphology probably due to the formation of high concentration of selenium compounds. X-ray diffraction spectra from films grown with 3 s exposure time to PH_3 + H_2Se flux showed reasonable crystallinity. The growth parameters were adjusted to achieve high n-type doping levels rather than to achieve the monolayer-per-cycle growth rate. Thicknesses of the samples were measured by a surface profilometer (Dektak). Carrier types and concentrations were determined by the Hall technique.

RESULTS AND DISCUSSION

Figure 1a shows the variation of n-type carrier concentrations of Se-doped GaInP with growth temperatures. N-type carrier concentrations of Se-doped GaInP showed a strong dependence on the

growth temperature, as in the case of Se-doped GaAs which was studied by Usui et al.[11] and shown in Fig. 1b. In our experiment, growth temperatures for Se-doped GaInP were varied from 400 to 550°C, and H_2Se flow rate was kept at 10 sccm. All the samples showed gallium composition around 51%, as determined from x-ray diffraction. As the growth temperature was reduced from higher temperature to 450°C, the carrier concentration increased quite rapidly, which is expected to be due to the high vapor pressure of Se at elevated temperatures.[11] In the growth temperature range of 400–450°C, the carrier concentration increased only slowly with decreasing growth temperature. This behavior is quite different from the previously reported Se-doped GaAs case shown in Fig. 1b, where the carrier concentration had a peak at around 440°C and decreased drastically on both sides of the peak. In Ref. 11, the fast decrease of the electron concentration on the lower temperature side was attributed to the formation of gallium selenides in GaAs at low temperatures, at which Se incorporation is so high as to form gallium selenides rather than isolated Se atoms in GaAs. It was also suggested that those Se atoms which formed gallium selenides such as GaSe, Ga_2Se_3, and Ga_2Se do not act as donors in GaAs, and the carrier concentration decreases when these are formed. To see if the difference between Se-doping behavior of GaInP in our experiment, and that of GaAs in Ref. 11 comes from the difference between two growth systems, rather than the properties of the two materials, we also performed Se-doping of GaAs by ALE. To make the growth conditions for Se-doped GaInP and Se-doped GaAs similar, flow rates of TMGa for GaAs were kept twice as high as those for $Ga_{0.51}In_{0.49}P$, and flow rates of AsH_3 and H_2Se for GaAs were kept the same as those of PH_3 and H_2Se for $Ga_{0.51}In_{0.49}P$. In our results shown in Fig. 1a, the carrier concentration of Se-doped GaAs had a peak value of 3.95×10^{19} cm^{-3} at 460 °C and decreased on both sides of the peak. This behavior is similar to the results shown in Fig. 1b. In our case, however, the decrease on the lower temperature side of the peak is not as drastic as in Fig. 1b. This may be due to the difference in growth methods used in the two experiments. In our case, AsH_3 and H_2Se were introduced together into the reactor. This does not allow for the formation of gallium selenides as effectively as in the case of Ref. 11, where AsH_3 and H_2Se were introduced separately at different ALE cycles. From the result of Se-doping of GaAs using our experimental setup, it is obvious that the difference between Se-doping behavior of GaInP in our experiment and that of GaAs in Ref. 11 comes from the difference between the properties of the two materials. In order to investigate the possible reasons for the difference between Se-doped GaInP and GaAs, we performed growths of Se-doped InP and GaP at 420 and 460°C, where the behaviors of Se-doping of GaInP and GaAs are quite different. Due to the slow growth rate, thicknesses of InP and GaP were limited to ~100 and ~40 nm, respectively. Carrier concentrations of Se-doped InP were as high as 9.05×10^{19} cm^{-3} at 420°C and 8.78×10^{19} cm^{-3} at 460°C, respectively, while carrier concentrations of Se-doped GaP were not high enough to be measured for the epitaxial layers as thin as ~40 nm. In the intensively studied GaAs case, due to surface and interface depletions, GaAs films of thickness ~50 nm even with electron concentrations around 5×10^{17} cm^{-3} show apparent Hall carrier concentrations 10^{15} cm^{-3},[16] which is difficult to be measured by our Hall measurement setup. From the results of Se-doping of InP and GaP by ALE, it could be suggested that, while a large portion of Se atoms incorporated in GaP sublattices of $Ga_{0.51}In_{0.49}P$ do not act as donors, as in the case of Se-doped GaAs grown at lower temperatures than 440°C. However, Se atoms incorporated in InP sublattices contribute to n-type conduction, thereby not resulting in the decrease of the carrier concentration of Se-doped GaInP grown at low temperatures. The difference in the Se-doping behavior of GaP and InP can be due to the relative stability of "second phases of selenium" in GaP and InP such as gallium selenides and indium selenides at the growing surface. More stable gallium selenides consume the selenium source more readily, at the growth temperatures, thus reducing the selenium incorporation as ionized impurities during the growth of GaP. It is also possible that indium selenides are not readily formed in InP, and, therefore, more selenium

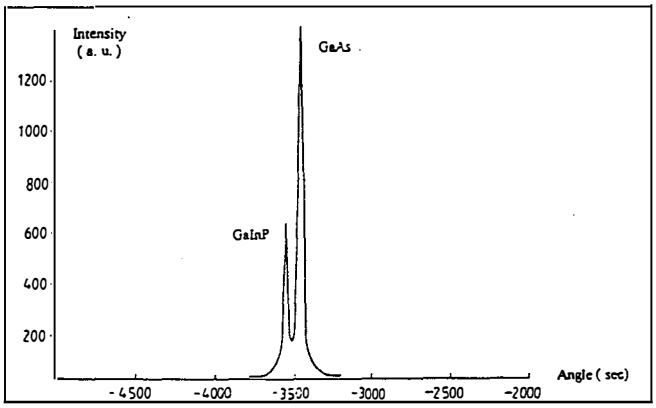

a

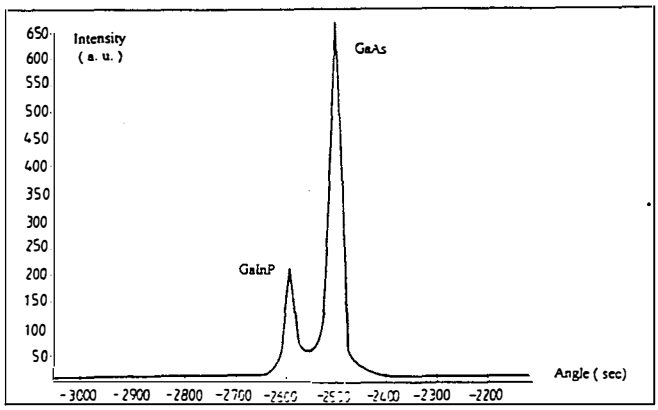

b

Fig. 2. X-ray diffraction patterns from Se-doped GaInP grown at 440°C (a) and 400°C (b).

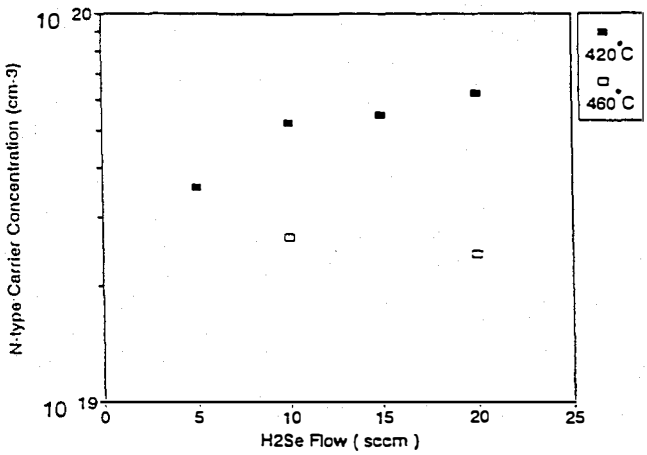

Fig. 3. Variation of n-type carrier concentrations in Se-doped GaInP with H_2Se flow rates. Se-doped GaInP was grown at 420 and 460°C.

atoms from the selenium source are consumed as shallow donor atoms in InP. More experiments such as secondary ion mass spectroscopy (SIMS) are needed to clarify the Se incorporation process in GaInP. At growth temperatures lower than 450°C, carrier concentrations in the range of $4–6 \times 10^{19}$ cm^{-3} were achieved. These are considered to be the highest doping levels ever reported for high bandgap ($E_g \approx 1.9$ eV) III-V compounds semiconductors.

Figures 2a and 2b are the x-ray diffraction spectra of GaInP films grown at 440 and 400°C, respectively. Lattice mismatches between the epilayers and the substrates are 4.6×10^{-4} and 4.5×10^{-4} for (a) and (b), respectively. The ratio of peak intensities of the deposited GaInP film and the GaAs substrate is higher in Fig. 2a than in Fig. 2b, implying a higher quality for the sample grown at 440°C. The degradation in the crystal quality of the samples grown at these low temperatures can be due to the second Se-phases in the epitaxial films. Selenium atoms which form these Se-phases such as GaSe and Ga_2Se_3 may act as defects in the epitaxial layers rather than donors. It should also be mentioned that GaInP can be deposited in ordered or disordered structures depending on the growth conditions. With these fairly high levels of doping, the disordered phase will be dominant as has been previously reported.[10]

The variation of n-type carrier concentration of Se-doped GaInP with respect to H_2Se flow rate was also investigated at two growth temperatures, 420 and 460°C, as shown in Fig. 3. At 420°C, as H_2Se flow rate was increased, the carrier concentration increased and then nearly saturated for H_2Se flow rates above 10 sccm. At 460°C, the carrier concentration stayed at the value of 2.5×10^{19} cm^{-3} with a H_2Se flow rate of 10 sccm. A higher flow rate of 20 sccm did not increase the carrier concentration. Under this growth condition, an opaque surface resulted. This indicates that in order to achieve high doping levels in GaInP using H_2Se as the dopant source, it is crucial to reduce the growth temperature. This is possible with atomic layer epitaxy.

SUMMARY

Selenium doping of $Ga_xIn_{1-x}P$ with $x \approx 0.51$ was performed using the atomic layer epitaxial technique. N-type carrier concentrations higher than 5×10^{19} cm^{-3} were achieved. The dependence of the carrier concentration on the growth temperature for Se doping of GaInP is quite different from that of Se doping of GaAs. This may be due to the difference in the properties of Se in InP and GaP. Reduced growth temperatures were found to be a crucial factor for achieving high doping levels in GaInP.

ACKNOWLEDGEMENT

This work is supported by NREL, NSF, and ONR.

REFERENCES

1. T. Iwamoto, K. Mori, M. Mizuta and H. Kukimoto, *J. Cryst. Growth* 68, 27 (1984).
2. I. Hino, A. Gomyo, K. Kobayashi, T. Suzuki and K. Nishida, *Appl. Phys. Lett.* 43, 987 (1983).
3. H. Kroemer, *J. Vac. Sci. Technol.* B1, 126 (1983); M. J. Mondry and H. Kroemer, *IEEE Electron Device Lett.* 6, 175 (1985).
4. Y.J. Chan, D. Pavlidis, M. Razeghi and F. Omnes, *IEEE Trans. Electron Devices* 37, 2141 (1990).
5. H. Tanaka, Y. Kawamura, S. Nojima, K. Wakita and H. Asahi, *J. Appl. Phys.* 61, 1713 (1987).
6. M.O. Watanabe and Y. Ohba, *J. Appl. Phys.* 60, 1032 (1986).
7. J.M. Olson, S.R. Kurtz, A.E. Kibbler and P. Faine, *Appl. Phys. Lett.* 56, 623 (1990).
8. D. Jung, C.A. Parker, J. Ramdani, M. Leonard, N. El-Masry and S.M. Bedair, *Proc. 1992 Electron. Mater. Conf.* Cambridge, MA (24 June 1992).
9. T. Ishikawa, T. Maeda and K. Kondo, *J. Appl. Phys.* 68, 3343 (1990).
10. S.R. Kurtz, J.M. Olson, J.P. Goral, G. Kibbler and E. Beck, *J. Electron. Mater.* 19, 825 (1990).
11. G. Usui and H. Sunakawa, *GaAs and Related Compounds*, Inst. Phys. Conf. Ser. No. 83 (Bristol, England: IOP, 1987), p.129.
12. G. Usui and H. Sunakawa, *Ext. Abs. 20th Conf. on Solid State Devices and Materials*, Tokyo, Japan, (1988), p. 379.
13. B.T. McDermott, N.A. El-Masry, F. Hyuga and S.M. Bedair, *J. Cryst. Growth* 107, 96 (1991).
14. M.A. Tischler and S.M. Bedair, *Atomic Layer Epitaxy*, ed. Suntola and Simpson (Glasgow and London: Blackie, 1990), Ch. 4.
15. P. Abraham, A. Bekkaoui, V. Souliere, J. Bouix and Y. Monteil, *J. Cryst. Growth* 107, 26 (1991).
16. A. Chandra, C.E.C. Wood, D.W. Woodard and L.F. Eastman, *Solid State Electron.* 22, 645 (1979).

$Al_{0.3}Ga_{0.7}As$/GaAs HETEROJUNCTION TUNNEL DIODE FOR TANDEM SOLAR CELL APPLICATIONS

G.M. Eldallal, N. Hayafuji[†], M.S. Abou Elwaffa[‡], M. A. Elgammal[‡], and S. M. Bedair.
North Carolina State University, Department of Electrical and Computer Engineering, Raleigh, NC 27695-7911 (USA)

ABSTRACT

A p^+-$Al_{0.3}Ga_{0.7}As$/n^+- GaAs heterojunction tunnel diode was fabricated using Atomic Layer Epitaxy (ALE) growth technique. Background carbon doping of ~ 10^{20} cm^{-3} was achieved in the p-side of the diode by optimizing growth conditions such as V/III ratio, exposure times to reactant gases, and growth temperature. In the n- side of the diode GaAs was doped with silane and doping concentrations as high as $7x10^{18}$ cm^{-3} were also achieved. The dopants are chosen to satisfy the high levels and low diffusion requirements. The diode can be used to interconnect the high and low band-gap cells in the AlGaAs/GaAs cascade solar cell structure. The reactor used in this investigation is a commercial MOCVD system which has been specially modified for dual operation of ALE and MOCVD growth modes.

INTRODUCTION

Tandem cells are attractive for concentrator terrestrial and space solar cells because they can achieve higher efficiencies than single-junction cells. In addition, the conversion efficiency of a concentrator cell usually, increases as concentration ratio increases up to the point where the power loss due to the growing series resistance begins to reduce the efficiency. Theoretically, for a two cell structure, conversion efficiencies of 30% and 40% can be achieved for one sun and 500 suns, respectively.[1] The AlGaAs/GaAs system has been considered as a potential candidate to illustrate this concept. To reduce internal power loss, the active junctions need to be connected with a low resistance but transparent structure.

[†] On leave from Optoelectronic & Microwave Devices Laboratory, Mitsubishi Electric Corporation, Japan.
[‡] Alexandria University, Department of Mathematics and Engineering Physics, Egypt.

Difficulties in obtaining appropriate tunnel junctions to interconnect the cascade structure have hampered the development of multijunction concentrator cells in this system. Metal interconnects have been used for GaAs-based multijunction tandem cells to overcome this problem.[2] However, metal grooves and contact grid lines on the surface usually reduce the effective area. The peak current density (J_p) of the tunnel junction should be greater than the short-circuit current density (J_{sc}) of the tandem solar cells (about 20 mA/cm^2 at 1 sun).

In this study we present a new approach to achieve a heterostructure tunnel diode in the AlGaAs/GaAs material system with performance suitable for high solar concentrations. AlGaAs was chosen for the p-type material rather than GaAs to avoid the high optical absorption of p-type GaAs. Also, the AlGaAs layer may act as a barrier to diffusion of optically generated electrons from underlying p-GaAs layer. Additionally, carbon concentrations in AlGaAs are substantially higher than in GaAs grown under the same conditions. This can be attributed to the stronger Al-C bond that leads to an enhanced incorporation of carbon into the film. GaAs was used for n-type side to avoid the problem of providing heavily-doped n-type AlGaAs.[3] Carbon was also chosen for the p^+-doping due to two reasons: First, Carbon has been reported to have a very low diffusion coefficient and relatively small ionization energy making it attractive for the heavily doped p^+-layer of the interconnecting junction in the multijunction structure where a highly controlled and thermally stable doping profile is required.[4,5] Second, the organometallic precursors present in the growth ambient are the sources of carbon. High levels of background carbon concentrations can be achieved without the need of any other dopant source such as CCl_4.[6-8] On the other hand, Si was selected for the n^+-doping because of its low vapor pressure and low diffusion coefficient to preserve abrupt doping profile.

RESULTS AND DISCUSSIONS

The reactor used in this study is based on the rotating susceptor concept. the deposition chamber is subdivided into six equally spaced compartments using quartz separators. A plan view schematic of the growth chamber is shown in Figure 1. The separators height above the substrate (H_p) can be finely controlled for improved confinement of reactant gases and boundary layer shearing.[9] The chamber as modified is capable of using up to two gas inlets for each reactant gas. ALE growth was conducted upon adjusting H_p to 1 mm and rotating the substrate, which results in an exposure to column III reactants, then flushing by H_2, followed by an exposure to column V reactants and flushing by H_2 at a system

pressure of 30 torr. MOCVD growth was also conducted without H_2 flow in the four purge injectors with $H_p = 10mm$, and a susceptor rotational rate of 300 rpm to promote gas phase mixing of the reactants at a system pressure of 60 torr.

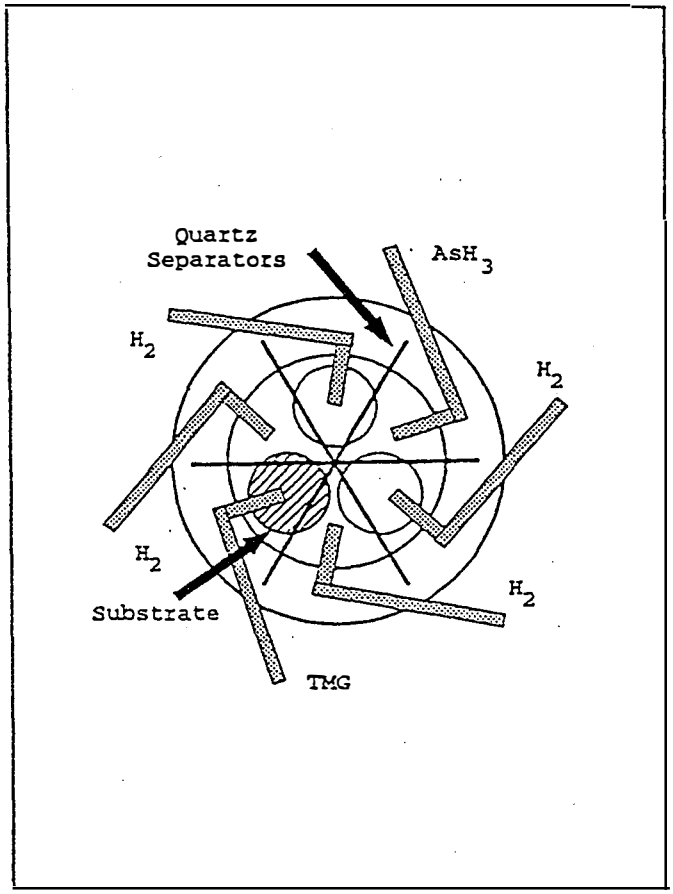

Figure 1. Plan View Schematic of the Growth Chamber.

ALE growth was chosen rather than MOCVD for epitaxial growth of this heavily doped heterostructure for two reasons:

(i) In general, carbon incorporation efficiency and electrically-active carbon concentrations are significantly higher in ALE grown films compared to MOCVD. As indicated in Figure 2, for the same V/III ratio, the background carbon incorporation in the ALE $Al_{0.3}Ga_{0.7}As$ grown films is about two orders of magnitude higher compared to MOCVD grown films. This is due to gas phase mixing in MOCVD growth mechanism which allows reactions between AsH_3 and (TMG or TMA) to form CH_4. This results in a reduction of the concentration of methyl groups available for decomposition and incorporation as carbon into the growing film.

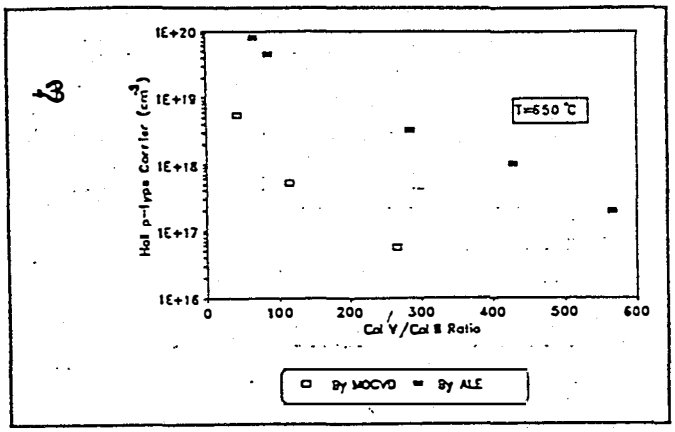

Figure 2. Background Carbon Doping of ALE and MOCVD Grown $Al_{0.3}Ga_{0.7}As$ as a Function of V/III Ratio.

Also shown in Fig.2, $Al_{0.3}Ga_{0.7}As$ with background carrier concentrations of 8×10^{19} cm^{-3} were achieved using ALE growth mode upon rotating the substrate at 60 rpm, corresponding to 167 ms exposure to either column III and column V reactants with growth rate of 1 μm/hr and V/III ratio of 66.

(ii) Consistently with other observations, where increasing the Si concentration beyond ~ 5×10^{18} cm^{-3} does not typically result in any further increase in the free carrier concentration in MOCVD GaAs grown films[10], Figure 3 shows that the electron concentration in MOCVD Si-doped GaAs grown films reaches a maximum value of 5×10^{18} cm^{-3}. However, ALE of GaAs with electron carrier concentrations as high as 7×10^{18} cm^{-3} were achieved using V/III ratio of 470, exposure times of 2.2 sec, 1.1 sec to TMG and AsH_3 respectively, and a growth rate of 0.15 μm/hr. It is believed that this is due to ALE growth mechanism that provides complete surface coverage which results in a more ideal surface for planar doping.

The tunnel diode structure was grown on n-type GaAs substrate at 650°C. It consisted of 300 Å n^+-GaAs layer ($n = 7 \times 10^{18}$ cm^{-3}), 300 Å p^+-$Al_{0.3}Ga_{0.7}As$ layer ($p = 8 \times 10^{19}$ cm^{-3}) and 0.7 μm p^+-GaAs contacting layer ($p = 5 \times 10^{18}$ cm^{-3}). For electrical evaluation purposes, a 0.1 μm AuGe/300 Å Ni/0.2 μm Au were deposited on the back side of the n-GaAs substrate and 0.2 μm Au was deposited on the p-GaAs top layer using photolithography techniques. Mesas with an area of 200×200 μm^2 were etched using (5 H_2O :2 H_3PO_4 :1 H_2O_2 by volume).

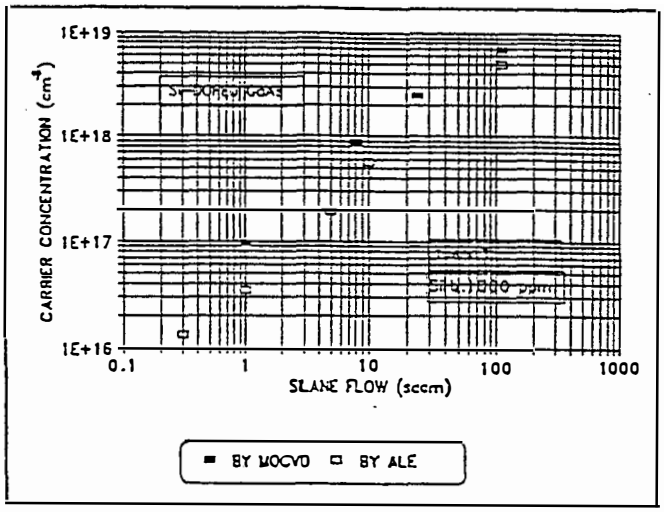

Figure 3. Hall n-Type Doping of GaAs Films Grown by ALE and MOCVD Modes of Growth.

Figure 4 shows the current- voltage (I-V) characteristics of the as-grown tunnel diodes at room temperature for three different growth conditions. Diode (A) was grown using the two growth conditions illustrated in Fig.2 and Fig.3 which give heavy doping levels. During the growth of the n^+-GaAs layer in diode (B), the exposure time of AsH_3 was increased to 2.2 sec while keeping the same V/III ratio as in diode (A) case. Diode (C) was also grown using the same growth conditions as in diode (A) case except that during the deposition of the heavily doped heterojunction interfaces, the substrate was kept under AsH_3 flux for 15 sec to establish steady state conditions and to resume abrupt interfaces.

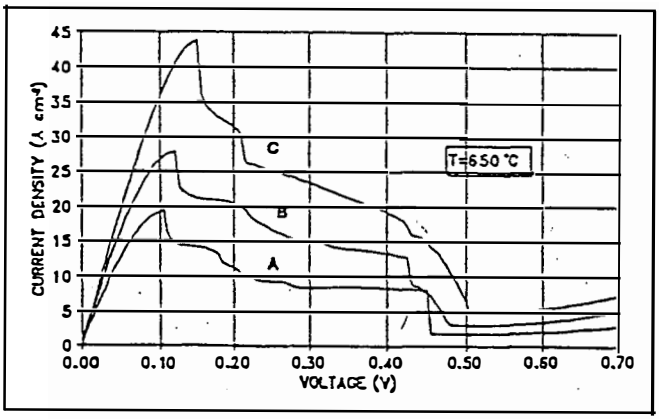

Figure 4. Typical I-V Characterisitics of n-GaAs/p-$Al_{0.3}Ga_{0.7}As$ Tunnel Junctions Grown at Different Growth Conditions.

High peak-to-valley ratio (J_p/J_v) of 10 were realized in all junctions, showing the dominance of interband tunneling, which indicates that band-gap blocking was effective in suppressing inelastic as well as elastic tunneling

process. This well defined negative resistance (NR) of the diodes makes them useful in digital applications. The main features of the fabricated tunnel junctions are summarized in Table (1).

Table (1): Main features of "as-grown" tunnel diodes.

Diode #	J_p/J_v	J_p (A/Cm^2)	V_p (V)	ϱ (Ω.Cm^2)
A	10	20.3	0.11	3.2×10^{-3}
B	10	27.8	0.12	2.6×10^{-3}
C	10	43.8	0.15	2.2×10^{-3}

From Table (1), we conclude that the diode characteristics are sensitive to the growth conditions since the peak current density (J_p) of the tunnel junction (C) is significantly higher, and the specific resistivity (ϱ) is correspondingly smaller compared to junction (A) without any decrease in the well-marked negative differential region. The high peak current density (44 A/cm^2) and the low series resistance (2.2×10^{-3} Ωcm^2) of diode (C) make it a good interconnector for the high and low band-gap cells in the AlGaAs/GaAs cascade structure operating at high solar concentrations. At 1000 suns operation, there will be only 44 mV voltage drop across the tunnel junction. This voltage drop is the upper limit since no corrections for the probe, metal contact, and substrate resistance are considered.

The above tunnel junction was used to connect GaAs bottom cell with $Al_{0.3}Ga_{0.7}As$ top cell, to form two junctions cascade solar cell structure. Figure 5 shows the I-V characteristics at 1 sun, and 53 suns. These results indicate that, up to 53 suns, the P^+-$Al_{0.3}Ga_{0.7}As/n^+$-GaAs tunnel junction does not seem to result in any appreciable deterioration in the solar cell performance.

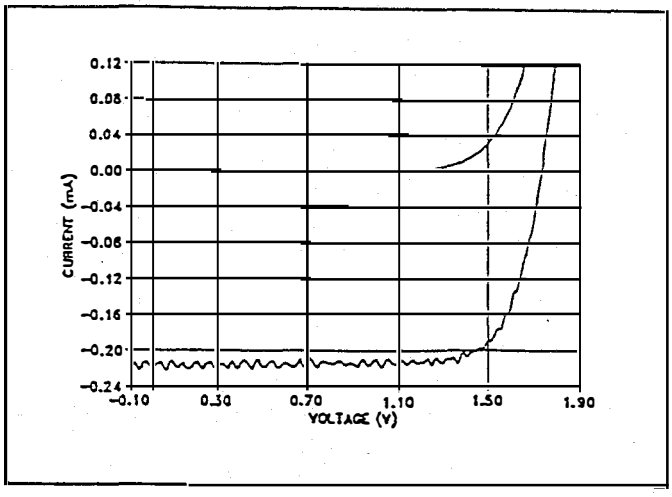

Figure 5(a). I-V Characteristics of $Al_{0.3}Ga_{0.7}As$/GaAs Multijunction Solar Cell Using p^+-$Al_{0.3}Ga_{0.7}As/n^+$-GaAs Connecting Tunnel Junction at 1 Sun.

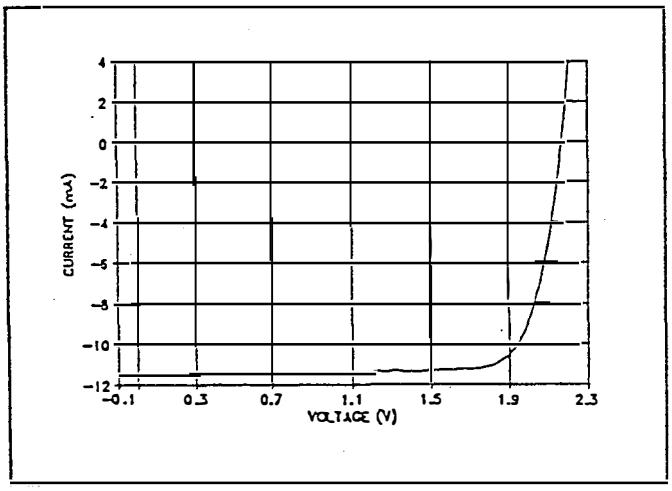

Figure 5(b). I-V Characteristics of $Al_{0.3}Ga_{0.7}As/GaAs$ Multijunction Solar Cell Using p^+-$Al_{0.3}Ga_{0.7}As/n^+$-GaAs Connecting Tunnel Junction at 53 Suns.

CONCLUSION

ALE with its low growth temperature, excellent thickness control, and capability to provide abrupt junctions at high doping levels, was used to grow a p^+-$Al_{0.3}Ga_{0.7}As/n^+$-GaAs heterojunction tunnel diode suitable as intercell ohmic contact for the AlGaAs/GaAs multijunction solar cell concentrator. C and Si have been chosen as the p- and n-type dopants , respectively to achieve abrupt and thermally stable doping profiles for the heterojunction interfaces. ALE is also suitable candidate for low temperature growth of the top cell to prevent further degradation of the tunnel junction during the growth of the whole cascade structure.

ACKNOWLEDGEMENT

This work is supported by NREL and NSF.

REFERENCES

1. R.L. Moon, L.W. Janes, H.A. VanderPlas, Y.G. Chai, and G.A. Antypas, Thirteenth IEEE Photovoltaic Special Conference, Washington, D.C. (IEEE, New York,1978), p.859.
2. B.-C. Chung, G.F. Virshup, and J.G. Werthen, *Appl. Phys. Lett.* **52**, 1889 (1988).
3. P.M. Mooney, *J. Appl. Phys.* **67**, R1 (1990).

4. T.F. Kuech, M.A. Tischler, P.J. Wang, G. Scilla, R. Potemski, and F. Cardone, *Appl. Phys. Lett.* **53**, 1317 (1988).
5. C.R. Abernathy, S.J. Pearton, R. Caruso, F. Ren, and J. Kovalchik, *Appl. Phys. Lett.* **55**, 1750 (1989).
6. J.R. Gong, D. Jung, N.A. El-Masry, and S.M. Bedair, *Appl. Phys. Lett.* **57**, 400 (1990).
7. K.G. Reid, H.M. Urdianyk, and S.M. Bedair, *Appl. Phys. Lett.* **59**, 2397 (1991).
8. B .C. Chung, R.T. Green, and H.F. Machmillan, *J. Cryst. Growth* **107**, 89 (1991).
9. A. Dip, G. Eldallal, P. Colter, N. Hayafuji, and S.M. Bedair, *Appl. Phys. Lett.* **62**, 2378 (1993).
10. T.N. Theis, P.M. Mooney, and S.L. Wright, *Phys. Rev. Lett.* **60**, 361 (1988).

SECTION(4)
Effect Of Strain And Heavy Doping On $Ga_xIn_{1-x}P/Ga_{.51}In_{.49}P$ Band Structure For BSF And Window Layer Applications

4.1 Strain effect:

The effect of strain on material parameters (energy gap, conduction and valence bands,...) was studied using two models, Van de Walle's [1] model and Hrivnak's [2] model. The materials used in this study are GaInP and GaAsP, since these materials are used in our experimental work either as BSF regions or as window layers. Since there is a lack of measured data about strained GaInP and GaAsP, we applied these strain models on the strained GaInAs material, which has some experimental published data. A comparison between Van de Walle's model and Hrivnak's model was carried out to check the models and to test our calculation process. The two models were found to be comparable but not exactly matched specially at high strain values .

4.1.1 GaInAs/GaAs:

Figure (4-1) shows the calculated $Ga_xIn_{1-x}As$ unstrained and strained with respect to GaAs, energy gaps versus composition x using Van de Walle's model "V" and Hrivnak's model "H". The strained values of the two models are comparable for the range $Ga_{.5}In_{.5}As$ to GaAs. However, for Ga % less than 50, where there are high values of lattice mismatch between the $Ga_xIn_{1-x}As$ and the GaAs substrate, there is a big difference between the two models. It seems that Van de Walle's model is more acceptable in this range because it suggests that the change of InAs energy gap due to strain is around 0.121 eV, while the Hrivnak's model gives a change of 0.36 eV. That means the energy gap was almost doubled. A comparison between our calculated data using the two models, and some published data was carried out. We found that data for the strained $Ga_xIn_{1-x}As$ alloy over GaAs are usually given for the low mismatch range, $x \geq 0.8$. In this range both models are comparable. We summarized in table 4-I our calculated ΔE_{g1} and ΔE_{g2} with some published measured values. Where, $\Delta E_{g1} = E_{gs}(Ga_xIn_{1-x}As) - E_g(Ga_xIn_{1-x}As)$ and $\Delta E_{g2} = |E_{gs}(Ga_xIn_{1-x}As) - E_g(GaAs)|$. Where, E_{gs} and E_g are the strained and the unstrained energy gaps.

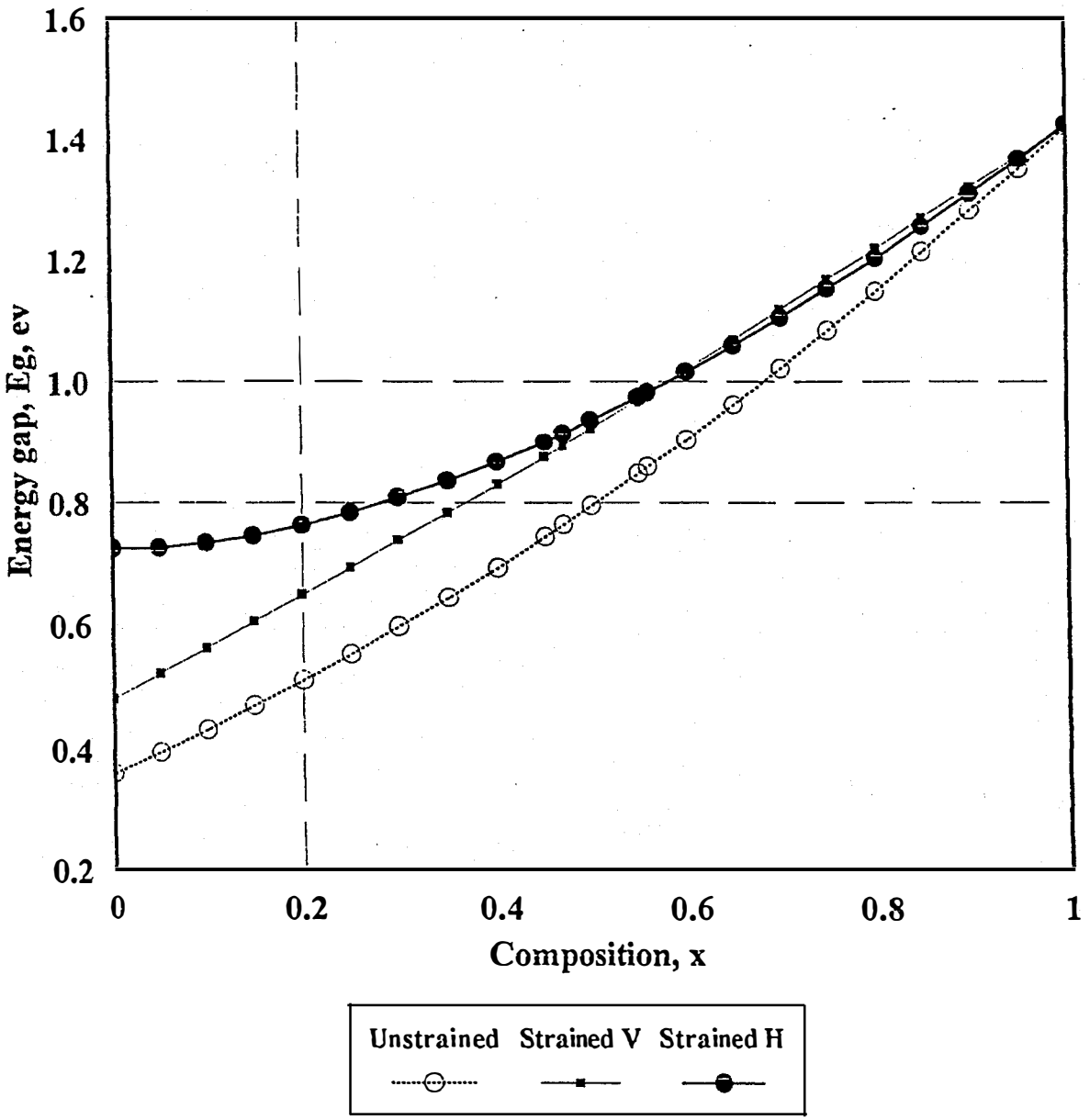

Fig. 4-1 The unstrained, and the strained $Ga_xIn_{1-x}As$ band gaps versus composition x. "V", Van De Walle's model and "H", Hrivnak's model.

Table 4-I: A comparison between our calculations and some published measured data for the increase in the $Ga_xIn_{1-x}As$ energy gap due to strain ΔE_{g1}, and the bandgap misfit between strained $Ga_xIn_{1-x}As$ and GaAs ΔE_{g2}.

Model or reference	x	ΔE_{g1} eV	ΔE_{g2} eV
Current calculations "V"	0.8	0.0703	0.2025
Current calculations "H"	0.8	0.0789	0.2207
Marie [3]	0.8		0.21
Current calculations "V"	0.85	0.05539	0.1521
Current calculations "H"	0.85	0.05997	0.1686
Niki [4]	0.85	0.06	0.162
Current calculations "V"	0.9	0.0389	0.101
Current calculations "H"	0.9	0.0405	0.114
Niki [4]	0.9	0.0446	0.11

It seems from the last figure and table that both models are acceptable to be applied for the practical range of mismatch. However, for InAs (x = 0), where the mismatch is maximum for this material, the two models give completely different values and to the best of our knowledge, no experimental values are found.

4.1.2 $Ga_xIn_{1-x}P$/GaAs

Since $Ga_xIn_{1-x}P$ grown over GaAs substrate is the main material in our experimental work, the study of this material is in details.

Figure (4-2) shows the variation of the unstrained $Ga_xIn_{1-x}P$ bandgap with composition x, for the direct Γ and indirect X and L energy gaps. Clearly, the material is a direct gap material for $x \leq 0.65$ and tends to be indirect X for x greater than that. In our experimental study, we used $Ga_xIn_{1-x}P$ mainly with $x \leq 0.65$. Therefore, we limit our investigations of the effect of strain to the direct energy gap materials.

Figure (4-3) shows the dependence of the unstrained lattice constant, a, the strained lattice constant parallel to the interface, a_p, and the strained lattice constant normal to the interface, a_n, on the gallium composition x. This figure shows how the unstrained lattice constant decreases with gallium composition x. The a_p is tied to the GaAs lattice constant (= 5.653 Å). That means that, the GaInP is under bi-axial compression strain for $x < 0.51$, and under bi-axial tensile strain for $x > 0.51$. The point (x = 0.51), where the three lattice constants (a, a_p, a_n) are equal, is the GaAs lattice constant (the lattice matching point).

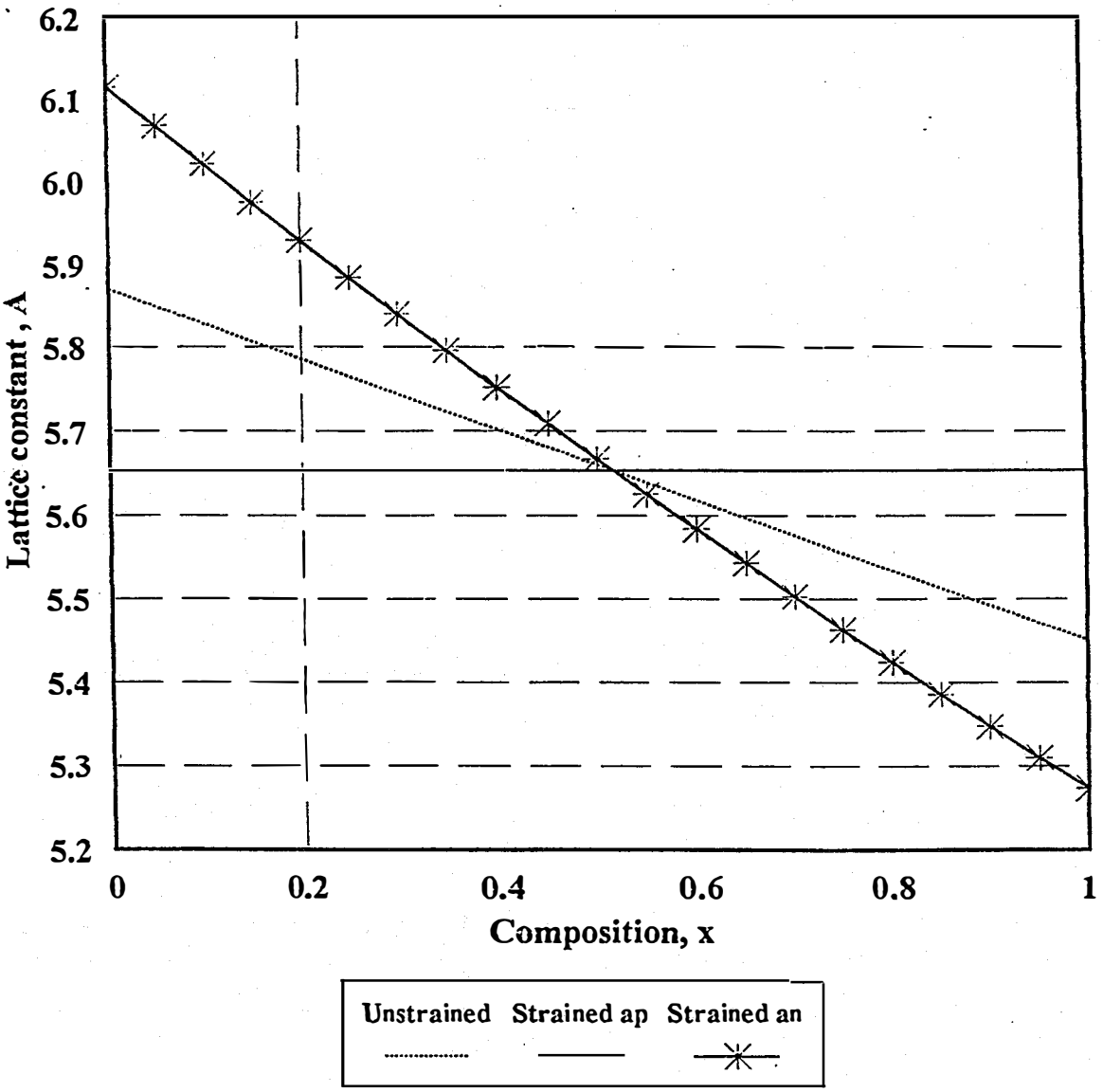

Fig. 4-2 The unstrained $Ga_xIn_{1-x}P$ direct Γ and indirect X and L band gaps versus composition x.

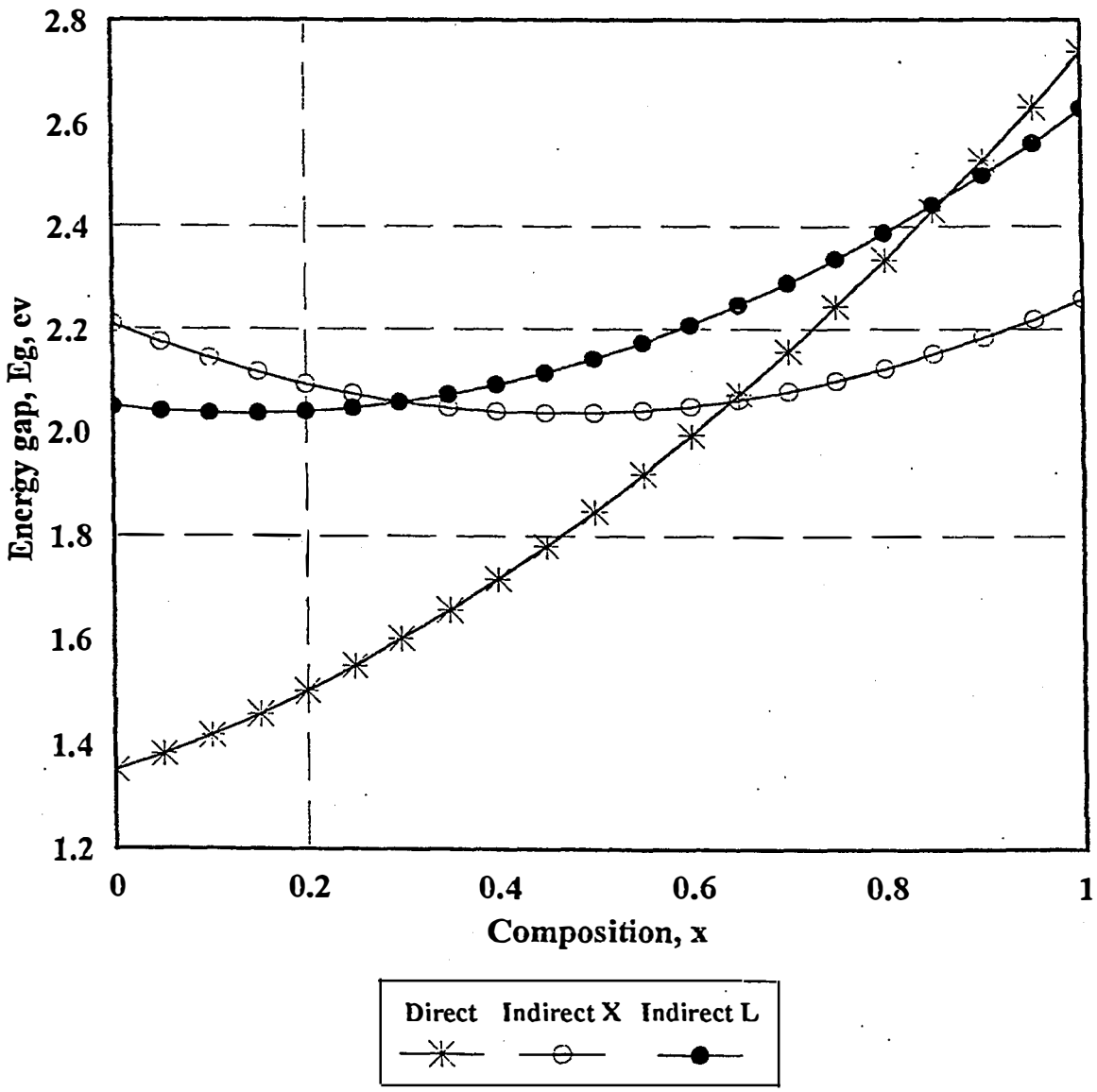

Fig. 4-3 The unstrained $Ga_xIn_{1-x}P$ lattice constant, a, the strained parallel lattice constants, a_p, and strained normal lattice constant an versus composition x.

Figure (4-4) shows the variations (shifts) in the valence bands due to strain effect, versus the composition x. These shifts are namely, the hydrostatic shift in the average electrostatic potential, $\Delta E_{v,av}$(hy), the shear shifts in the heavy hole, ΔE_{hh}(sh), light hole, ΔE_{lh} (sh), and spin-orbit, ΔE_{so}(sh), valence bands. Clearly, at x = 0.51, all the variations are zeros except that for the spin-orbit splitting. As mismatch increases (that is an increase in the strain either tensile or compression), the change in spin-orbit band increases in magnitude (shifts down). Figure (4-5) shows the effect of these shifts on the valence bands. The unstrained values of the valence bands were represented in addition to the strained ones. It is clear from both figures that, for $x < 0.51$, where, bi-axial compression strain takes place, the material is heavy-hole type, while for the range $x > 0.51$, it is a light hole type. That means that bi-axial compression strain shifts the heavy hole band up while the bi-axial tensile strain shifts the light hole.

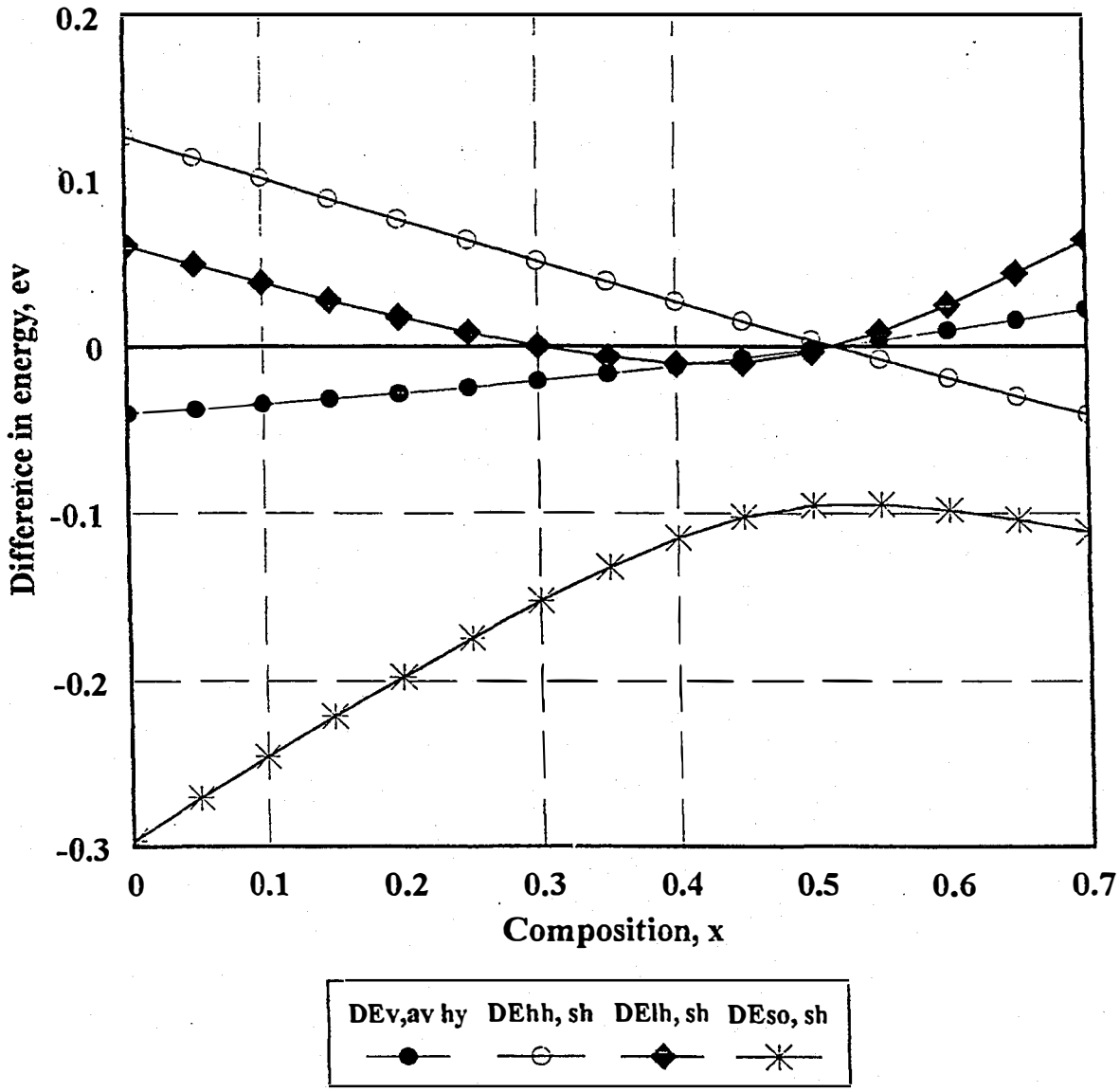

Fig. 4-4 The shifts (variations) in the $Ga_xIn_{1-x}P$ valence bands due to hydrostatic and shear strains versus composition x.

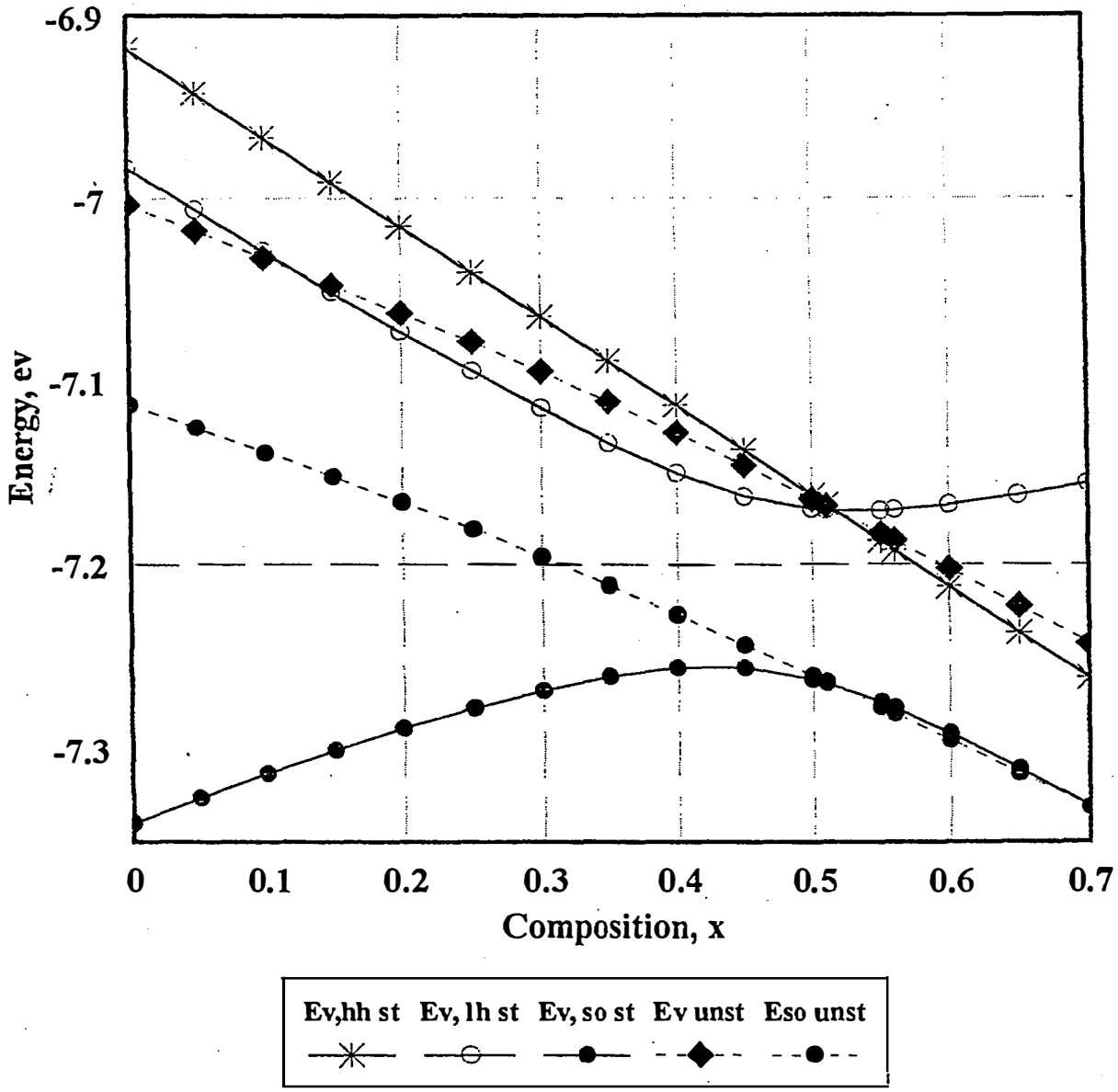

Fig. 4-5 The unstrained and strained $Ga_xIn_{1-x}P$ valence bands versus composition x.

Figure (4-6) shows the variation of the unstrained energy gap, E_g, the strained energy gap, E_{gs} with composition x, calculated using the two models, Van de Walle "V" and Hrivnak, "H". It is clear that the energy gap under compression strain ($x \leq 0.51$) increases from the unstrained value, whereas it decreases from the unstrained value when it is under tensile strain ($x \geq 0.51$). Although there is a big difference between the strained energy gap calculated using the two models in the range $x < 0.51$, there is almost matching in the other range $x \geq 0.51$ between the two models. However, Hrivnak's model is very sensitive to the effective masses values. Since there is a wide variety in the effective masses values reported in different literature, Van de Walle is more suitable to be used. A comparison between some of our calculations with published experimental results, was done which is summarized latter in table 4-II. From figure (4-6) we can recognize that the energy

gap under bi-axial tensile strain decreases considerably. Therefore, the energy gap of the strained $Ga_{.56}In_{.44}P$ which is used as a BSF region in our experimental work, was decreased from the unstrained 1.93 eV value to 1.897 eV.

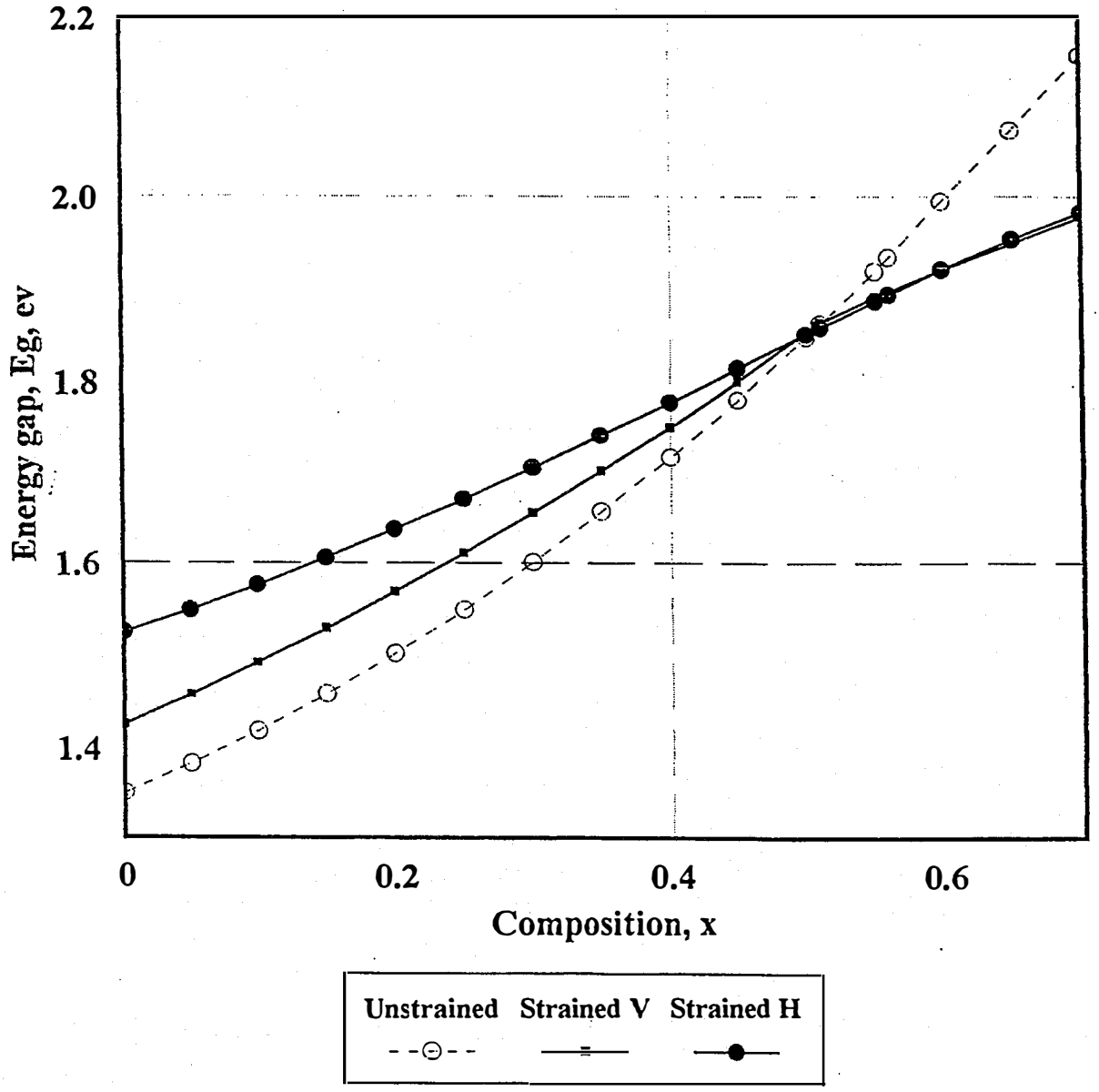

Fig. 4-6 The unstrained and strained $Ga_xIn_{1-x}P$ band gaps versus composition x. "V" is Van De Walle's model and "H" is Hrivnak's model.

This means that the difference in the energy gap between this BSF region and the $Ga_{.51}In_{.49}P$ base region is just 0.0355 eV, which is much lower than expected from the unstrained value for heterojunction BSF. This may be a reason for the low improvement in the experimental measurements of the cells parameters under BSF compared to the "No BSF" case.

Figure (4-7) shows the variation of the conduction band edge, E_c, and the three valence band edges (heavy hole E_{vhh}, light hole E_{vlh} and spin orbit split E_{vso}), with composition x for strained $Ga_xIn_{1-x}P$. The absolute values of the energy levels, have no meaning except they are measured. It is clear from figure (4-7) that for values of $x > 0.51$ the material is a light-hole like material. The light hole valence band which is the upper most valence band in the $x > 0.51$ region is almost flat in this range. Therefore, there is no heterojunction discontinuity in the valence band between $Ga_xIn_{1-x}P$ and $Ga_{.51}In_{.49}P$ in the range $x > 0.51$. Consequently, for a $Ga_{.56}In_{.44}P$, n-type, low doped, BSF, there is no BSF barrier at the base-BSF interface for the minority-carrier holes in the valence band.

Thus, our calculations point out that the strain tends to wipe out any beneficial BSF minority carrier confinement effects that may be expected on the basis of unstrained band offsets. In our experimental grown cells, although this BSF region is heavily doped, which suppose to create an acceptable (even homojunction) barrier to the minority holes in the base region, the doping is very high with respect to the $Ga_{.56}In_{.44}P$ such that it leads to other effects (band gap narrowing and even degeneracy) which will be explained latter. Figure (4-8) shows the variations of the band-offsets:

$\Delta E_g = E_{gs}(Ga_xIn_{1-x}P) - E_g(Ga_{.51}In_{.49}P)$, the conduction band discontinuity;

$\Delta E_c = E_c(Ga_xIn_{1-x}P) - E_c(Ga_{.51}In_{.49}P)$, and the valence band discontinuity;

$\Delta E_v = E_v(Ga_xIn_{1-x}P) - E_v(Ga_{.51}In_{.49}P)$, with composition x using Van de Walle's model.

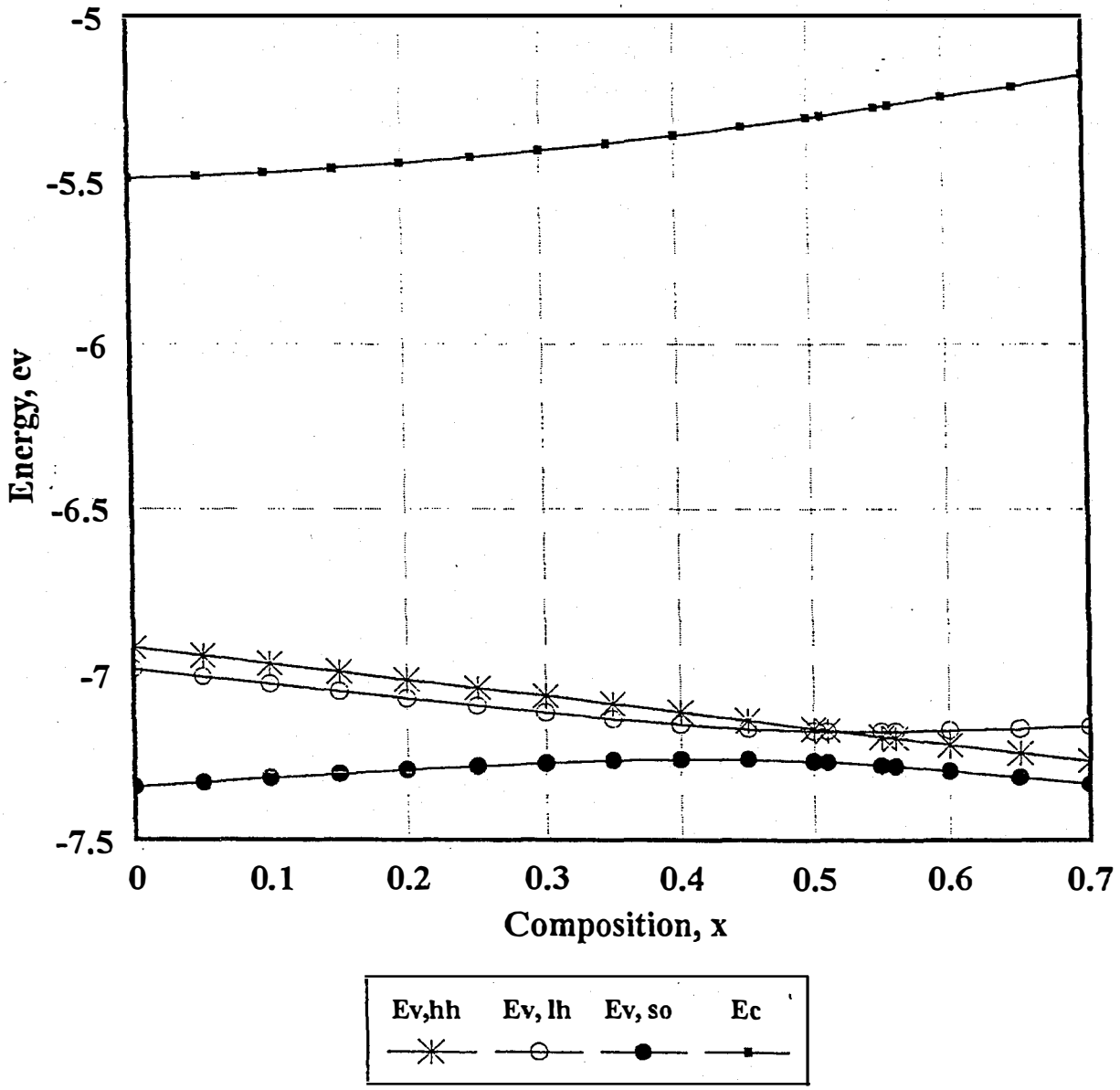

Fig. 4-7 The $Ga_xIn_{1-x}P$ strained conduction and valence band levels versus composition x.

We can get some conclusions from this figure (4-8). For the range $x < 0.51$, ΔE_v is positive and ΔE_c is negative that means we have a type I heterojunction interface. In this region also ΔE_g is negative that means that we can not use the strained $Ga_xIn_{1-x}P$ of this region as a BSF region. This is because the BSF layer must have energy gap greater or equal to the cell's bandgap. In addition to that, since ΔE_c is negative in this range, no barrier exists (instead a sink) for the minority electrons in the conduction band for the $n/p/p^+$ cells.

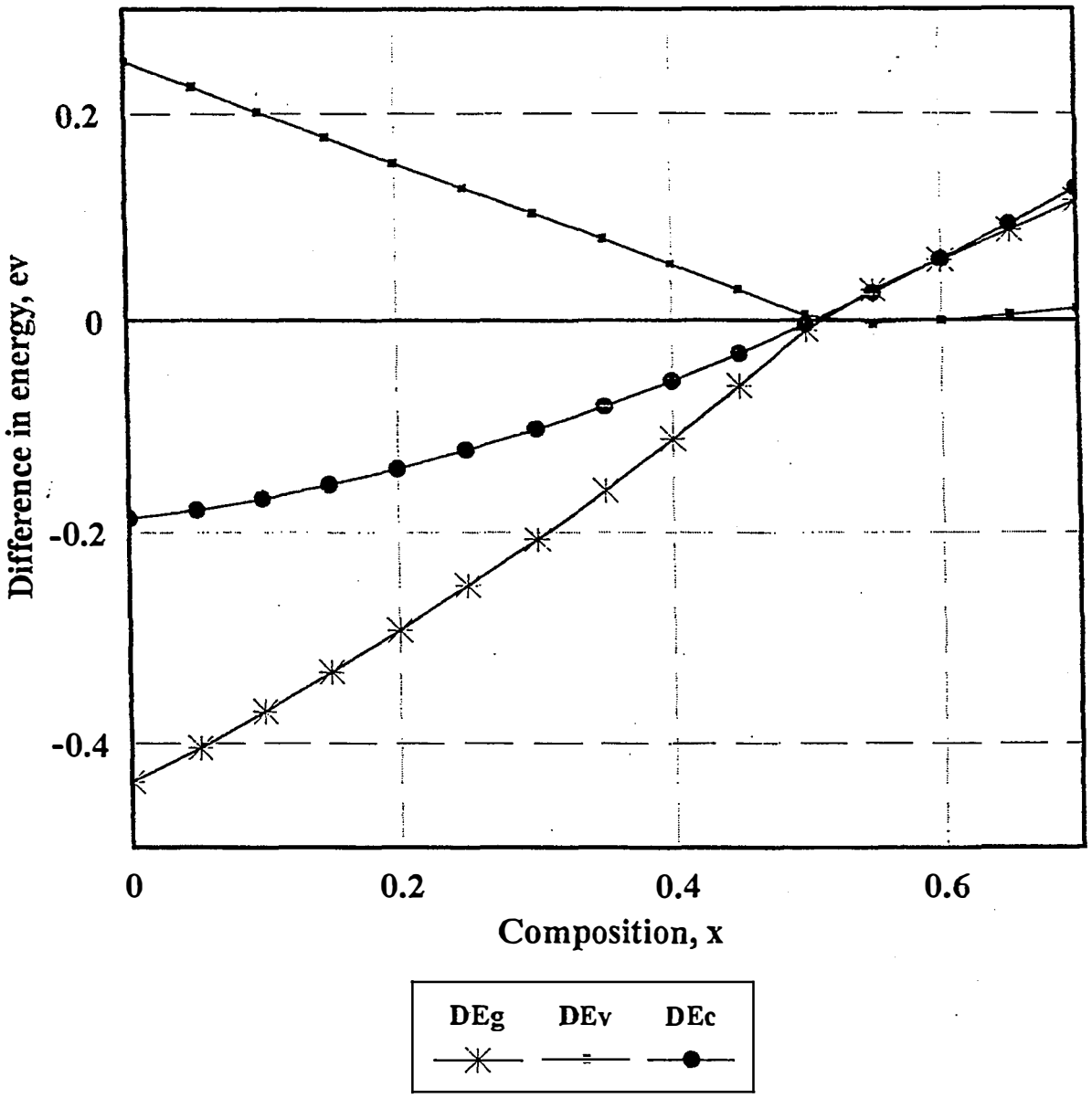

Fig. 4-8 The band offsets, ΔE_g, ΔE_c, and ΔE_v, between $Ga_xIn_{1-x}P$ and $Ga_{.51}In_{.49}P$ versus composition x.

For the other range, where $x > 0.51$, we can use the strained $Ga_xIn_{1-x}P$ as a BSF where ΔE_g and ΔE_c are positives. In this region the ΔE_v is almost zero, where it was seen in the previous figure, which means that the variation in composition x leads directly to a variation in the conduction band with no significant variation in the valence band. This result shows that for a compositional graded strained layer in this range, the graded field lies completely in the conduction band. As a result of that we can assume that the conduction band varies with composition linearly while the valence band can be considered flat through the graded region.

Figure (4-9) shows the same parameters as those shown in figure (4-8) except the band-offsets are between the strained $Ga_xIn_{1-x}P$ and the GaAs, where, $\Delta E_g = E_{gs}(Ga_xIn_{1-x}P) - E_g(GaAs)$, the conduction band discontinuity, $\Delta E_c = E_c(Ga_xIn_{1-x}P) - E_c(GaAs)$, and the valence band discontinuity, $\Delta E_v = E_v(Ga_xIn_{1-x}P) - E_v(GaAs)$. The energy levels at the heterojunction interface give a type II heterojunction for $x < 0.35$ and a type I heterojunction for $x > 0.35$. The calculations of the energy levels at the $Ga_xIn_{1-x}P/GaAs$ interface, are useful for the comparison between our theoretical calculations and the published experimental results.

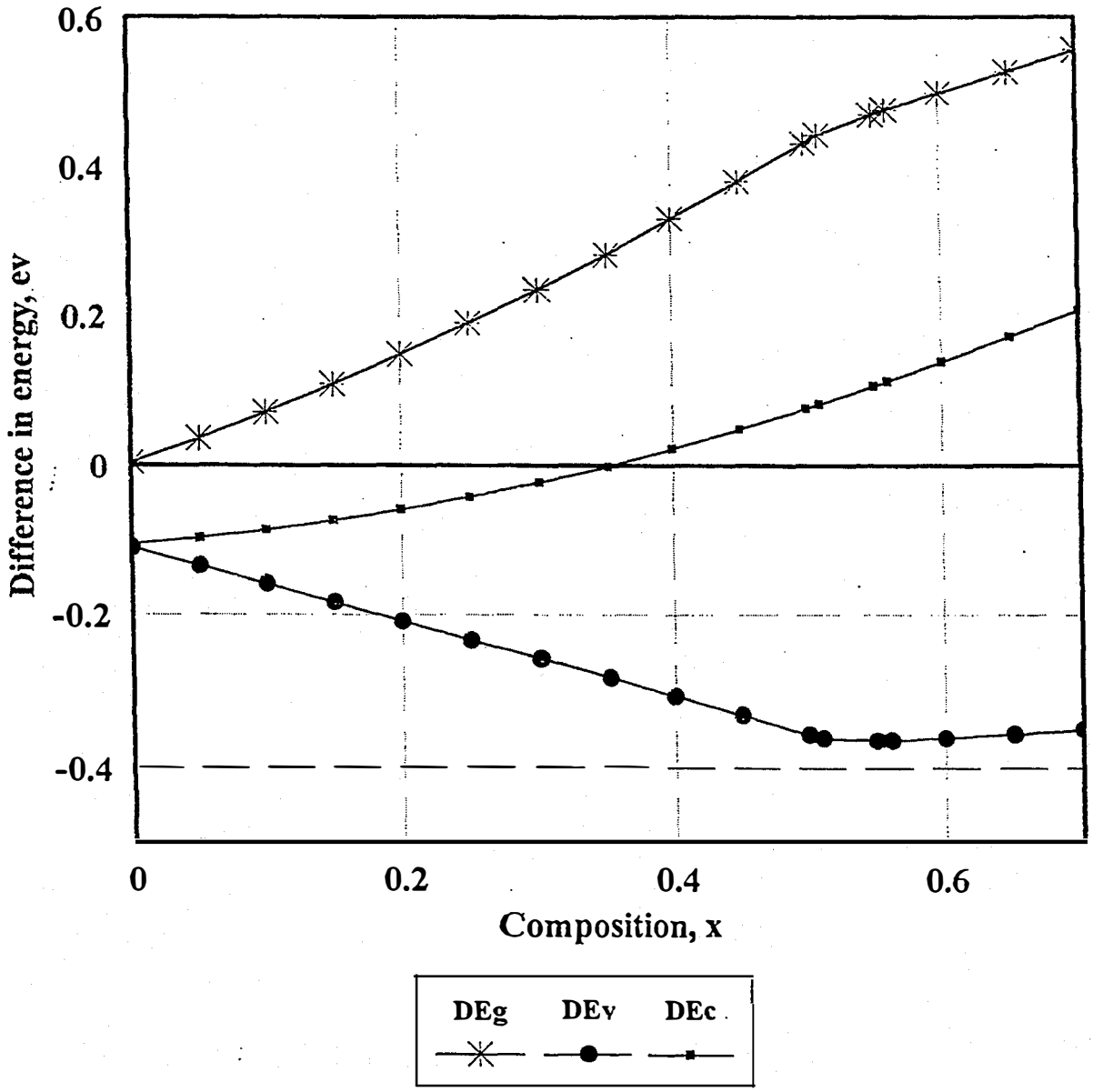

Fig. 4-9 The band offsets, ΔE_g, ΔE_c, and ΔE_v, between $Ga_xIn_{1-x}P$ and GaAs versus composition x.

Since, to our knowledge, the band offsets between strained $Ga_xIn_{1-x}P$ and GaAs have not been accurately determined yet, we made comparisons between our band offsets at the unstrained $Ga_{.51}In_{.49}P$/GaAs interface with other published experimental results. These values differ from one reference to another. Hasse [5] has values that are comparable to our unstrained offsets. Kobayashi [6] has experimental offset results of strained $Ga_xIn_{1-x}P$ grown over GaAs. These values are comparable to ours for the strained offsets. Table 4-II contains these experimental offset values between the $Ga_xIn_{1-x}P$ and the GaAs.

Table II: Experimental published band offsets between $Ga_xIn_{1-x}P$ and GaAs and our calculated ones.

Reference	x	$\|\Delta E_c\|$ eV	$\|\Delta E_v\|$ eV	ΔE_g eV
Current calculations "V"	0.51	0.083	0.361	.446
Kobayashi[6]	0.51	0.03		0.428
Rao[7]	0.51	10.22	0.24	0.428
Hasse [5]	0.51	0.108	0.353	0.461
Biswase [8]	0.51	0.198	0.285	0.483
Tiwari [9]	0.51	0.223	0.24	0.463
Lee [10]	0.51	0.21		
Bhattachayara [11]	0.51	0.2	0.28	0.48
Feng [12]	0.51	0.24-0.25		
Kobayashi [13]	0.51	0.14	0.45	
Current calculations "V"	0.56			0.477
Kobayashi [6]	0.56			≈0.47

4.2 Effect of heavy doping on the band structure:

Heavy doping can also have an important effect on the band offsets of heterojunctions. For GaAs material, the effective density of states in the conduction band, N_C $4.7x10^{17}$ cm^{-3} and in the valence band,, N_V $7x10^{18}$ cm^{-3}. These low values (compared to Si) mean that with just 10^{18} cm^{-3} doping concentration, the p-type GaAs is heavily doped and the n-type GaAs is degenerate. Most III-V semiconductors have N_C and N_V in the same order of magnitude as those of GaAs.

In our experimental work, we use doping values up to $3x10^{18}$ cm^{-3}. We studied the effect of heavy doping on the band offsets and the band levels of the strained GaInP. We calculated the effective density of states [14] from the electron and hole effective masses.

The band gap narrowing is calculated using the most common expression for p or n doped material:

$$BGN = AN^{1/3} \quad (4\text{-}1)$$

Where, BGN is the energy gap narrowing in eV, N is the doping concentration in cm^{-3} and A is a constant. The A values for the $Ga_xIn_{1-x}P$ were taken from Jain [15]. However, Jain suggested more terms to be added to equation (4-1). We used the common expression (4-1) following the approach of several published works.

Hannon [16], chung [17], and Jain [15] suggested expression for the effect of degeneracy on the band gap narrowing which leads to an apparent band gap narrowing, BGN*, given by,

$$BGN^* = BGN + KT \ln [F_{1/2} (E_f/KT)] - E_f \qquad (4\text{-}2)$$

where, $F_{1/2}$ is the Fermi-Dirac integral, and E_f is the Fermi level position with respect to the majority band edge in eV.

Band gap narrowing leads to shifts in both the conduction band and the valence band positions. Jain [15] suggested that the shifts of the two bands (conduction and valence) divided by their effective masses are equal, in the limit of high $>10^{18}$ cm^{-3} carrier concentrations. He assumes that the heavy and light hole bands move together into the gap due to heavy doping.

4.2.1 Effect of band structure calculations on the performance of BSF in the GaInP cells:

Figure (4-10) shows the band levels of the $Ga_{.51}In_{.49}P/Ga_{.56}In_{.44}P/GaAs$ structure. This is a typical structure of the (base/back surface field region (BSF)/substrate) of our grown solar cells. Figure (4-10a) shows the three regions as each region was grown alone. In this figure the $Ga_{.56}In_{.44}P$ layer is unstrained. The $Ga_{.56}In_{.44}P$ region looks as a good choice as a BSF to our cells from the discontinuity values between it and the base. The band gap discontinuity between the BSF and the base is about 73 meV divided between 53.5 meV in the conduction band and 18.7 meV in the valence band. This makes the structure a good one to be used in solar cells. However, the effect of strain that has to take place due to the difference in lattice constants, deteriorates these barriers that can be seen in figure (4-10b). The energy gap offset between $Ga_{.56}In_{.44}P$ and $Ga_{.51}In_{.49}P$ was reduced to 36 meV and lies mostly in the conduction band - 33.4 meV, as we seen before in fig. (4-8). From this structure we can predict that this may work as a BSF with a barrier for electrons in n/p/p+ structure but not for holes in p/n/n+ structure (not better than an isotype homojunction BSF $Ga_{.51}In_{.49}P$). The effect of heavy doping on the band gaps has to be taken into consideration. For an n-type $Ga_{.56}In_{.44}P$ doped with $2x10^{18}$ cm^{-3}, an additional narrowing to the energy gap takes place due to this heavy doping as seen in figure (4-10c). This leads to a conversion of the barrier in the valence band interface to a sink. This result shows that the existence of the heterojunction BSF is worse than a normal homojunction BSF. However, this heavy doping value, leads to a shift in the Fermi level inside the conduction band and the material becomes degenerate. This leads to an apparent widening in the band gap that opposes the shrinkage due to heavy doping effect alone. This widening can cancel this shrinkage. Our results indicate that the net result become widening rather than shrinkage which is seen in figure (4-10d). In this figure the sink in the valence band was changed to a barrier again and this figure is looking exactly as figure (4-10b) even with slightly higher barrier. The p-type $Ga_{.56}In_{.44}P$ material with $2x10^{18}$ cm^{-3} doping, does not reach the degeneracy limit (the Fermi level still in the band gap over the valence band), and only shrinking in the band gap is the only result of heavy doping as seen in figure (4-10e) and (4-10f). We have a sink in the valence band interface and a reasonable barrier in the conduction band interface. This can work as a good structure for p-type BSF.

In our experimental measurement for the GaInP cells with strained $Ga_{.56}In_{.44}P$ BSF, we found that the effect of strained $Ga_{.56}In_{.44}P$ BSF on the cell parameters is not as expected from a heterojunction BSF. Figure (4-10d) may explain this behavior. At the valence band interface between the base and the BSF, a slight, negligible barrier to minority holes in a $p/n/n^+$ structure exists. This negligible barrier is not enough to enhance the short circuit current of such a cell. However, at the conduction band interface, there is a reasonable barrier to the electron majority carriers in a $p/n/n^+$ which is not the case for homojunction BSF or no BSF case. This barrier for majority carriers in a $p/n/n^+$ structure may lead to a reduction in the majority carriers losses at that interface. This leads to a reasonable increase in the dark current which with no reasonable enhancement in the

short circuit current leads directly to a reduction in the open circuit voltage. These theoretical results agree with our measured ones from our cells. For an n/p/p^+ structure, the barrier in the conduction band has to enhance the short circuit current over the no BSF case. In this case, there is no barrier for the majority carriers that let us expect an enhancement in the open circuit voltage and of course in the fill factor. Our experimental results do not show these enhancements over the No BSF case.

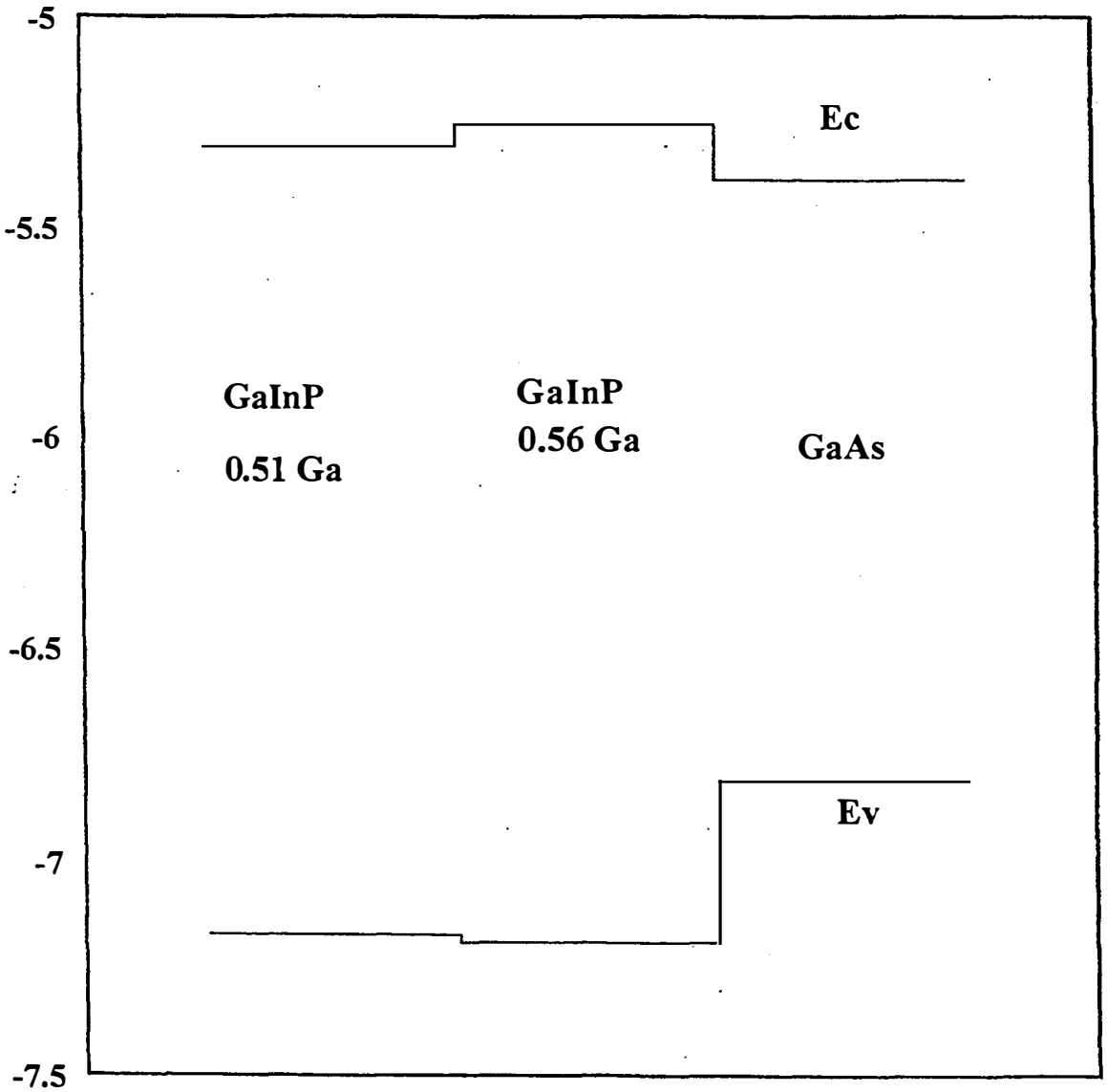

Fig. 4-10a The band levels and the interface discontinuities between GaAs, $Ga_{.56}In_{.44}P$, and $Ga_{.51}In_{.49}P$ materials. No strain or doping effects.

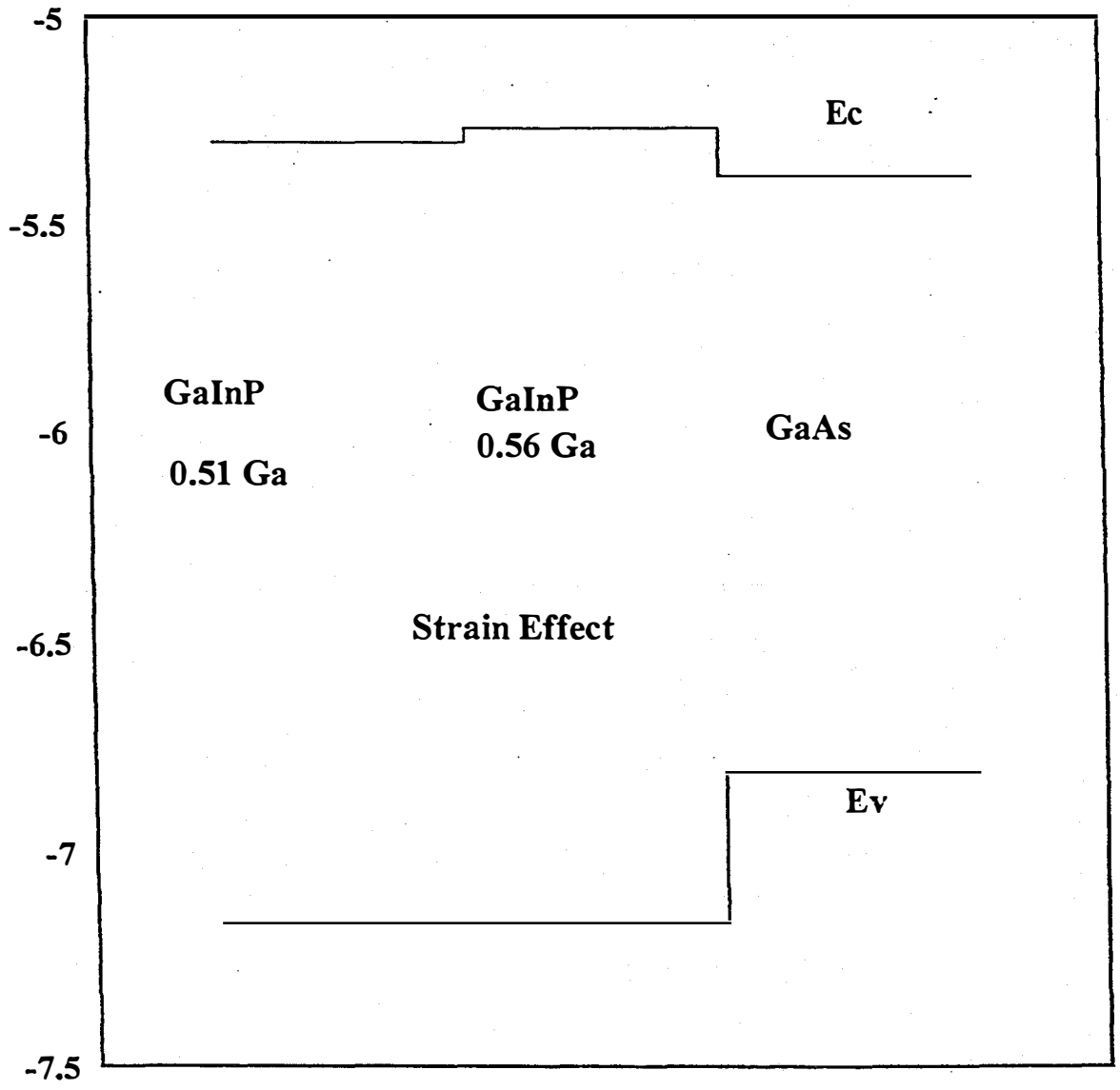

Fig. 4-10b The band levels and the interface discontinuities between GaAs, $Ga_{.56}In_{.44}P$, and $Ga_{.51}In_{.49}P$ materials. Strain effect is included.

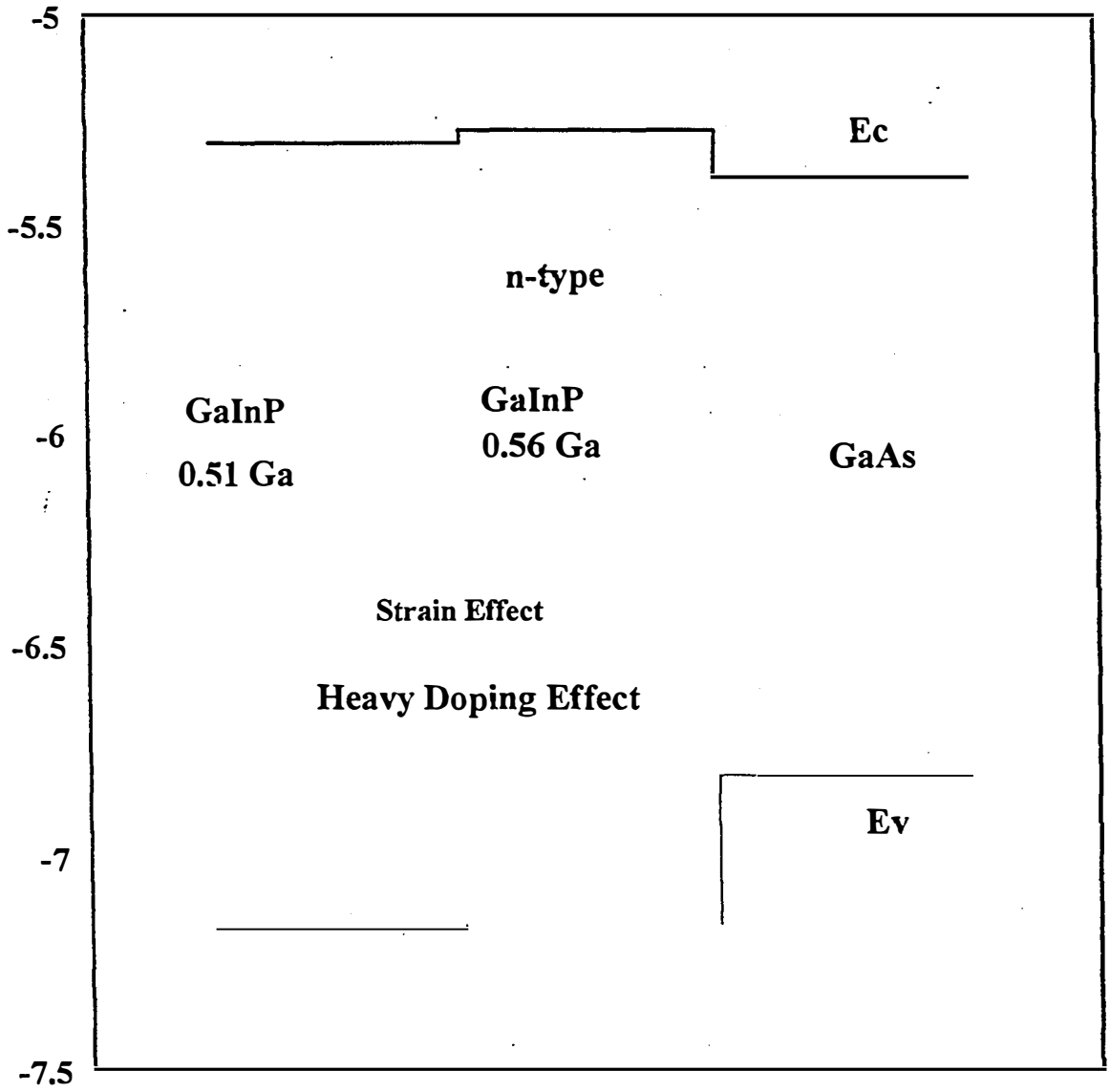

Fig. 4-10c The band levels and the interface discontinuities between GaAs, $Ga_{.56}In_{.44}P$, and $Ga_{.51}In_{.49}P$ materials. Strain effect and heavy doping effect are included (n-type material).

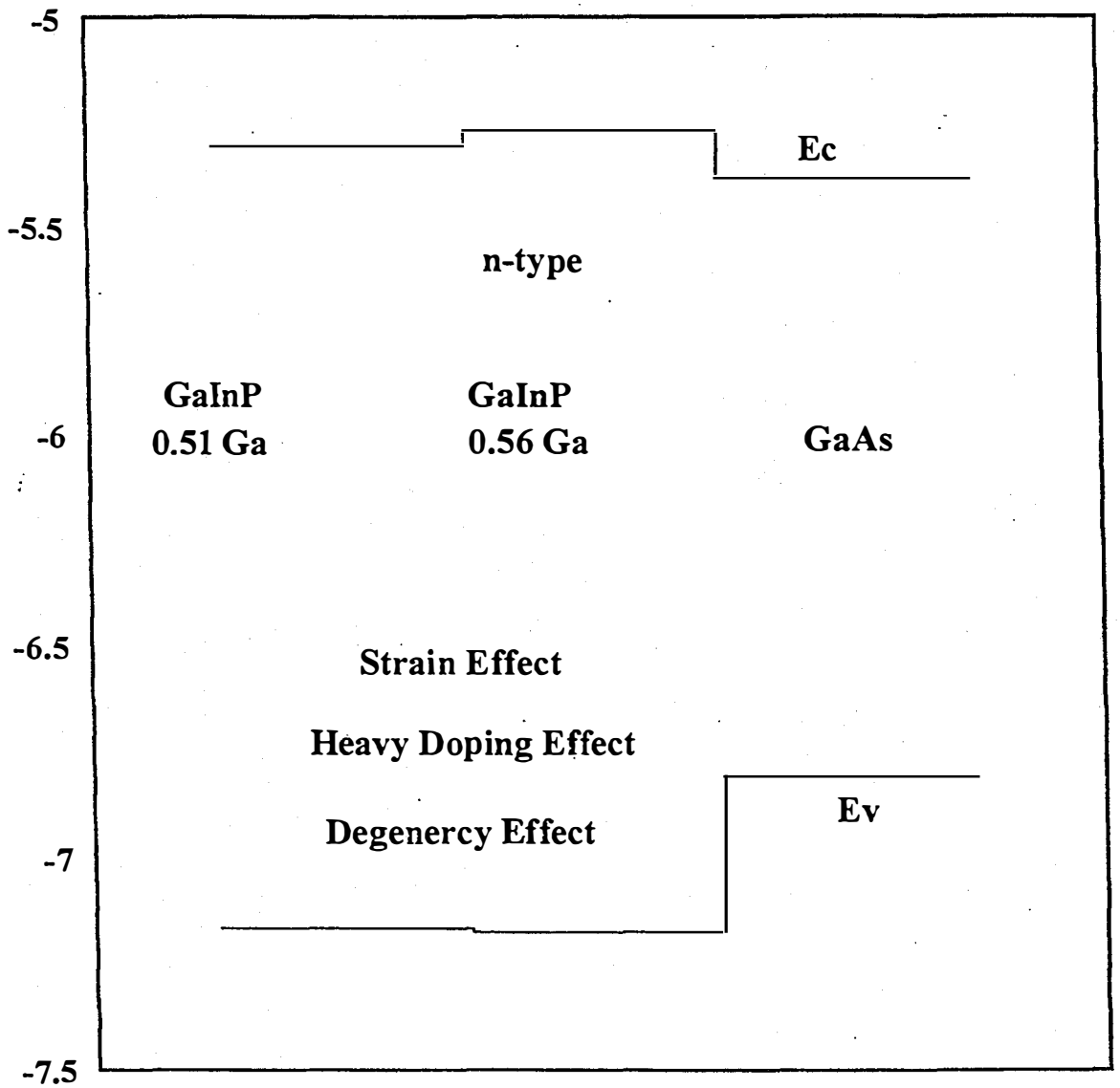

Fig. 4-10d The band levels and the interface discontinuities between GaAs, $Ga_{.56}In_{.44}P$, and $Ga_{.51}In_{.49}P$ materials. Strain effect, heavy doping effect, and degeneracy effect are included (n-type material).

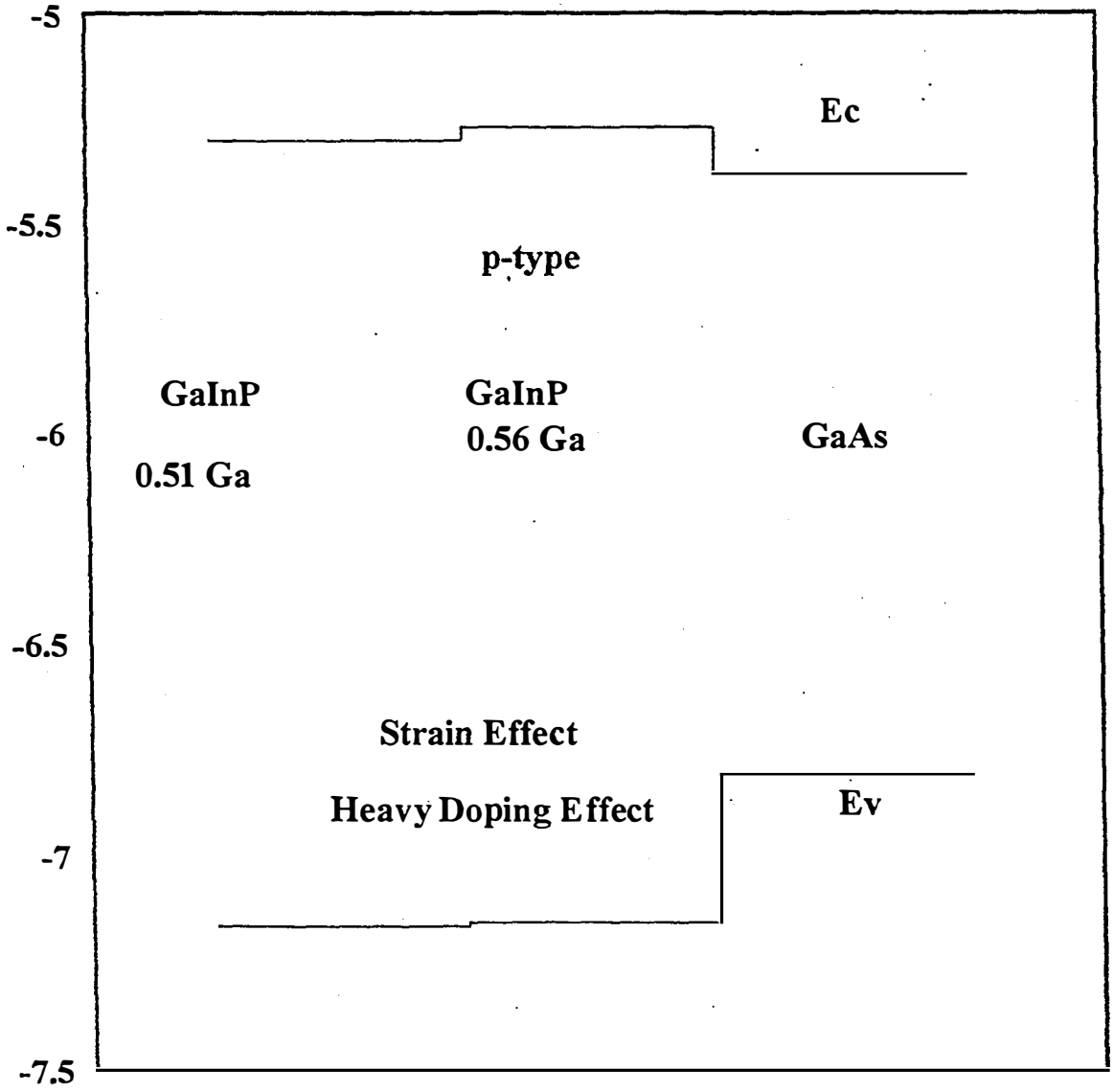

Fig. 4-10e The band levels and the interface discontinuities between GaAs, $Ga_{.56}In_{.44}P$, and $Ga_{.51}In_{.49}P$ materials. Strain effect, and heavy doping effect are included (p-type material).

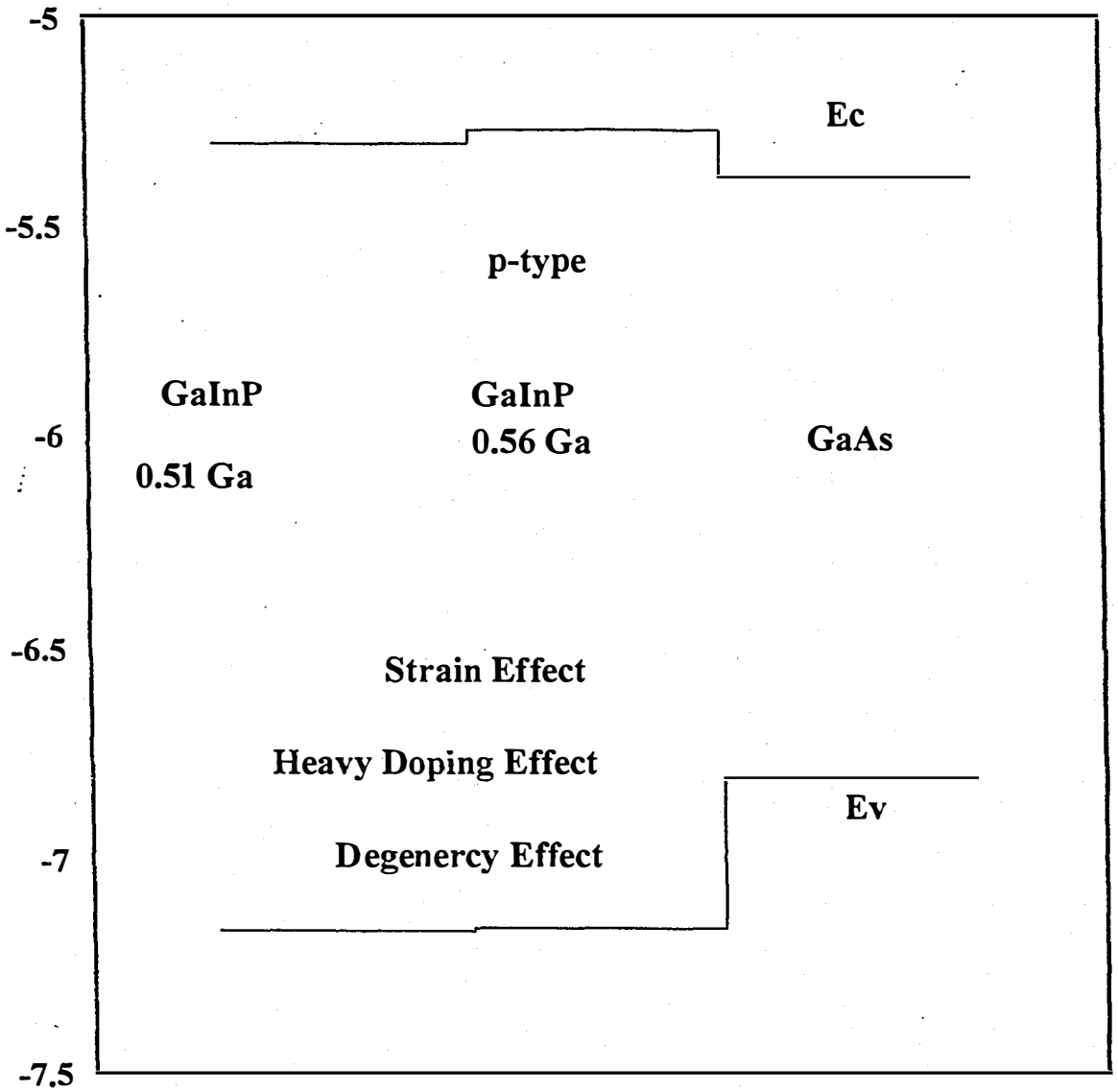

Fig. 4-10f The band levels and the interface discontinuities between GaAs, $Ga_{.56}In_{.44}P$, and $Ga_{.51}In_{.49}P$ materials. Strain effect, heavy doping effect, and degeneracy effect are included (p-type material).

Strained $Ga_{.63}In_{.37}P$ material which is used as a BSF region in our solar cells and/or with slightly increase in the Ga composition $Ga_{.65}In_{.35}P$ this material is used as a window layer for solar cells too. Figure (4-11) summarizes the effect of strain alone then heavy doping and strain on the band levels of this $Ga_{.65}In_{.35}P$ material. Although there is a high discontinuity between the unstrained $Ga_{.65}In_{.35}P$ material and the $Ga_{.51}In_{.49}P$ material, the effect of the strong strain on this $Ga_{.65}In_{.35}P$ material is severe, due to the high mismatch as seen in figure (4-11). Figure (4-11d) shows the effect of strain and heavy doping on n-type $Ga_{.63}In_{.37}P$. It is clear from

this figure that the valence band barrier has almost disappeared. This strained layer if used as BSF layer for $p/n/n^+$ gives a worse values than that of a lower strained BSF. This is the case in our experimental results where the short circuit current, the fill factor and the open circuit voltage were deteriorated. Due to the high mismatch, the probability of misfit dislocation creation increases which may lead to deterioration in the cell parameters. For the p-type $Ga_{.65}In_{.35}P$ as seen in figure (4-11e), even with strain and heavy doping effects, a good barrier for minority electrons in p-type region still exists at the interface. This makes this material a well material as a BSF for the $n/p/p^+$ structure. However, special care has to be taken in the growth of this strained material to avoid the misfit dislocation creation. This material with just slight increase in the Ga composition and care in fabrication, can work as a window layer for p/n $Ga_{.51}In_{.49}P$ solar cells.

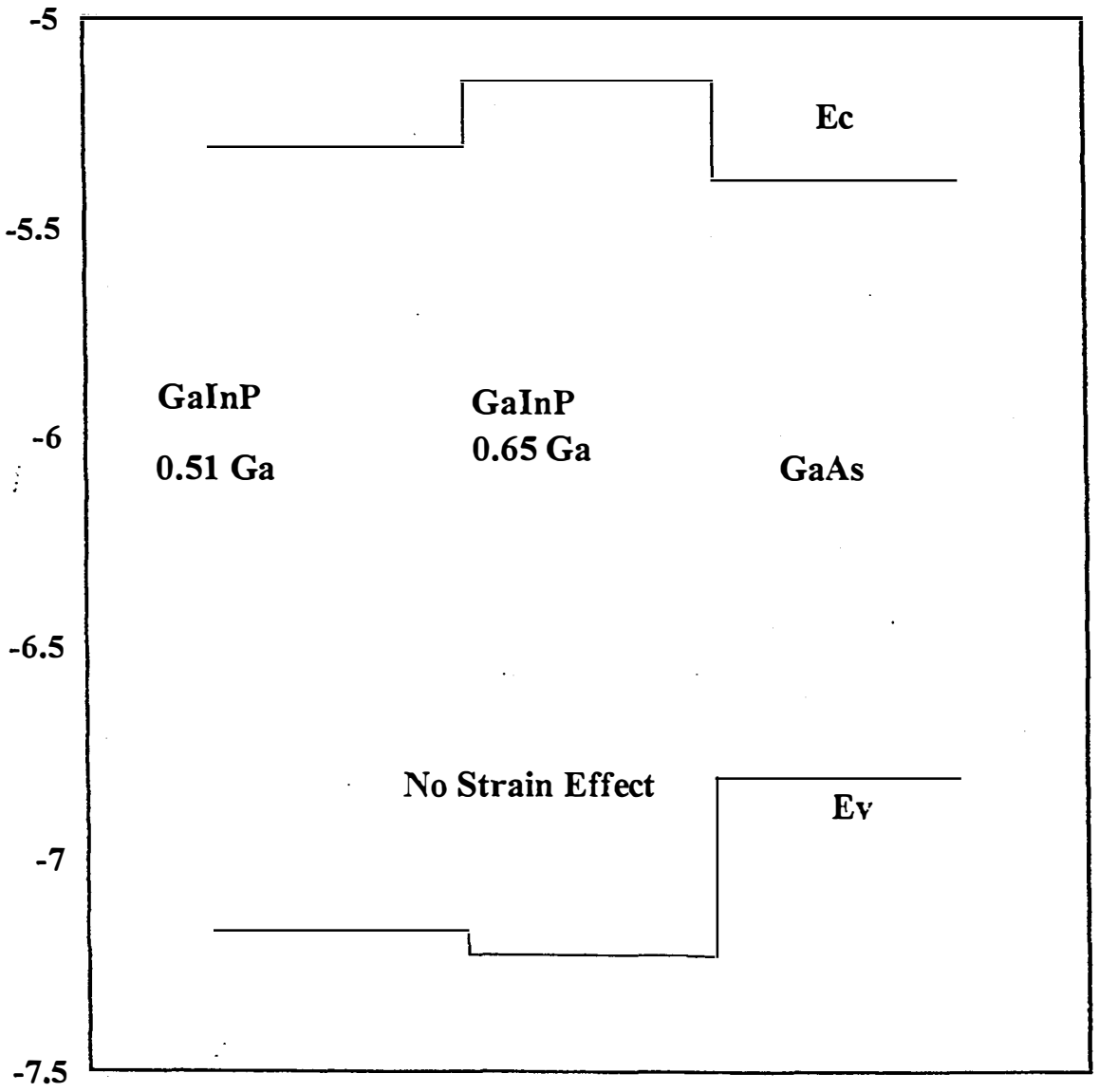

Fig. 4-11a The band levels and the interface discontinuities between GaAs, $Ga_{.65}In_{.35}P$ and $Ga_{.51}In_{.49}P$ materials. No strain or doping effects.

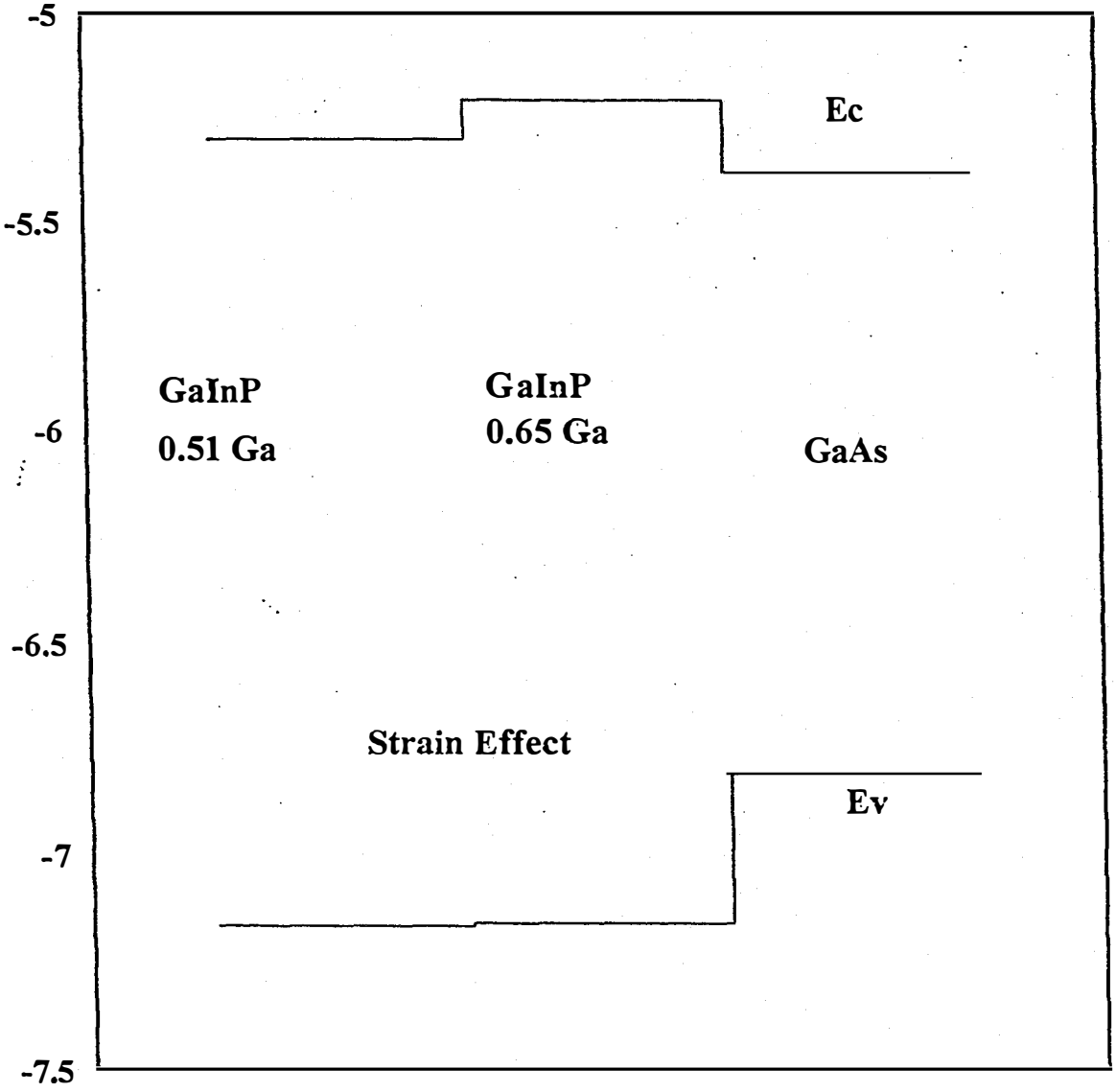

Fig. 4-11b The band levels and the interface discontinuities between GaAs, $Ga_{.65}In_{.35}P$, and $Ga_{.51}In_{.49}P$ materials. Strain effect is included.

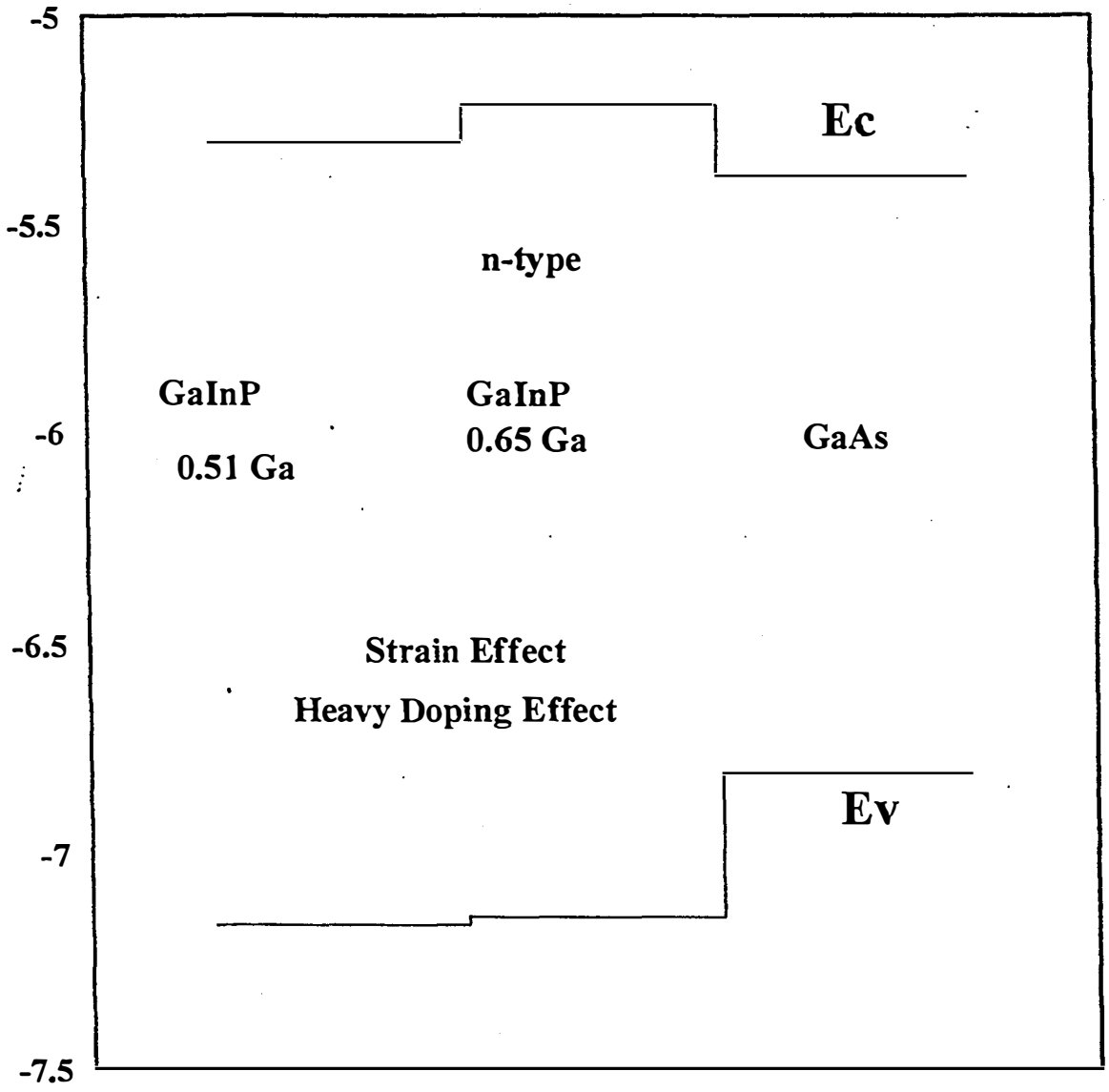

Fig. 4-11c The band levels and the interface discontinuities between GaAs, $Ga_{.65}In_{.35}P$, and $Ga_{.51}In_{.49}P$ materials. Strain effect and heavy doping effect are included (n-type material).

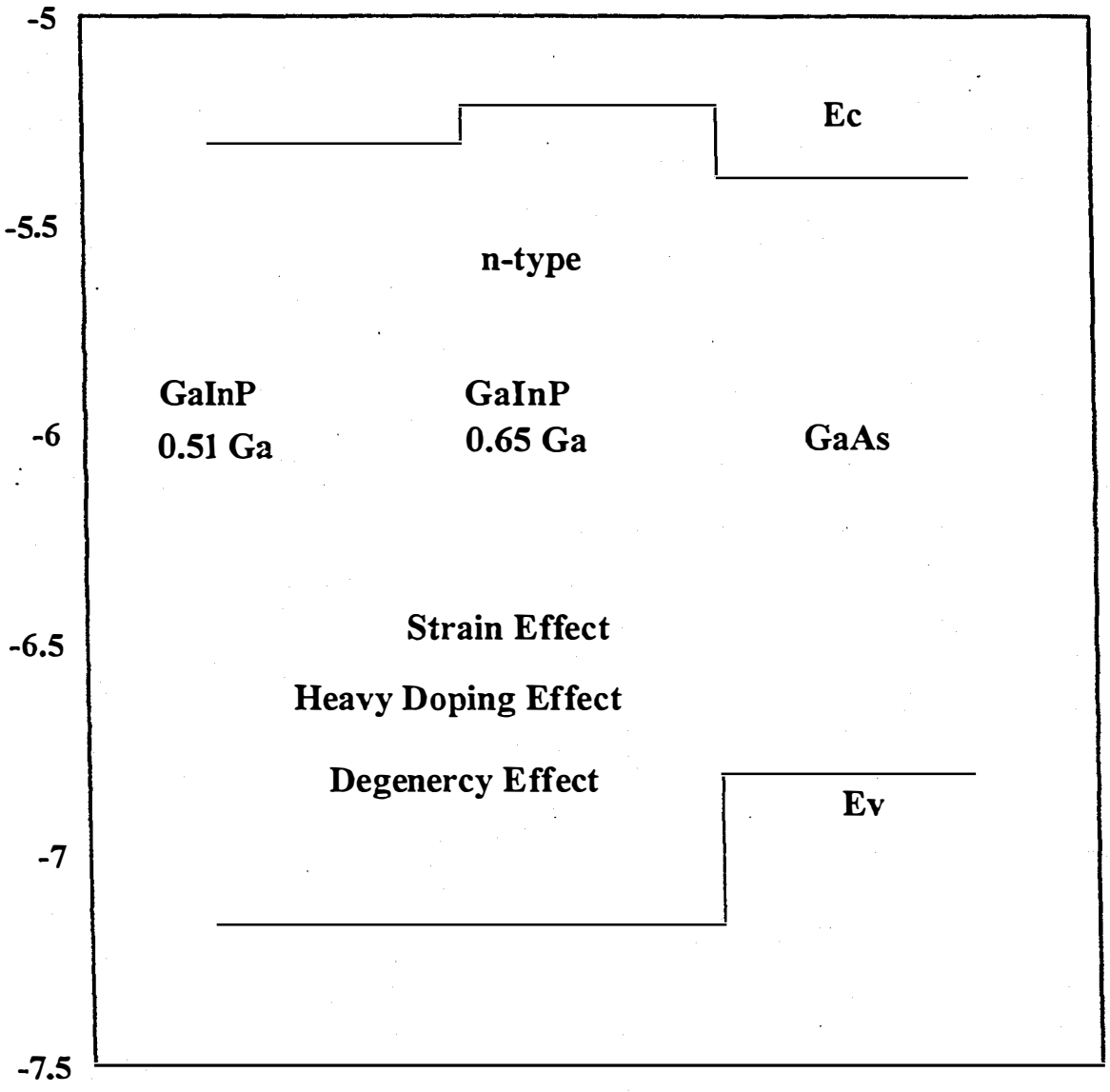

Fig. 4-11d The band levels and the interface discontinuities between GaAs, $Ga_{.65}In_{.35}P$, and $Ga_{.51}In_{.49}P$ materials. Strain effect, heavy doping effect, and degeneracy effects are included (n-type material).

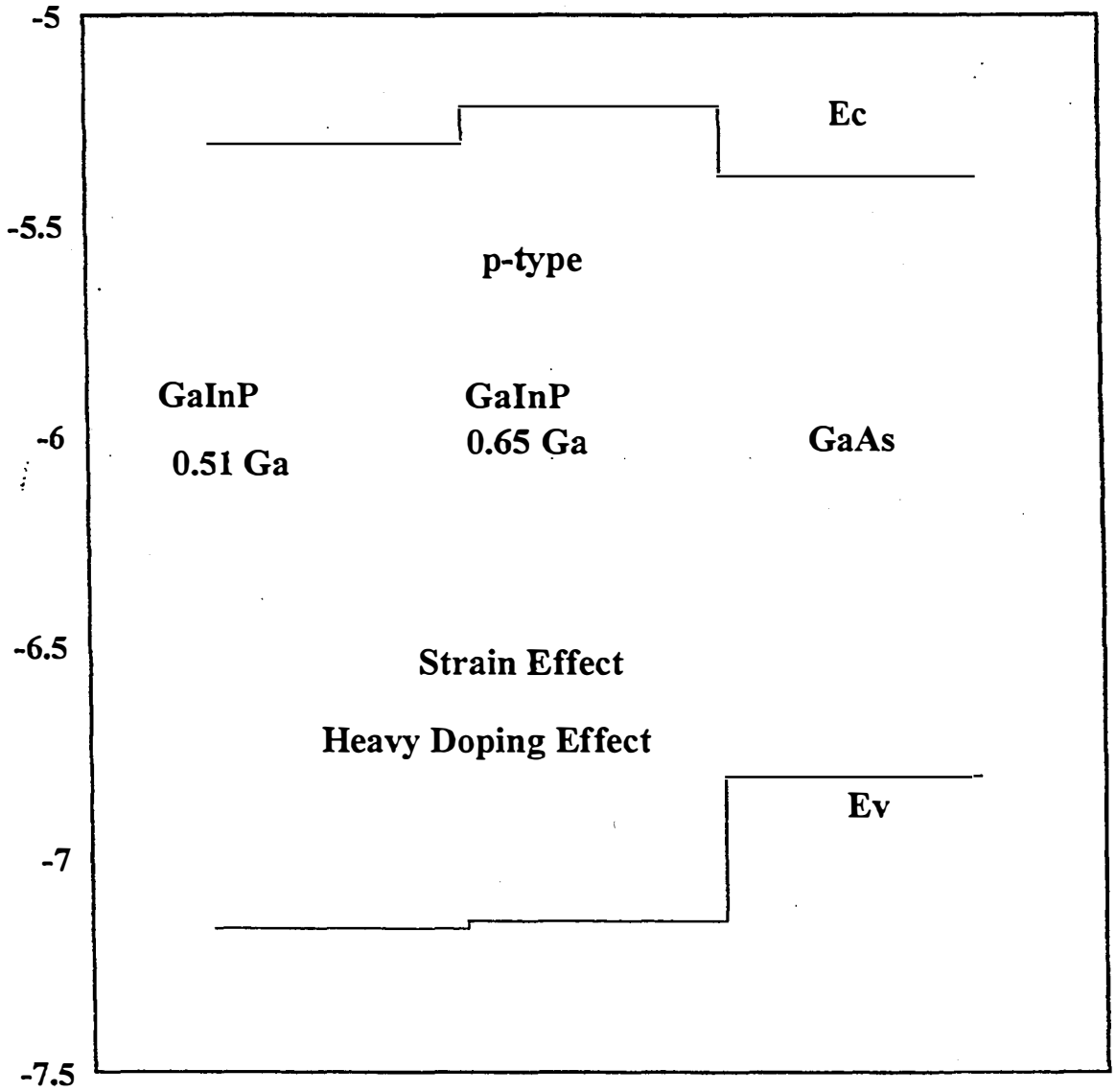

Fig. 4-11e The band levels and the interface discontinuities between GaAs, $Ga_{.65}In_{.35}P$, and $Ga_{.51}In_{.49}P$ materials. Strain effect, and heavy doping effect are included (p-type material).

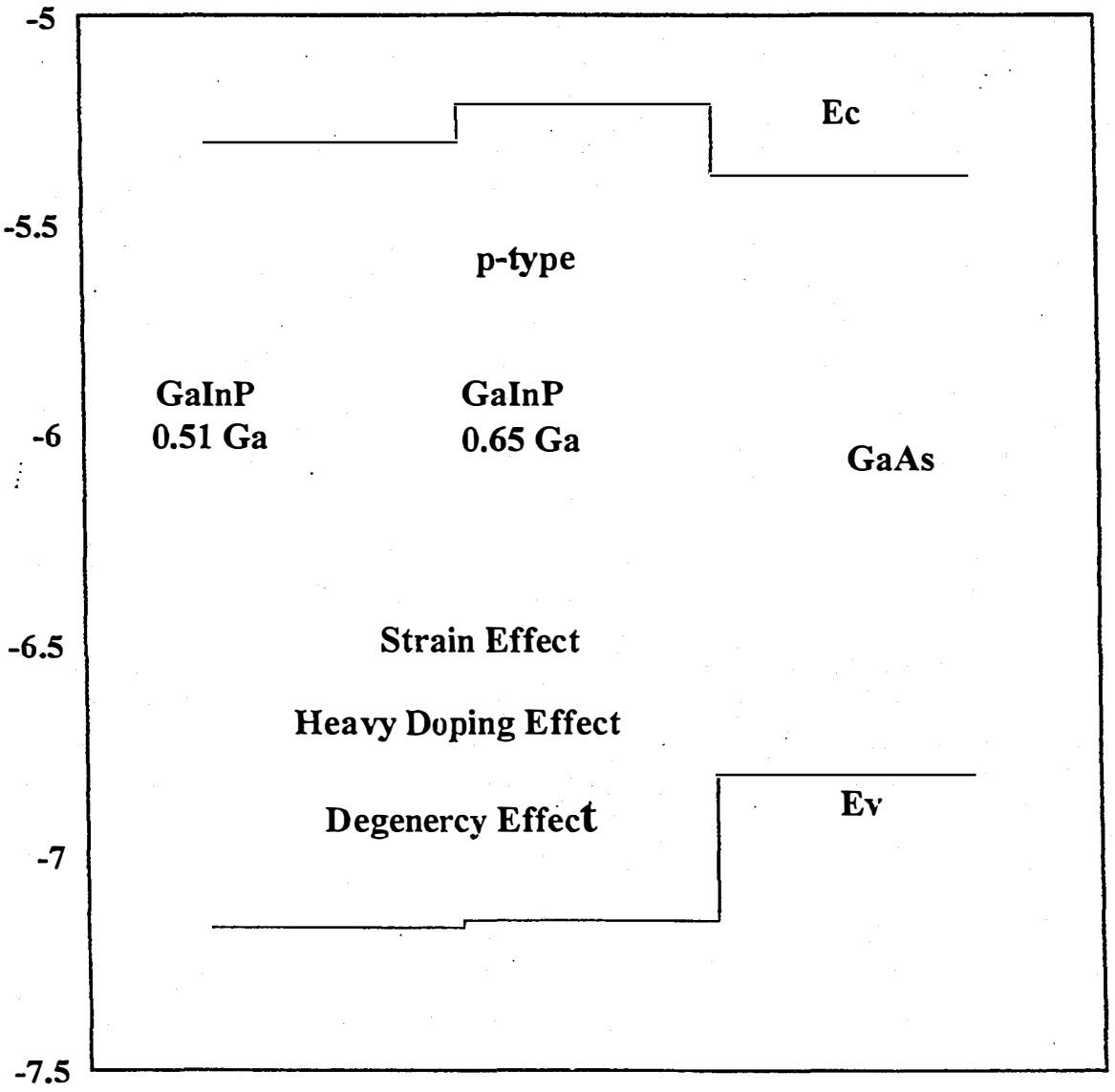

Fig. 4-11f The band levels and the interface discontinuities between GaAs, $Ga_{.65}In_{.35}P$, and $Ga_{.51}In_{.49}P$ materials. Strain effect, heavy doping effect, and degeneracy effects are included (p-type material).

References:

1) G. C. Van de Walle and R. M. Martin "Theoretical Calculations of Semiconductor Heterojunction Discontinuities", J. Vac. Tech. B. **4**(4), p. 8154 (1986).

2) L. Hrivnak "The Relation for Electron Effective Masses of Strained InGaAs Layers", Phys. Stat. Sol. (A) **123**, p. k133 (1991).

3) X. Marie, J. Barrau, B. Brousseau, Th. Amand, and M. Brousseau, "Interfacial-Band Discontinuities for Strained Layers of $In_xGa_{1-x}As$ Grown on (100) GaAs", J. Appl. Phys., **69** (2), pp. 812-815 (1990).

4) S. Niki, C. L. Lin, W. S. C. Chang, and H. H. Wieder, "Band-Edge Discontinuities of Strained-Layer $In_xGa_{1-x}As$/GaAs Heterojunctions and Quantum Wells", Appl. Phys. Lett., **55** (13), pp. 1339-1341 (1989).

5) M. A. Hasse, M. J. Hafich and G. Y. Robinson, "Internal Photoemission and Energy-Band Offsets in GaAs-GaInP p-I-N Heterojunction Photodiodes", Appl. Phys. Lett., **58** (6), pp. 616-618 (1991).

6) T Kobayashi, K Taira, F. Nakamura, and H. Kawai, "Band Lineup for a GaInP/GaAs Heterojunction Measured by a High-Gain Npn Heterojunction Bipolar Transistor Grown by Metalorganic Chemical Vapor Deposition" J. Appl. Phys., **65** (12) p. 4898 (1989).

7) M. A. Rao, E. J. Caine, J. Kroemer, S. I. Long, and D. I. Babic, "Determination of Valence and Conduction-Band Discontinuities at the (Ga,In)P/GaAs Heterojunction by C-V Profiling", J Appl. Phys., **61** (2), pp. 643-649 (1987).

8) D. Biswase, N. Debbar, and P. Bhattacharya, M. Razeghi, M. Defour, and F. Omnes, "Conduction and Valence Band Offsets in GaAs/$Ga_{0.51}In_{0.49}P$ Single Quantum Wells grown by Metaorganic Chemical Vapor Deposition", Appl. Phys. Lett., **56** (9), pp. 833-835 (1990).

9) Sandip Tiwari and David J. Frank, "Empirical Fit to Band Discontinuities and Barrier Heights in III-V Alloy System", Appl. Phys. Lett., pp. 630-632 (1992).

10) T. W. Lee, P. A. Houston, R. Kumar, X. F. Yang, G. Hill, M. Hopkinson, and P. A. Claxton, "Conduction Band Discontinuity in InGaP/GaAs Measured Using Both Current-Voltage and Photoemission Methods", Appl. Phys. Lett., **60** (4), pp. 474-476 (1992).

11) P. Bhattachaya, N. Debbar, and D. Biswas, M. Razeghi, M. Defour, and F. Omnes, "Band Offsets in GaAs/$Ga_{0.51}In_{0.49}P$ Heterostructures Grown By MOCVD", Int. Phys. Conf. Ser. **No. 106**: Chapter **6** pp. 351-356 (1990).

12) S. L. Feng, J. Krynicki, "Band Offset of GaAs-GaInP Heterojunctions", Semicond. Sci. Technol. **8** pp. 2092-2096 (1993).

13) T. Kobayashi, F. Nakamura, K. Taira and H. Kawai, "Band Lineup for GaInP/GaAs Heterojunction Measured by n-p-n and p-n-p Heterojunction Bipolar Transistor", Int. Phys. Conf. Ser. **No. 106:** Chapter 6 pp. 357-362 (1990).

14) S. M. Sze "**Semiconductor Devices: Physics and Technology**." Bell Telephone Laboratories, Inc. (1985).

15) S. C. Jain, J. M. McGregor and D. J. Roulston, "Band-Gap Narrowing in Novel III-V Semiconductors," J. Appl. Phys., **68** (7), p. 3747 (1990).

16) E. S. Harmon, M.R. Mellock, M. S. Lungstrom and M.L. Lovejoy, "Experimental Determination of the Effects of Degnerate Fermi Statistics on Heavily p-Doped GaAs," Appl. Phys. Let. **58** (15), p. 1647 (1991).

17) H. L. Chang, P. D. DeMoulin, M. E. Klausmeier-Brown, M. R. Melloch and M. S. Lundstrom, "Evidence for Band-Gap Narrowing Effects in Be-doped, p-p^+ GaAs Homojunction Barriers," J. Appl. Phys., **64** (11), p. 6361 (1988).

BACK SURFACE FIELDS FOR N/P AND P/N GAINP SOLAR CELLS

N.H. Rafat and S.M. Bedair
North Carolina State University, Raleigh, NC 27695-7911

P.R. Sharps, J.S. Hills, J.A. Hancock, and M.L. Timmons
Research Triangle Institute
Research Triangle Park, NC 27709-2194

ABSTRACT

We have grown n/p/p^+ and p/n/n^+ $GaInP_2$ top cells, lattice matched to GaAs for multijunction tandem solar cells. We have studied the effect of different types of back surface field (BSF) layers on the cell parameters of each cell. These layers are namely, abrupt strained $GaInP_2$, graded strained $GaInP_2$, disordered $GaInP_2$and AlGaAs layers. The measurements were done under 1-sun AM0 spectrum. The results show that the abrupt strained $GaInP_2$ BSF outperforms the disordered $GaInP_2$ BSF. Likely related to material quality, the AlGaAs layer clearly produce the least efficient BSF. It has been found that the abrupt strained $Ga_xIn_{1-x}P$ BSF with x=0.56 gives better results than the case with x=0.63 for the p/n/n^+ structure.

INTRODUCTION

'The multi-band gap multijunction tandem solar cells have attracted attention since the seventies [1]. The use of multijunctions in the photovoltaic field is done to achieve better matching to the solar spectrum than would be possible using single-junction solar cells. The III-V semiconductors are among the best materials to meet requirements of tandem solar cells. Numerous work has been done on the AlGaAs/GaAs lattice matched system. However, the AlGaAs has disadvantages. These disadvantages are: the formation of DX centers and the possibility of the Al to oxidize due to the sensitivity of AlGaAs for oxygen and water. The recombination velocity at the AlGaAs/GaAs interface is higher than that at the GaInP/GaAs interface [2]. We look for a material that is lattice matched to GaAs and has an energy gap as high as that of AlGaAs. One of the most promising material for the top cell is the $GaInP_2$ lattice matched to GaAs. To achieve high-efficiency multijunction solar cells, several parameters need optimization. Short-circuit current, open-circuit voltage, and fill factor must all be good simultaneously to produce high efficiency. An important source of losses is the recombination of minority carriers at the front and back surfaces of the cell. The BSF region at the back of the cell constitutes an energy barrier to the minority carriers in the base region. The interface states between the base and the BSF regions must be as low as possible to avoid another source of recombination. This could be achieved using lattice-matching materials. Reducing recombination at the back side of the cell could increase the short circuit current and reduce the saturation current and hence increase the open circuit voltage and the efficiency. Both window layer and back surface field layer for the top cell will affect performance of this junction. This top cell produces about two-thirds of the efficiency in a tandem stack, and it is not clear that either has been completely optimized. In previous work, both window layers for p/n $GaInP_2$ cells [3] and BSF layers for n/p $GaInP_2$ cells [4] have been studied. In the latter study, disordered $GaInP_2$ and quaternary $AlGaInP_2$ were examined and the disordered $GaInP_2$ was clearly superior to the Al- containing alloys.

p or n	GaAs	Cap	0.2 μ
p or n	AlInP	Window	250 A
p+ or n+	GaInP	Emitter	0.2μ
n or p	GaInP	Base	0.35μ
n+ or p+	BSF	Region	150-200 A
n+ or P+	GaAs	Buffer	0.2 μ
n+ or p+	GaAs	Substrate	

Fig. 1. The structure of the $GaInP_2$ Cell with all layers and the cap layer before etching (not to scale).

In this work, the study of BSF layers extends for n/p $GaInP_2$ to include lattice-matched AlGaAs layers, lattice-mismatched strained $Ga_xIn_{1-x}P$ (x>.51) and layers graded from x=0.56 to x=0.51, in addition to disordered $GaInP_2$. The present work also includes p/n devices since it is not clear whether an n/p or p/n tandem cell will be the most easily manufactured. Fig. 1 shows the structure of the cells used in this work. We have either n/p or p/n $GaInP_2$ lattice matched to GaAs with energy gap around 1.87 ev. The thickness of this cell is around 0.55 μm to ensure current matching with the bottom GaAs cell in the

multijunction structure. This thickness was also suggested [5] for the optimum thickness for this band gap under AM0. However, the theoretical work [6] from which this conclusion has been produced suggested a higher efficiency than one could expect from experimental results. This is because in this theoretical work, two main assumptions have been made. First, the collection efficiency is assumed 100 %, and second, the recombination in the depletion region is neglected. If it was not neglected, it would add a limit to the efficiency because of the 10^{17} cm^{-3} doping of the base which leads to a non negligible thickness in the depletion region. In addition to the main junction and the BSF layer, each cell has a buffer layer, , a window layer and a cap layer. The purpose of the buffer layer is to provide a smooth surface between the GaAs substrate and the $GaInP_2$. The purpose of the window layer is to reduce the recombination at the front surface without absorbing light. It also affects the reflection at the top. The purpose of the cap layer, after etching, is to provide selected, highly doped areas on the surface to achieve good ohmic contact. The short circuit current, the open circuit voltage and the fill factor have been measured for a number of cells of each structure. These measurements were done under 1-sun AM0 solar spectrum using a solar simulator.

EXPERIMENTAL

The $GaInP_2$ were grown using atmospheric pressure OMVPE growth. All the cells were grown at 650 ^0C with growth rate of 0.04 μ/min for GaAs, 0.08 μ/min for $GaInP_2$ and 0.15 μ/min for AlGaAs. Trimethylgallium (TMGa), trimethylaluminum (TMAl), ethyldymethyle indium (EDMIn), arsine (AsH_3) and phosphine (PH_3) are the source materials for the growth. Diethylzinc (DEZn) and hydrogen selenide (H_2Se) are used as the p-type and n-type dopants, respectively. The cells were processed as small-area devices using a concentrator grid metallization with a junction active-area of 0.141 cm^2 and total-area of 0.169 cm^2. The evaporated metallization was done using Au:Ge/Ni/Au for the n-type and using Ti/Au for p-type. In this work we have not used an anti-reflecting coatings, which would enhance our short circuit current by about 20% and the open circuit voltage and the efficiency.

Disordered $GaInP_2$ was grown by doping the material heavily while using a low V/III ratio namely (50:1). Strained layers used in all comparisons between different BSFs have compositions of $Ga_{.56}In_{.44}P$, which should produce unstrained band gaps of about 1.95 ev. Another strained layer with a composition of $Ga_{.53}In_{.37}P$, which has unstrained band gap of about 2.05 ev, was used for the comparison between different abrupt strained BSFs for p/n cells. This strained layers are thin (about 150-200 A) to avoid exceeding the critical thicknesses of the alloys, thereby minimizing introduction of mismatch-related defects. The $Al_xGa_{1-x}As$ (x about 0.8) BSF layer was not Included in the n/p device because most of the energy gap discontinuity is in the valence band (between GaInP and AlGaAs), and poor minority carrier confinement results at the back surface (identical situation was observed in attempting to use AlGaAs as a window layer for p/n cells. That is, minority carrier electron confinement was almost non-existent.). A BSF layer graded from $Ga_{.56}In_{.44}P$ to $Ga_{.51}In_{.49}P$ over 150 A was also evaluated and is referred to as graded BSF compared to the abrupt BSF for the other strained layer.

RESULTS AND DISCUSSION

Fig. 2 shows the short circuit current (over an active area = 0.141 cm^2 and without an anti-reflecting coatings) under different types of BSF for both $n/p/p^+$ and $p/n/n^+$ cells. The values of the short circuit current are comparable for the different types of BSF In the $n/p/p^+$ and $p/n/n^+$ structures. The short circuit currents for the abrupt and the graded strained layers $GaInP_2$ (case C and D) give the best results for both $n/p/p^+$ and $p/n/n^+$. These values are (J_{sc} = 10 mA/cm^2 for $p/n/n^+$ and J_{sc} =5.6 mA/cm^2 for $n/p/p^+$). In both structures, the short circuit currents for the disordered $GaInP_2$ (case B) give the worst results. Although the energy gap of the disordered $GaInP_2$ layer is higher than the strained one, the short circuit current is lower in this case. The main result in this figure is that the short circuit current in case of $p/n/n^+$ Is much higher than that of $n/p/p^+$. This means that, it is better to work with a $p/n/n^+$ cell with an abrupt or graded back surface field layers rather than an $n/p/p^+$ cell. According to this results the work has been extended to look for the effect of using a more strained $Ga_xIn_{1-x}P$ BSF layer (x=0.63) with a p/n cell rather than an n/p cell.

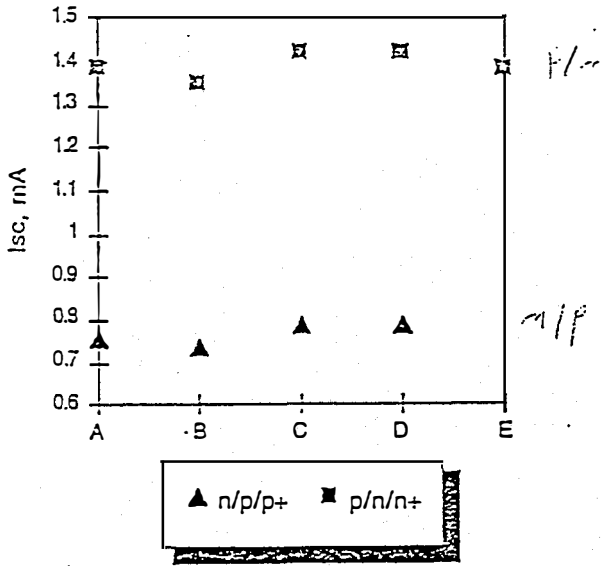

Fig. 2. The short circuit current in mA over an active area (0.141 cm^2) for different types of BSF for both $n/p/p^+$ and $p/n/n^+$ cells (no anti- reflecting coatings). A) no BSF layer, B) disordered $GaInP_2$, C) abrupt strained $GaInP_2$, D) graded strained $GaInP_2$, and E) AlGaAs.

Fig. 3 shows the values of the fill factor under different types of BSF for both structures. The values for the $p/n/n^+$ structure still outperforms the $n/p/p^+$ structure. The abrupt strained BSF and the disordered BSF give the best results for the $p/n/n^+$ structure and for the $n/p/p^+$

structure the abrupt strained BSF outperforms the disordered BSF. The AlGaAs BSF gives the worst results for p/n/n+. That means that inserting the AlGaAs layer between the substrate and the cell instead of enhancing the cell parameters as expected from a BSF layer, deteriorate the FF. This is also the case for all the n/p/p+ types of BSF, since the no BSF layer gives very good fill factor values.

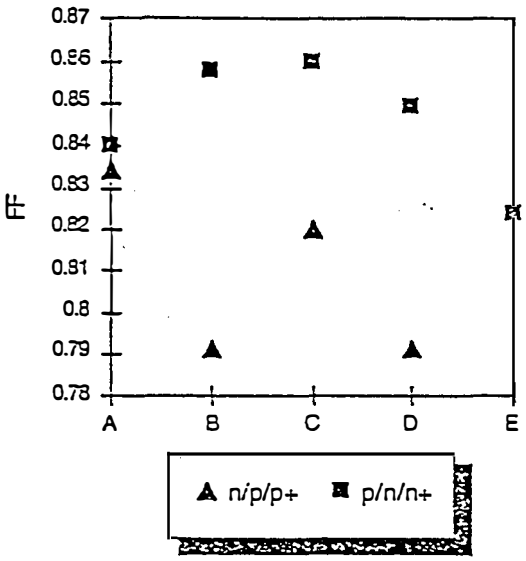

Fig. 3. The fill factor for different types of BSF for both n/p/p+ and p/n/n+ cells. A) no BSF layer, B) disordered $GaInP_2$, C) abrupt strained $GaInP_2$, D) graded strained $GaInP_2$, and E) AlGaAs.

Fig. 4 shows the open circuit voltage for all BSF types. The disordered BSF for the p/n/n+ gives the best result which is a negligible enhancement over the no- BSF case. The AlGaAs is still the worst type of BSF for the p/n/n+cells. For the n/p/p+ structure, the abrupt strained $GaInP_2$ gives the best open circuit voltage over all BSF types in this structure. The results from this figure show that there is no enhancement in the open circuit voltage for the p/n/n+ structure which was not expected. However, for the n/p/p+ structure there is a reasonable enhancement (40 mev) in the open circuit voltage for the case of abrupt strained $GaInP_2$ over the no BSF case. The reason for that, is that the $GaInP_2$ BSF layer is under tensile strain which will lead to a decrease in its energy gap than that of unstrained layer with the same composition. This decrease will lead to a lower band offset between the BSF layer and the base region. For the case of the strained $Ga_xIn_{1-x}P$ with x=0.56 BSF, the band offset between this layer with the base $Ga_xIn_{1-x}P$ with x=0.51 lies almost in the conduction band. This is why we could find a barrier for electrons as minority carriers in the p- base region (and hence an enhancement in the cell parameters), while we could not find this barrier for the holes in the n-base region.

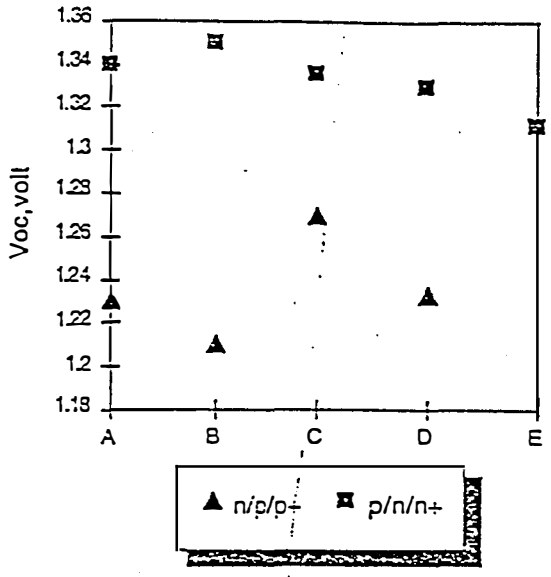

Fig. 4. The open circuit voltage for different types of BSF for both n/p/p+ and p/n/n+ cells. A) no BSF layer, B) disordered $GaInP_2$, C) abrupt strained $GaInP_2$, D) graded strained $GaInP_2$, and E) AlGaAs.

As a general conclusion from the previous results one can conclude that, although the abrupt strained $GaInP_2$ BSF for the n/p/p+ is the most effective structure, the absolutely highest results over the different BSF types in the two structures are that of the p/n/n+ with a $GaInP_2$ abrupt strained BSF layer.

To estimate the extent to which the Ga content of the BSF layer could be increased (to increase bandgap) without introducing a number of defects, a p/n/n+ cell with a $Ga_{.63}In_{.37}P$ BSF layer has been grown. The performance was compared with the cell containing $Ga_{.56}In_{.44}P$ BSF layer and with the cell without BSF layer. Table I show these data for the open circuit voltage, V_{oc}, the short circuit current, I_{sc}, and the fill factor, FF that reveal expected results. For the $Ga_{.63}In_{.37}P$ layer in which tensile strain increases, performance drops off dramatically for all parameters after the improvements observed with a smaller amount of strain. As the mismatching between the base and the BSF layer increases as the critical thickness of the BSF region decreases and the possibility of creating misfit dislocations increases. These data certainly suggest the limits to which the strained layer concept can be extended. From all measurements, the best values we have obtained is the p/n/n+ structure with a strained abrupt layer of $Ga_{.56}In_{.44}P$. Fig. 5 gives the I-V characteristics of this cell which has V_{oc} =1.336 volt, I_{sc} = 1.418 mA (J_{sc}= 10 mA/cm^2) (no anti-reflecting coatings) and FF = 0.86. With a proper optimization to the window layer and including anti-reflectings layers, the results would increase by a significant amount.

PROPERTIES OF HIGHLY STRAINED GaP and GaP/GaAs/GaP QUANTUM WELLS GROWN ON GaAs SUBSTRATES BY ATOMIC LAYER EPITAXY

C.A.Parker, J.R.Gong, D.Jung, F.Huga[a)], N.A.El-Masry, and S.M.Bedair

Department of Electrical and Computer Engineering

North Carolina State University

Raleigh, North Carolina 27695-7911

[a)]On leave from NTT LSI Laboratories, 3-1, Morinosato

Wakamiya, Atsugi-shi, Kanagawa, 243-01 Japan.

To be submitted.

Abstract

Atomic layer epitaxy (ALE) has been employed for the growth of highly strained (3.6%) GaP films and GaP/GaAs/GaP single quantum wells on (100) GaAs substrates at 500°C. Misfit dislocation formation in GaP was observed by Scanning Transmission Electron Microscopy (STEM) and chemical delineation of dislocations. The onset of dislocations in the GaP layers was also determined by the onset of degradation in electrical properties (breakdown voltage and reverse current) of GaP/GaAs Schottky diodes and in low temperature photoluminescence (FWHM and intensity) of GaP/GaAs/GaP single quantum wells. All techniques experimentally indicate a critical layer thickness (CLT) greater than 60 Å. This value is several times larger than the theoretical value (h_c<20 Å) predicted by the force balance model. This result may be related to the low growth temperature and the two dimensional (2-D) nature of the ALE growth process.

Introduction

Due to the tailorable nature in the optical and electrical properties, pseudomorphic strained layer epitaxy has attracted much attention in recent years as a source for alternative heterostructure materials. Several systems such as GaInAs/InP[1,2], GeSi/Si[3,4], InGaAs/GaAs[5-9], GaAsP/GaP[10], and GaAsP/GaAs[11,12] have already been investigated intensively from both material and device aspects. In strained layer epitaxy, layers are grown lattice mismatched to the substrate where pseudomorphic growth is supported for layers less than the critical layer thickness (CLT)[13]. When the layer thickness exceeds the CLT, the mismatch is accommodated by both elastic strains and generations of misfit dislocations[13]. These misfit dislocations degrade the structural, optical and electrical properties of materials[13]. Therefore, it is very important to determine clearly the CLT value in strained layer systems. Large lattice-mismatch strained-layer systems that have very thin critical thicknesses require precise control of deposition rate and thickness uniformity. Atomic layer epitaxy (ALE) is a suitable candidate for growth of ultra-thin highly strained pseudomorphic layers due to its unique self-limiting mechanism.

The highly strained GaP/GaAs system grown on GaAs substrates with a mismatch of 3.6% can utilize GaP as a wide bandgap (2.26 eV at room temperature) alternative to the more commonly used semiconductor compounds with Al as a group III species. However,

the thickness of a single dislocation-free GaP layer grown on a GaAs substrate is limited to a CLT of approximately 16 Å as predicted by the theoretical force balance model of Matthews and Blakeslee[12]. If thicker barrier layers are required to provide better confinement of carriers and prevent tunneling, the thickness of the high bandgap GaP layer must exceed the theoritical CLT. We report in this paper that the monolayer-by-monolayer and low temperature ALE growth can achieve GaP with layer thickness greater than the theoretical CLT that can be suitable for device potential applications. A single GaP overgrown layer and GaP/GaAs/GaP single quantum well structures grown on GaAs will be studied to determine the CLT in ALE grown layers.

Growth

The ALE growth of GaP and GaAs was achieved in an atmospheric-pressure quartz reactor with a specially designed graphite susceptor which has been described in detail elsewhere[14]. TMGa was employed as the source of column III metal with bubbler temperature kept at -10 °C. The PH_3 and AsH_3 were utilized as column V source materials. The ALE growth for each layer entailed alternatively exposing the substrate to column III and column V streams of organometallic and hydride precursors. A constant 4 slm hydrogen flow was injected into the reactor by a central inlet tube during the growth.

All GaP layers in this study were grown by ALE at 500 °C. To prevent the growth of the ternary compound GaAsP and ensure interfacial abruptness after growth of a GaAs layer, the GaAs

sample was first positioned under the AsH_3 flux for 15 seconds; then the AsH_3 flux was turned off while the PH_3 flux was turned on. Prior to growth of the GaP layer, the sample was held stationary under the PH_3 flux for several seconds with a high hydrogen flow at low temperature (500 °C) to ensure removal of the AsH_3 gas from the reactor. An inversion of this technique was employed when switching from PH_3 to AsH_3 before growing GaAs on GaP in the strained quantum well studies.

The substrates used in the GaP/GaAs Schottky diode studies were semi-insulating (100) GaAs wafers. First, a 2000 Å undoped GaAs buffer layer was grown at 650°C utilizing a conventional MOCVD approach where the substrate is stationary and exposed to the TMGa and AsH_3 fluxes simultaneously. The buffer layer was followed by a 2000 Å Si-doped (3x17 cm^{-3}) GaAs layer grown by ALE at 550°C. Finally, an ALE GaP layer was grown at 500°C. The planar Schottky device was fabricated first by evaporating a AuGe/Au (350 Å/1500 Å) Ohmic contact with an E-beam evaporator on a photoresist patterned surface followed by an anneal step at 425°C for 30 seconds in N_2. Next, a Schottky Ti/Au (600 Å/1500 Å) contact by E-beam evaporation was fabricated with a diode area 280 μm x
280 μm.

The characterization techniques used to determine the CLT of GaP on (100) GaAs were Transmission Electron Microscopy (TEM), chemical etch delineation of dislocations, electrical characterics of GaP/GaAs Schottky diodes, and low temperature photoluminescence spectroscopy of strained GaP/GaAs/GaP single quantum wells.

Results and Discussion

TEM was used to view dislocation formation in GaP layers. Figures 1(a)-(c) show the plan-view TEM micrographs of the GaP layers on GaAs characterized by a Hitachi 800 Transmission Electron Microscope operating at 200 KV. The thickness of these GaP layers are 60, 80, and 200 Å, respectively, as determined from the ALE number of cycles. It appears a dislocation density was observed when the thickness of GaP layers increased from 60 to 80 Å. As revealed in Figure 1(c), most of the dislocation lines are of the misfit type running along [110] and [1-10] directions when the GaP layer thickness reaches approximately 200 Å. The rapid increase in dislocation density is an indication of strain relaxation by dislocation formation due to the very large lattice mismatch. From a the dislocation onset, TEM suggest a CLT occuring between 60 and 80 Å.

Delineation of dislocations at the interface surface by chemical etching was also applied to study dislocation formations in the GaP layer grown on GaAs. The GaP layer was first removed by HCl followed by H_3PO_4: H_2O_2: H_2O (3:1:50) to remove the GaAs epilayer. Possibly due to cluster 3-D nucleation, discussed later in detail, in GaP layers exceeding a critical layer thickness, delineation of the 3-D clusters and associated dislocations in these GaP layers can be seen. This dislocation delineation shown in Figure 2(a) and 2(b) are photographs taken from an optical microscope of the 60 Å GaP and 140 Å GaP samples after the mesa etch. A photograph of the 100 Å GaP sample was the same as the 60 Å GaP sample. This

technique is clearly not as sensitive as the TEM technique for determining dislocation onset, even though TEM is not the most sensitive technique, however; it illustrates, as did the TEM technique, a plan-view of the dislocations and that the theoretical CLT of GaP on GaAs has been exceeded.

The degradation of electrical properites for a fabricated GaP/GaAs Schottky diode was employed to determine the onset of misfit dislocations in the GaP layer or defects at the GaP/GaAs interface. The degradation of electrical properties in devices has been previously used to determine CLT's, for example, increase in leakage current for a p-i-n diode utilizing a GaInAs/InP strained layer superlattice[1] or increases in reverse current and ideality factor for Schottky diodes formed from GaInP/InP strained material system[15]. In our experiment, samples with GaP thicknesses of 0 Å, 20 Å, 40 Å, 60 Å, 100 Å, and 140 Å were grown to determine the CLT. The breakdown voltage at I=-280 μA and the reverse current at V = -1V were measured using a Hewlett-Packard 4145B semiconductor parameter analizer. Figure 3 and 4 show the dependence of the breakdown voltage and the reverse current on the GaP layer thickness. From the figures, degradation of the electrical properties of these Schottky diodes occurs for GaP films thicker than 60 Å. This is in good agreement with the onset of misfit dislocations seen by TEM.

Degradation of optical properties of GaP/GaAs/GaP strained single quantum wells by low temperature photoluminescence (PL) spectroscopy was also used to verify the onset of dislocations at

the interface. Since the presence of dislocations act as nonradiative recombination centers, PL intensity and linewidth degradation has been used before for determining the CLT[16]. For these quantum well experiments, a series of GaP/GaAs/GaP strained single quantum wells were grown by ALE at 500 °C directly on a (100) GaAs substrate. The thicknesses of the GaP barrier layers (20 Å, 40 Å, 60 Å, 80 Å, 120 Å, and 150 Å) were varied while the GaAs well width was held constant at 40 Å. All layer thicknesses were verified with cross-section transmission electron microscopy. A very uniform, two-dimension ALE growth of both GaP and GaAs with abrupt interfaces can be seen in Figure 5, a cross-sectional TEM micrograph of a GaP/GaAs/GaP strained single quantum well grown on a (100) GaAs substrate with barrier and well thicknesses of 60 Å. A plot of the relative PL intensities and the FWHM measured at 22 K (Figure 6) indicates an increase in FWHM in samples with GaP thicknesses in the range and greater than 80 to 120 Å. Similarily, a maximum in relative PL intensity at barrier thicknesses of 120 Å can be seen. The lower PL intensity for barrier layers less than 120 Å is due to reduced quantum confinement; while the increase in FWHM and the associated decrease in intensity for GaP layers greater than 120 Å is due to defect generation at the interfaces. This degradation range (80-120 Å) of the PL emmisions from GaP/GaAs/GaP quantum wells is slightly greater than the onset of dislocations seen by TEM (60-80 Å). This discrepancy possibly may be due to strain sharing in the thin GaAs quantum well layer, thereby, increasing the experimentally measured CLT, or it may

simply be a less sensitive detection method.

Experimental CLT values greater than the predicted theoretical CLT values imply that the CLT depends not only on the amount of strain magnitude but on the mode of growth and the growth temperature. Important modes of growth are the three-dimensional (3-D) cluster formation or island growth and the two-dimensional (2-D) Frank-van der Merwe (FM) mode where the film covers the substrate and thickens uniformly. The FM mode is supported for growth temperatures below a certain roughening transition temperature (TR)[17]. For thin overlayers the epitaxial strained film is coherent and the mismatch is completely accommodated by elastic strain. As the value of the equilibrium critical thickness is exceeded, it becomes energetically favorable for dislocations to start to appear at the strained interfaces. Therefore, the mismatch will be accommodated by a combination of elastic strain and interfacial misfit dislocations, rather than by elastic strain alone. This behavior is associated with kinetic barriers to the formation and motion of misfit dislocations. Therefore, it is currently believed that during this initial relaxation behavior, if the growth follows a 2D mode, dislocation sources are originated either from substrate threading dislocations[18,12] or by heterogenous nucleation.[19,20] The heterogenous nucleation center can be due to small clusters of impurity atoms, localized structural surface defects, or other sources that can produce localized stress concentration. These surface defects can play a major role in the initial stages of relaxation of strained-layer structures, and

their suppression can lead to the retardation of this relaxation process; thus, higher strain can be sustained for a given layer thickness. Therefore, ALE can yield high quality interfaces free from many defects and heterogeneous nucleation centers that can exist in other conventional growth technologies; thereby, higher CLT's can be achieved. Two-dimensional growth is supported by ALE due to the one layer per cycle process where deposition of organometallic group III molecules migrate to their proper lattice sites followed by a reaction with group V hydride for growth of III-V compounds. In this manner, stoichimetric growth is achieved, thus reducing anti-site defects.

Growth at low temperatures is also desirable for maintaining high CLT's. Research of InGaAs films with x=0.33 on GaAs substrates[21] reports the onset of interfacial dislocations and 3D island growth for higher growth temperatures. Therefore, 3D growth is thermodynamically favored in lattice mismatch systems grown at high temperature which can lead to heterogeneous nucleation sites. Furthermore, in a recent publication, InGaAs with In as high as 45% was grown on GaAs well above the CLT at low substrate temperatures[9]. The high CLT's obtained in our results can also be contributed to low temperature growth (500°C) of GaP and ALE 2-D stoichiometric growth.

A potential application of the growth of thick GaP on GaAs is its use as a substitute for AlGaAs in high electron mobility transistors (HEMT's) where the thickness of the AlGaAs layer is used for threshold voltage control[22]. From preliminary results, we

have found that the etch rate of the ALE grown GaP layers is more than 50 times slower than that of GaAs for H_3PO_4-based and NH_4OH-based etchants. Even though AlGaAs has a high etching selectivity ratio to GaAs[23], the results suggest that GaP could be a suitable replacement for AlGaAs as an effective stop-etch layer. Furthermore, due to the high surface states of GaAs, passivation of GaAs with a wide-bandgap material lowers the surface recombination velocity[24]. It has been reported that the interface between phosphorus compounds and GaAs has a lower recombination velocity than the AlGaAs/GaAs interface[25,26]. The gate Schottky barrier is also increased by the wide-bandgap material. Thus, GaP potentially could be used as an effective stop-etch, passivating layer and increase the Schottky barrier height in metal semiconductor field effect transistor (MESFET) structures.

Conclusion

Highly strained GaP films and GaP/GaAs/GaP single quantum wells were grown on (100) GaAs by low temperature atomic layer epitaxy with GaP layer thicknesses exceeding the theoretical CLT. All charaterization techniques confirmed a CLT greater than 60 Å. This high value suggest that the onset of misfit disloctions in the GaP layer can be impeded due to low temperature 2-D ALE growth.

This work is supported by NSF, ONR/SDIO, and NTT.

References

1. H. Tempkin, D.G. Gershon, S.N.G Chu, J.M. Vandenberg, R.A. Hamm, and M.B. Panish, Appl. Phys. Lett. **55**, 1668 (1989).

2. Munecazu Tacano, Yoshinobu Sugiyama, and Yukihiro Takeuchi, Appl. Phys. Lett. **58**, 2420 (1991).

3. R. People and J.C. Bean, Appl. Phys. Lett. **47**, 322 (1985).

4. D.C. Hougton, D.D. Perovic, J.M. Baribeau, and G.C. Weatherly, J. Appl. Phys. **67**, 1850 (1990).

5. W.D. Laidig, C.K. Peng, and Y.F. Lin, J. Vac Sci. Technol. **B2**, 181 (1984).

6. I.J. Fritz, S.T. Picraux, L.R. Dawson, T.J. Drummond, W.D. Laidig and N.G. Anderson, Appl. Phys. Lett. **46**, 967 (1985)

7. I.J. Fritz, P.L Gourley, and L.R. Dawson, Appl. Phys. Lett. **51**, 1004 (1987).

8. N.G. Anderson, W.D. Laidig, R.M. Kolbas, and Y.C. Lo, J. Appl. Phys. **60**, 7 (1986).

9. B. Elman, Emil S. Koteles, P. Melman, K. Ostreicher, and C. Sung, J. Appl. Phys. **70**, 2634 (1991).

10. G.C. Osbourn, R.M. Biefeld and P.L. Gourley, Apl. Phys. Lett. **41**, 172 (1982).

11. G.C. Osbourn, J. Appl. Phys. **53**, 1586 (1982).

12. J.W. Matthews and A.E. Blakeslee, J. Cryst. Growth **27**, 118 (1974)

13. J.H. van der Merwe, CRC Crit. Rev. Solid State Mater. Sci. **7**, 209 (1978).

14. M.A. Tischler and S.M. Bedair in *Atomic Layer Epitaxy*, edited by T. Suntola and M. Simpson (Blackie, Glasgow and London, 1990), Chap. 4.

15. S. Loualiche, A. Ginudi, A. LeCorre, D. Lecrosnier, C. Vaudry, L. Henry, and C. Guillemot, Appl. Phys. Lett. **55**, 2099 (1989).

16. T.G. Anderson, Z.G. Chen, V.D. Kulakovskii, A. Voldin, and J.T. Vallin, Appl. Phys. Lett. **51**, 752 (1987).

17. G.H. Gilmer and M.H. Grabow, Journal of Metals **June**, 19 (1987).

18. J.W. Matthews, S. Mader, and T.B. Light, J. Appl. Phys. **41**, 3800 (1970).

19. Brian W. Dodson, Appl. Phys Lett. **53**, 394 (1988).

20. E.A. Fitzgerald, G.P. Watson, R.E. Proano, D.G. Ast, P.D. Kirchner, G.D. Pettit, and J.M. Woodall, J. Appl. Phys. **65**, 2220, (1989).

21. G.J. Whaley and P.I. Cohen, J. Vac. Sci. Technol. **B6**, 525 (1988).

22. M. Abe, T. Mimura, K. Nishiuchi, A. Shibatomi, and M. Kobayashi, IEEE J. Quantum Electronics **22**, 1870 (1986).

23. K. Hikosaka, T. Mimura, and K. Joshin, Jpn. J. Appl. Phys. **20**, 1847 (1981).

24. F. Capasso and G.F. Williams, J. Electrochem. Soc. **129**, 821 (1982).

25. J.M. Olson, R.K. Ahrenkiel, D.J. Dunlavy, B. Keyes, and A.E. Kibbler, Appl. Phys. Lett. **55**, 1208 (1989).

26. Fumiaki Hyuga, Tatsuo Aoki, Suehiro Sugitani, Kazuyoshi Asai, and Yoshihiro Imamura, MRS Conference **Fall** (1991).

Figure Captions

Figure 1. Plan-View TEM Micrographs of GaP Layers Grown On (100) GaAs. (a) 60 Å GaP layer, (b) 80 Å GaP layer, (c) 200 Å GaP layer.

Figure 2. Chemical Etch Delineation of Dislocations in GaP layer. (a) Mesa Etch of 60 Å GaP Grown on GaAs, (b) Mesa Etch of 140 Å GaP Grown on GaAs

Figure 3. GaP/GaAs Schottky Diode Breakdown Voltage measured at I=-280μA for different GaP Thicknesses.

Figure 4. GaP/GaAs Schottky Diode Reverse Current Measured at V=-1V for different GaP Thicknesses.

Figure 5. A Cross-Sectional TEM Micrograph of a 60 Å GaP/ 60 Å GaAs/ 60 Å GaP Strain Quantum Well Grown on (100) GaAs Substrate.

Figure 6. PL Intensity and FWHM for a GaP/GaAs/GaP SQW's with a Constant GaAs Well Thickness of 40 Å and Various GaP Barrier Thicknesses.

Plan-View TEM Micrographs of GaP Layers Grown On (100) GaAs

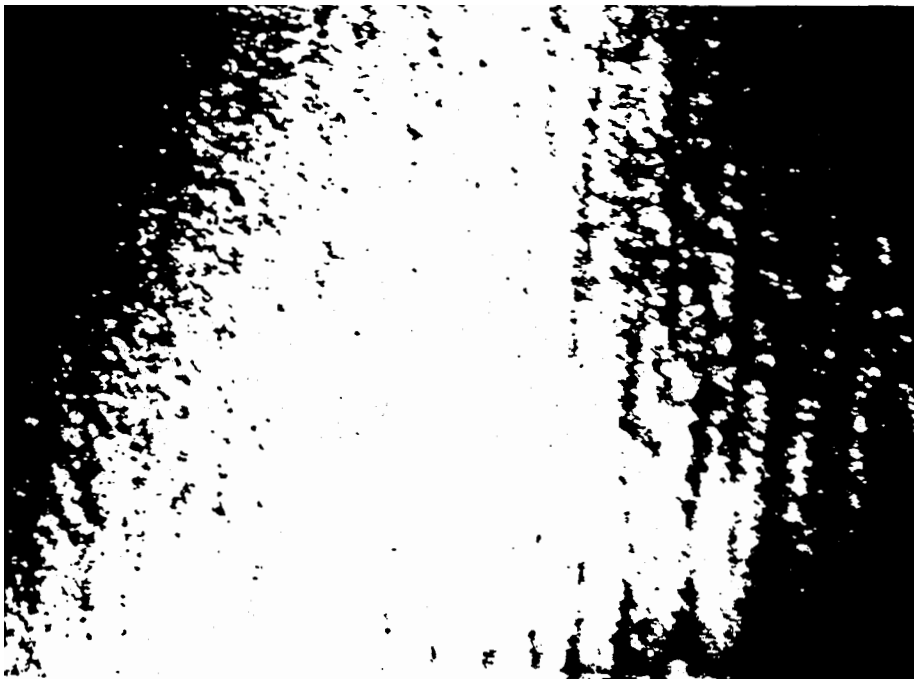

Figure 1(a) 60 Å GaP layer

Plan-View TEM Micrographs of GaP Layers Grown On (100) GaAs

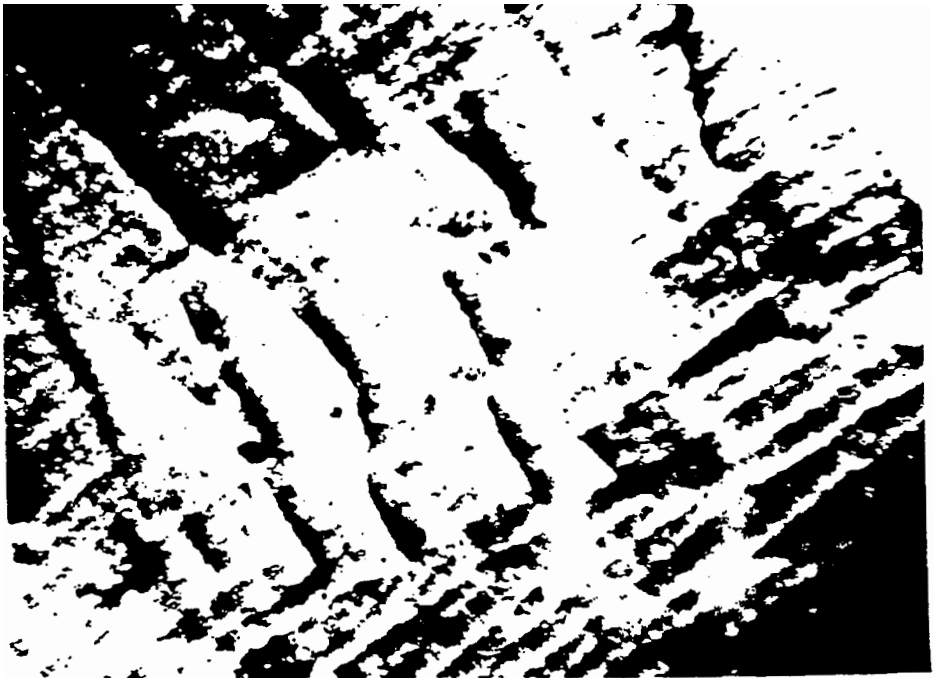

Figure 1(b) 80 Å GaP layer

Plan-View TEM Micrographs of GaP Layers Grown On (100) GaAs

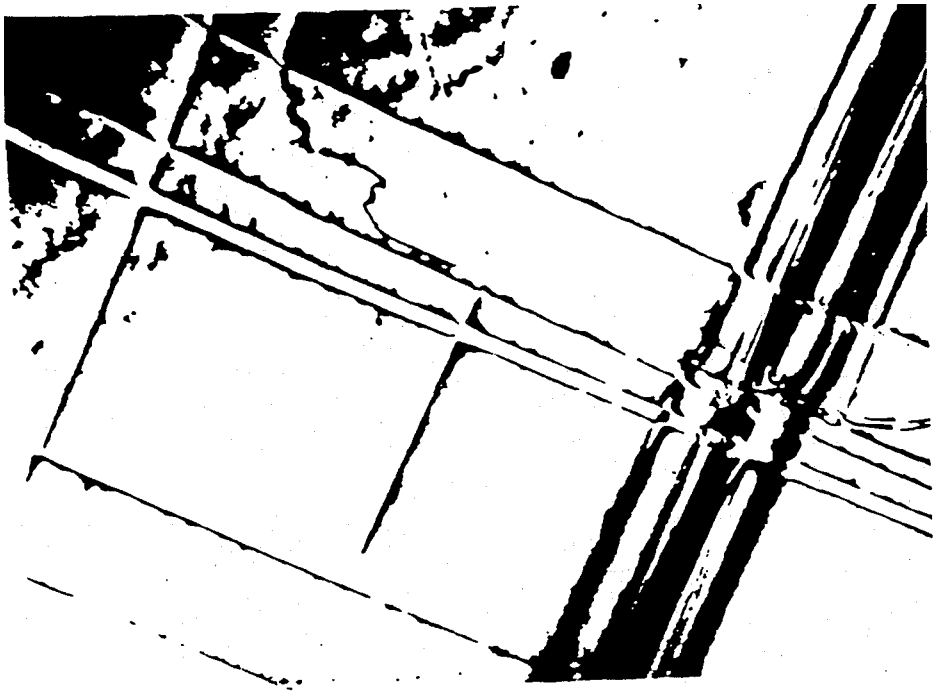

Figure 1(c) 200 Å GaP layer

Chemical Etch Delineation of Dislocations
Formed in the GaP Layer

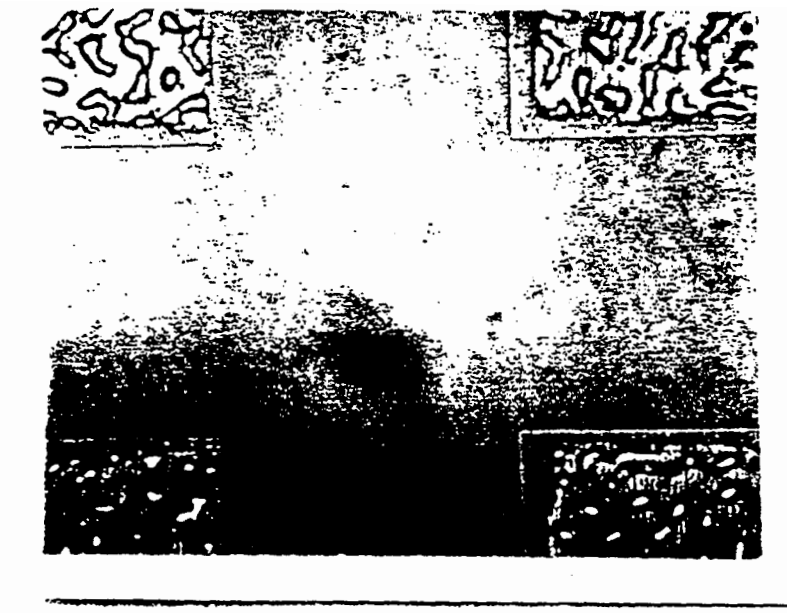

Figure 2(a). 60 Å GaP grown on GaAs after Mesa Etch

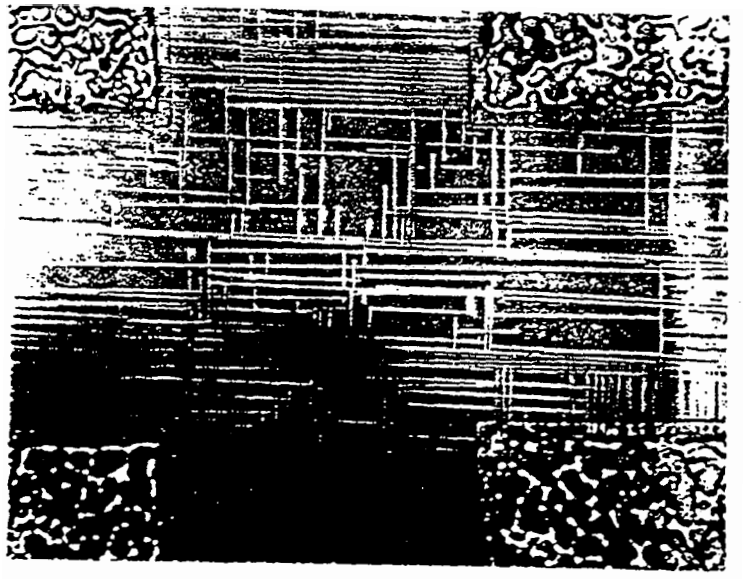

Figure 2(b). 140 Å GaP grown on GaAs after Mesa Etch

GaP/GaAs Schottky Diode Characteristics

Ti/Au Schottky (280um x 280um)

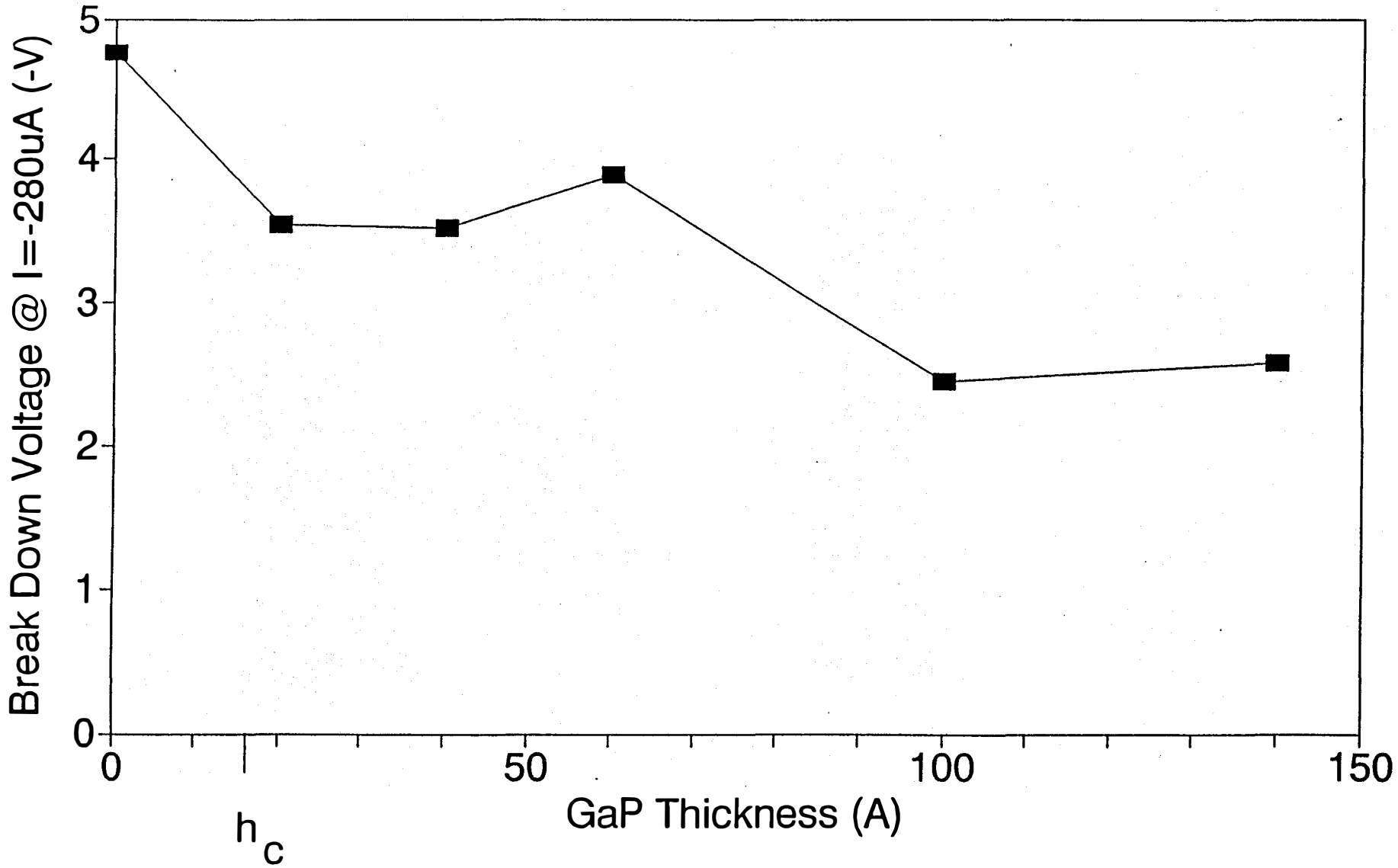

FIGURE 3

GaP/GaAs Schottky Diode Characteristics

Ti/Au Schottky (280um x 280um)

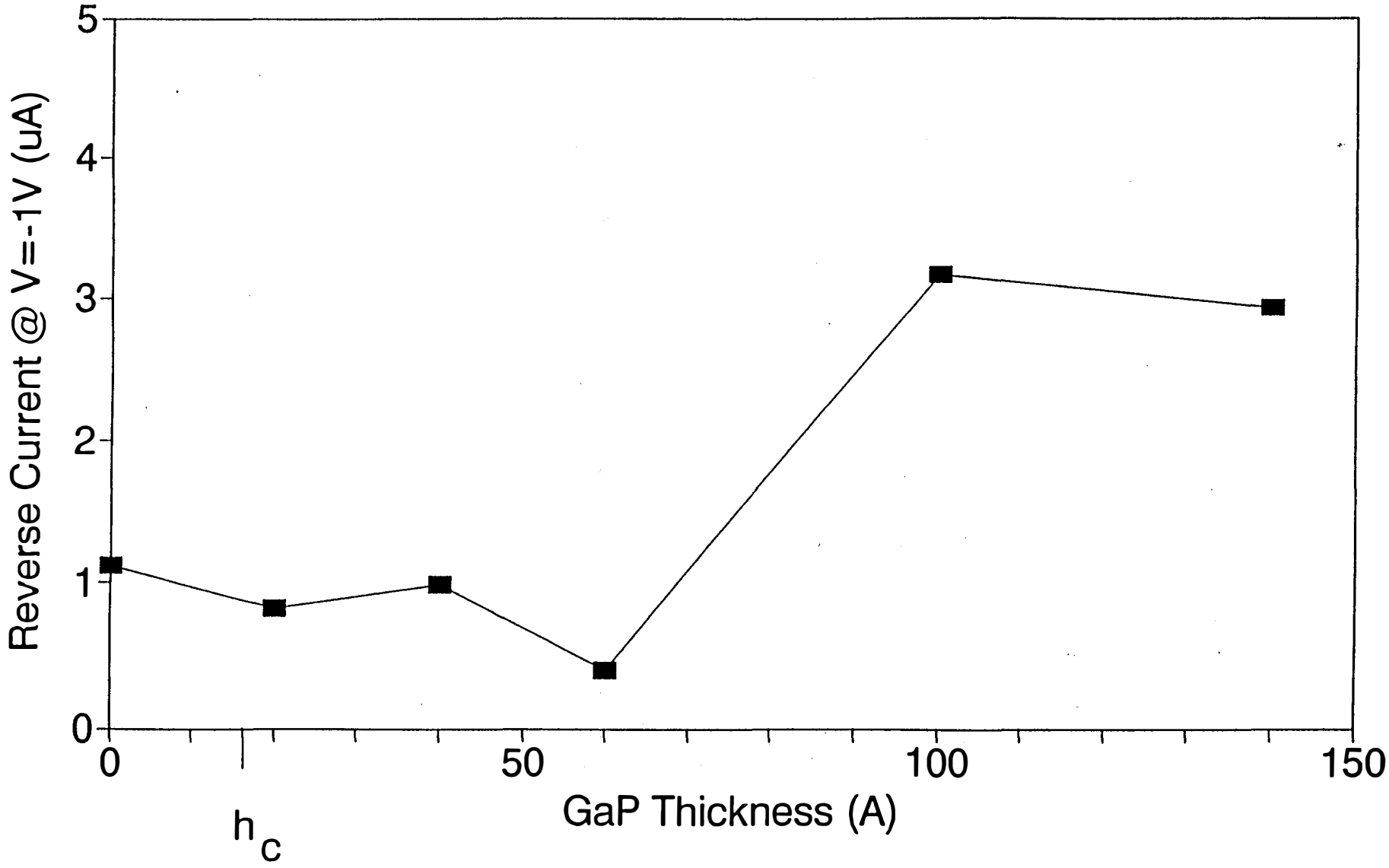

FIGURE 4

A Cross-Sectional TEM Micrograph of a GaP/GaAs/GaP Strained Quantum Well Grown on (100) GaAs Substrate

Figure 5. 60 Å GaP/ 60 Å GaAs/ 60 Å GaP SQW

PL Data of GaP/GaAs SQW

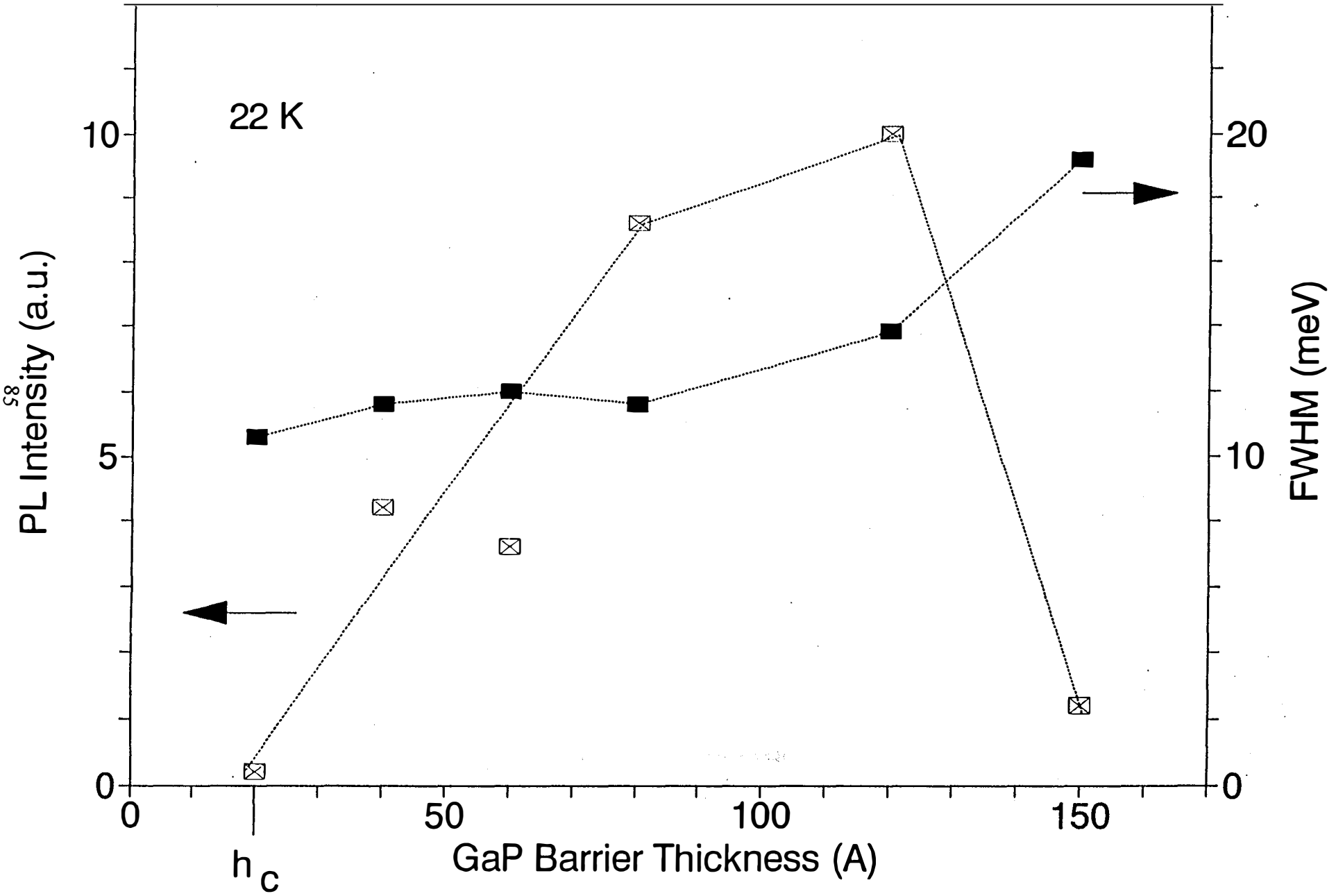

FIGURE 6

AlGaAs/GaInP heterojunction tunnel diode

6.1 Introduction

Multijunction or cascade solar cells may be considered the only promising approach for achieving high conversion efficiency by more efficient utilization of the solar spectrum. Theoretical studies for a two cell structure have shown, for example, conversion efficiencies of 30% and 40% for one sun and 500 suns, respectively [1]. A major challenge in the development of these multijunction solar cells is the requirement of a low resistance, optically transparent interconnect between the adjacent junctions [2]. The use of a tunnel junction is considered the most appealing approach for interconnecting the high and low band-gap cells. The tunnel junction should operate under forward bias at a current density of about 20 A/cm^2 for 1000 suns operation. The band- gap in the tunnel junction should be slightly larger than that of the top cell i.e. $E_g \geq 1.8$ eV when GaAs ($E_g = 1.43$ eV) and AlGaAs ($E_g = 1.8$ eV) are used as the bottom and top cells, respectively. These requirements necessitate both n and p doping levels approaching 10^{20} cm^{-3} in these high band-gap ternary alloys. Also dopants should have very low diffusion properties to minimize the junction degradation during the subsequent epitaxial growth processes. Previous efforts have only limited success. Tunneling was achieved in AlGaAs with $E_g \simeq 1.6$ eV whereas a backward diode was obtained for $E_g \simeq 1.9$ eV [3].

We present a new approach to achieve a heterostructure tunnel diode in the p^+-AlGaAs/n^+-GaInP material system with $E_g \approx 1.9$ eV and with performance suitable for 1000 suns solar concentration. The atomic Layer Epitaxy (ALE) growth approach was used for epitaxial growth of this heavily doped heterostructure. The material systems and dopants weree chosen to satisfy the high levels and the low diffusion requirements. Carbon was chosen for the p^+-doping since high levels, in the 10^{20} cm^{-3} range, can be achieved both in GaAs and AlGaAs [4]. Also carbon has a diffusion coefficient several orders of magnitude lower than other conventional p-type dopants such as Zn and Be [5]. $Al_{0.36}Ga_{0.64}As$ is not the best candidate for n^+ material due to the problem associated with DX-centers, resulting in doping levels only in the low 10^{18} cm^{-3} range [6]. Most of the donor atoms behave as deep levels rather than ionized impurities especially for a composition close to the Γ, L and X valleys cross-over. The band-gap of $Ga_{0.51}In_{0.49}P$ ($E_g \approx 1.9$ eV) is about 0.3 eV lower than the band-gap at the direct-indirect transition which occurs at 2.2 eV. Thus the role of the deep levels " DX centers " is not as pronounced in $Ga_{0.51}In_{0.49}P$ as in $Al_{0.36}Ga_{0.64}As$. DX center densities less than 10^{14} cm^{-3} were reported in n-type GaInP with $n \sim 10^{17}$ cm^{-3} [7]. Selenium was used for n^+-type dopant because it has relatively shallow donor levels [8]. ALE growth rather than MOCVD was chosen for several reasons. First, for p^+-AlGaAs, carbon is readily extracted from the decomposition products of the organometallic sources without the need of any new dopant source such as CCl_4 [9-11]. Second, low temperature growth, known to be essential for high Se incorporation [12] in the n^+-GaInP layer, is possible in ALE growth. Third, for n^+-GaInP, since in ALE growth the H_2Se, dopant

source, is introduced separately from the organometallic sources, exposure times to H_2Se can be optimized for high doping levels independent of the growth rate. In ALE growth, the growth conditions for both p^+-AlGaAs and n^+-GaInP were optimized to achieve high doping levels rather than to maintain a monolayer per ALE cycle.

6.2 Experiment

In ALE growth, we use a specially designed growth chamber and susceptor, which has been described in chapter 2. The susceptor rotates between the column III and column V streams of organometallic and hydride precursors. Trimethylgallium (TMGa), trimethylaluminum (TMAl), trimethylindium (TMIn) , arsine (AsH_3, 100%), and phosphine (PH_3, 100%) were the source materials. Hydrogen selenide (H_2Se, 45ppm in H_2), used as an n-type dopant source for the GaAs and GaInP layers, was introduced into the column V line during the ALE growth cycle.

p^+-AlGaAs and n^+-GaInP were grown by the methods described in chapters 4 and 5. $Al_{0.36}Ga_{0.64}As$ with $p = 1 \times 10^{20}$ cm^{-3} was obtained by background carbon incorporation in the ALE growth. Se-doped $Ga_{0.51}In_{0.49}P$ with $n \simeq 5 \times 10^{19}$ cm^{-3} was successfully grown at a growth temperature as low as 460 °C. These two heavily doped materials were combined together to fabricate an AlGaAs/GaInP heterojunction tunnel diode.

The tunnel diode structure shown in Figure 6.1 was grown on a Zn-doped p-type GaAs substrate and consisted of a 1000 Å p^+-AlGaAs layer ($p = 1 \times 10^{20}$ cm^{-3}), a 1000 Å n^+-GaInP layer ($n \simeq 5 \times 10^{19}$ cm^{-3}) and a 5000 Å n^+-GaAs contacting layer.

Care was taken at the p^+-AlGaAs /n^+-GaInP heterointerface to reduce the intermixing of As and P. After the growth of p^+-AlGaAs at 600 °C, the sample was kept under an AsH_3 flux while the substrate temperature was reduced to 460 °C. After the temperature was stabilized, the AsH_3 flux was turned off and a PH_3 flux was turned on. After 20 sec, the growth of Se-doped GaInP was begun. After growth the sample was cut into several pieces. One piece was then annealed at 650 °C for 30 minutes and one at 750 °C for 30 minutes, both under an AsH_3 atmosphere. These two pieces, plus a third piece not annealed, were used to fabricate tunnel diodes. This annealing experiment was performed to simulate the growth of the top cell, usually AlGaAs, in the cascade solar cell structure. For electrical evaluation 2000 Å Au was deposited on the back side of the p-type GaAs substrate, and 1000Å AuGe / 300Å Ni / 2000Å Au were deposited on the GaAs top layer using photolithography techniques. Mesas with an area 200μm × 200μm were etched using a 3-step etching method. First H_3PO_4 : H_2O_2 : H_2O = 3 : 1 : 50 solution was used to etch the GaAs top layer followed by HCl : H_2O = 1 : 1 solution to remove the n^+-GaInP layer. Finally H_3PO_4 : H_2O_2 : H_2O = 3 : 1 : 50 solution was used again to etch the p^+-AlGaAs layer and part of the p-type GaAs substrate.

6.3 Results and discussion

Figure 6.2 shows the current-voltage (I-V) characteristics of the as-grown tunnel diode at room temperature and at 150 °K. The diode does not exhibit a well-pronounced negative differential resistance region and has a peak to valley current

density ratio J_p/J_v of 1.3 at room temperature and 1.9 at 150 °K. While a tunnel diode without a well-pronounced negative differential resistance region is not suitable for digital applications, it is still suitable as the connecting junction in the cascade solar cell structure. In the latter case the value of the peak current density and the voltage drop across the connecting junction are the important parameters since they affect the open circuit voltage and fill factor in this solar cell structure. At room temperature, the total resistance of the tunnel diode structure is 2.6 Ω which corresponds to a specific resistivity of 1×10^{-3} Ωcm^2. At 20 A/cm^2, which is the approximate current density for an AlGaAs/GaAs two junction solar cell operating at 1000 suns, the voltage drop across this tunnel junction is only 21 mV. This voltage drop is an upper limit since no corrections for the probe, metal contact and substrate resistance have been considered. This is the best performance reported for a high band-gap tunnel diode ($E_g \approx 1.9$ eV) as the connecting junction in the cascade solar cell structure. A GaAs tunnel diode with a peak current density of $\sim$ 45 A/cm^2 and a specific resistivity of 2×10^{-3} Ω cm^{-2} has been reported [13]. The performance of the present heterojunction tunnel diode is comparable to the previously reported GaAs tunnel junction.

The fact that this high E_g tunnel junction has fairly high J_p can be attributed to several factors. The presence of a high excess current density enhances the value of J_p while reducing the J_p/J_v ratio. The excess current exist primarily due to the electron tunneling via energy states within the forbidden gap and can be represented by [14]

$$J_x \approx A_1 D_x \exp \{-\alpha_x [E_g - qV + 0.6 q (V_n+V_p)] \}$$

Eq. (6 - 1)

where A_1 and α_x are constants and D_x is the volume density of energy states within the band-gap via which electron tunneling occurs and E_g is the band-gap of the tunnel junction. V is the applied voltage and qV_n and qV_p are the fermi level penetrations into the conduction and valence band, respectively. As can be seen by Eq.(6 - 1), the excess current density will increase with the density of band-gap states and will exponentially increase as the applied voltage increases. In our tunnel diode, since both the p- and n-side of the junction are heavily doped, a high density of forbidden gap states may exist [13] and J-V measured at room temperature shows high excess current density. The excess current density will decrease at lower temperatures, because the band-gap E_g will increase with decreasing temperature. In Figure 6.2 the decrease of the excess current density at lower temperature 150 °C is clearly shown. In addition to the high excess current density, the band-to-band tunnel current density is also fairly high. From Figure 6.2, at 150 °K $J_p - J_v$ is about 40 A/cm^2. If the high excess current density is taken into account, the actual band-to-band tunnel current density would be higher than 40 A/cm^2. Although this high band-to-band tunnel current density (hereafter called the tunnel current density) is primarily due to the heavy doping on both sides of the junction, it may also have to do with the band line-up at the AlGaAs/GaInP interface. It has been reported that the $Al_{0.36}Ga_{0.64}As/Ga_{0.51}In_{0.49}P$ interface has a staggered band line-up where both the conduction and valence bands of

AlGaAs have higher energies than those of GaInP [15]. Figure 6.3 (a) shows the energy band diagram of isolated p^+-$Al_{0.36}Ga_{0.64}As$ and n^+-$Ga_{0.51}In_{0.49}P$ [16]. E_g is the band-gap and E_c and E_v are conduction and valence band edges, respectively. X is the electron affinity and Z is the work function. X and Z are the amount of energy needed to take the electron at the bottom of the conduction band and in the fermi level just outside the semiconductor, respectively. ΔE_c is the conduction band discontinuity. Anderson's model says that ΔE_c is the difference in the electron affinity of the two materials *i.e.* $\Delta E_c = X_1 - X_2$. E_{fn} and E_{fp} are the the fermi level in the n^+ and p^+-layer, respectively. The expected band line-up at the heterointerface when these two heavily doped materials are brought together is shown in Figure 6.3 (b). qV_d is the built-in potential and it is defined as the difference in the work function of the two materials *i.e.* $qV_d = Z_2 - Z_1$. The built-in potential of the heterojunction with the conduction band discontinuity ΔE_c will be lower by ΔE_c than that of the junction without ΔE_c. In the AlGaAs/GaInP heterointerface, if E_n and E_p are the fermi level penetration into the conduction and valence band, respectively, then qV_d can be set equal to $E_{g2} - \Delta E_c + E_n + E_p$. In the AlGaAs/GaInP heterojunction, the depletion layer thickness W can be represented by Eq.(6 - 2) [16].

$$W = \sqrt{\frac{2\varepsilon_1\varepsilon_2(V_d - V)(N_a + N_d)^2}{q\,(\varepsilon_1 N_d + \varepsilon_2 N_a)\, N_d\, N_a}}$$

Eq. (6-2)

where q is the electric charge, V is the applied voltage, and ε_1 and ε_2 are the dielectric constants of n- and p-side, respectively. N_d and N_a are n- and p- type carrier concentration, respectively. Due to the conduction band discontinuity ΔE_c, which results in the lower built-in potential, W in the heterojunction with ΔE_c will be decreased compared with that in the junction without ΔE_c as can be seen in Eq. (6-2). The decrease of the depletion width W is quite small (several angstroms) since the conduction band discontinuity of the $Al_{0.36}Ga_{0.64}As/Ga_{0.51}In_{0.49}P$ is ~ 150 meV, which is much smaller than band-gaps of the two semiconductors, both of which are ~ 1.9 eV. However, even such a small variation in W can affect the peak tunnel current density J_p significantly [17] because the tunnel current density is very sensitive to the value of W as shown below in Eq.(6-3), which is from Refs. [14] and [18]. In Eq. (6-3) W is included in F, which is defined as the force on the tunneling electron by the electric field in the depletion region and can be represented by ~ (tunneling barrier height)/W.

$$J_t = \frac{qm^*}{18\hbar^3} \exp\left[- \frac{\pi m^{*1/2} E_g^{3/2}}{2\sqrt{2}\hbar F} \right] \left(\frac{\hat{E}}{2}\right) D$$

$$\hat{E} = \frac{\sqrt{2}\hbar F}{\pi m^{*1/2} E_g^{1/2}}$$

$$D = \int_{E_{c1}}^{E_{v2}} [\, f_1(E) - f_2(E) \,][\, 1 - \exp(-\frac{2E_s}{\hat{E}}) \,]\, dE$$

Eq. (6-3)

where J_t is the tunnel current density, m^* is the effective mass of the tunneling electron, E_g is the band-gap of the depletion layer, and $f_1(E)$ and $f_2(E)$ are the Fermi-Dirac

)/n^+-$Ga_{0.51}In_{0.49}P$ ($n^+ = 5 \times 10^{19}$ cm^{-3}) with $\Delta E_c = 0.150$ eV. The left side of the vertical axis refers to diodes (A),(C) and (D), while the right side refers to diode (B), whose current density is too small to be displayed on the same scale with (A),(C) or (D). The programs used to calculate J-V curves for diodes (A) and (D) at room temperature are included in the Appendix. For (A) and (B), the program in Ref.[18] was followed with some changes such as values of electron and hole effective masses and dielectric constants. For $Al_xGa_{1-x}As$ with $0 \leq x \leq 0.45$, the band-gap E_g at room temperature was calculated using

$$E_g(x) = 1.424 + 1.247x \text{ (eV)} \qquad \text{Eq. (6-4).}$$

The effective masses of the conduction band electrons and the valence band holes were represented by

$$m_e^* = (0.067 + 0.083x)m_0 \qquad \text{Eq. (6-5)}$$

and

$$m_h^* = (0.48 + 0.31x)m_0 \qquad \text{Eq. (6-6)}$$

respectively. Eqs. (6-4), (6-5) and (6-6) are from Ref.[20]. The dielectric constant of $Al_xGa_{1-x}As$ was estimated using

$$\varepsilon = 12.9 - 2.0 \times ((E_g(x) - 1.424)/(3.03 - 1.424)) \qquad \text{Eq. (6-7)}$$

which differs from the corresponding equation in Ref.[18] only in the direct band-gap values of GaAs and AlAs. For the p^+-$Al_{0.36}Ga_{0.64}As/n^+$-$Ga_{0.51}In_{0.49}P$ heterojunction tunnel diodes, (C) and (D), further modification such as the incorporation of the depletion width narrowing due to ΔE_c and the change of the tunneling electron effective mass was made in the program used for diodes (A) and (B). The electron effective mass

for $Ga_{0.51}In_{0.49}P$ was taken as $m_e^* = 0.1\ m_0$ [21]. $\varepsilon_i = 12.016$ was used as the $Ga_{0.51}In_{0.49}P$ dielectric constant. Since the presence of ΔE_c at the heterointerface is not considered to affect the tunnel barrier height, F in Eq. (6-3) should be represented by $F = [\ q(V_d - V) + \Delta E_c\ ]/W$ for the calculation of J_p of the heterojunction. The value of ΔE_c can be estimated by combining the reported values of the conduction band discontinuities of AlGaAs/GaAs and GaInP/GaAs heterostructures. ΔE_c of the $Ga_{0.51}In_{0.49}P$/GaAs structure is reported to be in the wide range of 30 - 390 meV [22]. If ΔE_c of $\sim$ 100 meV is taken for the $Ga_{0.51}In_{0.49}P$/GaAs heterointerface [22] and ΔE_c of the AlGaAs/GaAs heterostructure is assumed to be 60% of the difference in the band-gaps of AlGaAs and GaAs, ΔE_c of the $Al_{0.36}Ga_{0.64}As/Ga_{0.51}In_{0.49}P$ heterojunction can be assumed to be 150 meV, which was used in our calculation. ΔE_c at 150 °K was assumed to be equal to that at room temperature.

J-V curves for diodes (A) and (C), show only a small difference, which is attributed mainly to the differences in physical constants of two structures such as electron effective mass and dielectric constants. However, the J-V curve for diode (D) shows significant differences from those for diodes (A) and (C). J_p of diode (D) is increased by $\sim$ 35% and $\sim$ 50% compared with those of diodes (A) and (C) at room temperature and at 150 °K, respectively. At 150 °K, the peak tunnel current density for all of the diodes is lower than at room temperature, mainly due to the increase of the band-gap and, thus, the increase of tunneling barrier height. Our calculation succeeded in showing that ΔE_c, which results in the decrease of depletion layer thickness, indeed affects the tunnel current density, although it produced lower J_p value

than the observed J_p - J_v value at 150 °K in Figure 6.2, which is expected to be closer to the actual band-to-band tunnel current density due to lower excess current density at lower temperature.The difference between the calculated and experimental results can be attributed to the uncertainties in the physical constants such as the electron effective mass and to the deviation of the tunneling barrier shape assumed in the calculation from the exact shape. In a hypothetical extreme case of $\Delta E_c \sim E_{g2}$, W would be almost zero and the tunnel current density would be infinitely high.

Even though a p^+-$Al_{0.36}Ga_{0.64}As$ ($p^+ = 1 \times 10^{20}$ cm^{-3})/n^--$Al_{0.36}Ga_{0.64}As$ ($n^+ = 5 \times 10^{19}$ cm^{-3}), diode (A), was compared with a p^+-AlGaAs/n^+-GaInP heterojunction in Figure 6.5 (a) and (b), in practice it is almost impossible to grow n^+-$Al_{0.36}Ga_{0.64}As$ with $n^+ \geq 1 \times 10^{19}$ cm^{-3} due to DX centers. The maximum reported value of n-type carrier concentration in AlGaAs with $E_g \geq 1.8$ eV is limited to the mid 10^{18} cm^{-3}. With this value of n-type carrier concentration, p^+-AlGaAs/n^+-AlGaAs with $E_g \sim 1.9$ eV does not seem to be suitable as the interconnect part of the cascade solar cell operating at high solar concentrations as can be seen from the curve (B) in Figure 6.5 (a) and (b). The change of the peak tunnel current density J_p with the variation of the depletion layer thickness W is shown in Figure 6.6 (a). J_p was calculated simply by deleting the integral part D of Eq. (6-3) [17]. J_p decreases exponentially as W increases as is the case of the GaAs tunnel diode [17]. Figure 6.6 (b) shows the variation of the depletion region width at equilibrium with the doping level in the n-side of the p^+-AlGaAs/n^+-GaInP heterojunction. The decrease of the depletion region width by ΔE_c is also shown. Figures 6.6 (a) and (b) demonstrate the necessity of achieving

high doping levels in the n-side of the junction, thereby achieving a high J_p value. The results in Figure 6.5 show, for the preparation of the high band-gap tunnel diode, the p-AlGaAs/n-GaInP material system is better than p-AlGaAs/n-AlGaAs system primarily due to the achievability of the high doping levels $\sim 5 \times 10^{19}$ cm^{-3} in the n^+-side of the tunnel junction. The conduction band discontinuity of the p^+-AlGaAs/n^+-GaInP also contribute to the high peak current density.

Figures 6.7 (a) and (b) show the performances of the tunnel diodes made with samples annealed at 650 °C and at 750 °C for 30 minutes. The performance of the diode annealed at 650 °C did not degrade seriously, while the diode annealed at 750 °C showed some degradation. At 20 A/cm^2 the voltage drops across the tunnel junctions were 58 mV and 100 mV for the samples annealed at 650 °C and at 750 °C, respectively. The peak current density J_p of the sample annealed at 750 °C decreased about a factor of three compared with J_p of the as-grown sample. This performance degradation may be attributed to the diffusion of the dopant atoms across the junction. Both carbon and selenium used as the dopant species are reported to have very low diffusion coefficients in GaAs. The reported value of the diffusion coefficient of carbon D_c in GaAs is $D_c = 2 \times 10^{-16}$ cm^2/sec at 800 °C [5], and that of selenium is $D_{se} = 3 \times 10^{-18}$ cm^2/sec at 700 °C [23]. Under the assumption that $D_c = D_{se} = D = 1 \times 10^{-16}$ cm^2/sec at 750 °C and D_c and D_{se} have the same value in both sides of the junction, a rough estimate of the increase of the depletion layer thickness and thus the decrease of J_p, after annealing, was made. From diffusion theory in Ref. [24], the concentration profile of C and Se atoms at the position x from the junction at time t is

$$N_C(x) = \frac{N_{Co}}{2} erfc\left[\frac{x}{2\sqrt{Dt}}\right] \qquad N_{Se}(x) = \frac{N_{Seo}}{2} erfc\left[\frac{-x}{2\sqrt{Dt}}\right]$$

Eq. (6-8)

where $N_c(x)$ and N_{Se} are the concentration profile of carbon and selenium, respectively. N_{Co} and N_{Seo} are the concentration of C and Se in the p- and n-side of the as-grown junction, which is expected to be close to an abrupt junction, and t is the annealing time and erfc is the complementary error function. The gradient of the doping profile, p - n, at $x = 0$ can be set equal to

$$\left(\frac{d\,[\,N_C(x) - N_{Se}(x)\,]}{dx}\right)_{x=0} = -\frac{N_{Co} + N_{Seo}}{2}\frac{1}{\sqrt{\pi Dt}}$$

Eq. (6-9)

If we make another assumption that the doping profile around the junction is linearly graded and the slope of the linearly graded junction a is equal to the absolute value of the doping profile gradient at $x = 0$, which is given by above equation, a is

$$a = \left(\frac{N_{Co} + N_{Seo}}{2}\right)\frac{1}{\sqrt{\pi Dt}}$$

Eq.(6-10)

The depletion region width W of the linearly graded junction with a slope a is given by [14]

$$W = \left(\frac{12\varepsilon_s V_{bi}}{q\ a} \right)^{1/3}$$

Eq.(6 - 11)

where ε_s is the dielectric constant, q is the electron charge and V_{bi} is the built-in potential. In our case, W can be represented by

$$W = \left(\frac{12\varepsilon_s V_{bi}}{q\ \frac{(N_{Co} + N_{Seo})}{2\sqrt{\pi Dt}}} \right)^{1/3} = \left(\frac{24\pi^{1/2}\varepsilon_s V_{bi}}{q\ (N_{Co} + N_{Seo})} \right)^{1/3} (Dt)^{1/6}$$

Eq.(6-12)

In our case $\varepsilon_s \sim 12.0\varepsilon_o$, $V_{bi} \sim 1.9$ V, $N_{Co} = 1 \times 10^{20}$ cm^{-3}, $N_{Seo} = 5 \times 10^{19}$ cm^{-3}. $Dt = 1 \times 10^{-16} \times 30 \times 60$ cm^2 $= 1.8 \times 10^{-13}$ cm^2 for 30 mins. annealing time. With these values, W $\sim$ 114 Å was estimated. In Figure 6.6 (a) J_p at W = 114 Å, the estimated value of W of the tunnel junction annealed at 750 °C, is about an order of magnitude less than J_p at W = 95 Å, which was the calculated value of W of the assumed abrupt junction of the as-grown tunnel diode. Our rough estimate of the decrease of the peak current density can partially explain the experimental results. Table 6.1 summarizes the main features of the tunnel diodes as-grown, annealed at 650 °C and 750 °C. The results for the GaAs tunnel diode were also included for comparison.

6.4 Conclusion

A p^+-AlGaAs/n^+-GaInP tunnel junction was grown by ALE using C and Se for

the p- and n-type dopants, respectively. There is only ~ 20 mV voltage drop across this junction at 20 A/cm^2, which is the expected current density for an AlGaAs/GaAs two junction solar cell at 1000 suns operation. Our calculation shows that p^+-AlGaAs/n^+-GaInP heterostructure can be considered as a better material system than p^+-AlGaAs/n^+-AlGaAs structure for the connecting tunnel diode in the cascade solar structure, primarily because doping levels as high as 5×10^{19} cm^{-3} can be achieved for the n^+-side material. In addition, the conduction band discontinuity at the heterointerface also contributes to high band-to-band tunnel current density. Even though the performance of the tunnel diode annealed at temperatures higher than the growth temperature, especially at 750 °C, showed degradations, probably due to the diffusion of the dopant species, the voltage drop across the junction at 20 A/cm^2 is still low enough for this junction to be suitable for 1000 suns operation. This p^+-AlGaAs/n^+-GaInP heterostructure diode is the first reported tunnel diode fabricated using high band-gap material systems suitable for a cascade solar cell structure operating at 1000 suns.

References

[1] R.L. Moon, L.W. Janes, H.A. VanderPlas, Y.G. Chai, and G.A. Antypas, *Thirteenth IEEE Photovoltaic Special Conference*, Washington,D.C. (IEEE, New York, 1978), p.859.

[2] S.M. Bedair, M.F. Lamorte, and J.R. Hauser, Appl. Phys. Lett. **34**, 38 (1979).

[3] S.M. Bedair, J. Appl. Phys. **51**, 3935 (1980).

[4] M. Konagai, T. Yamada, T. Akatsuka, K. Saito, E. Tokumitsu, and K. Takahashi, J. Cryst. Growth **98**, 167 (1989).

[5] N. Kobayashi, T. Makimoto, and Y. Horikoshi, Appl. Phys. Lett. **50**, 1435 (1987).

[6] P.M. Mooney, J. Appl. Phys. **67**, R1 (1990).

[7] M.O. Watanabe and Y. Ohba, J. Appl. Phys. **60**, 1032 (1986).

[8] T. Ishikawa, T. Maeda, and K. Kondo, J. Appl. Phys. **68**, 3343 (1990).

[9] J.R. Gong, D. Jung, N.A. El-Masry, and S.M. Bedair, Appl. Phys. Lett. **57**, 400 (1990).

[10] K.G. Reid, H.M. Urdianyk, and S.M. Bedair, Appl. Phys. Lett. **59**, 2397 (1991).

[11] B.C. Chung, R.T. Green, and H.F. MacMillan, J. Cryst. Growth **107**, 89 (1991).

[12] A. Usui and H. Sunakawa in *Inst. Phys. Conf. Ser. no.83, GaAs and Related Compounds*, 129 (1986).

[13] P. Basmaji, M. Guittard, A. Rudra, J.F. Carlin, and P. Gibart, J. Appl. Phys.

62, 2103 (1987).

[14] S.M. Sze, *Physics of Semiconductor Devices,* 2nd Edition, New York: Wiley (1981), Chap.9.

[15] M.A. Rao, E.J. Caine, H. Kroemer, S.I. Long, and D.I. Babic, J. Appl. Phys. **61**, 643 (1987).

[16] R.L. Anderson, Solid State Electron. **5**, 341 (1962).

[17] R.E. Hayes, P. Gibart, J. Chevrier, and S. Wagner, Solar Cells **15**, 231 (1985).

[18] G.A. DeJong, M.S. Thesis, North Carolina State University, Raleigh, N.C. (1978).

[19] J.S. Blakemore, *Semiconductor Statistics*, (Dover, New York, 1987)

[20] H.C. Casey and M.B. Panish, *Heterostructure Lasers*, Part A and B, New York, Academic Press (1978).

[21] T. Kobayashi, K. Taira, F. Nakamura, and H. Kawai, J. Appl. Phys. **65**, 4898 (1989).

[22] M.A. Haase, M.J. Hafich, and G.Y. Robinson, Appl. Phys. Lett. **58**, 616 (1991).

[23] B. Goldstein, Phys. Rev. **121**, 1305 (1961).

[24] J.S. Kirkaldy and D.J. Young, *Diffusion in The Condensed State*, (The Institute of Metals, London, U.K. 1987)

Table 6.1 Main features of the heterojunction tunnel diodes as-grown, annealed at 650 °C and annealed at 750 °C. Results for a GaAs tunnel diode from Ref.[13] were also included for comparison.

Sample	As-grown	Annealed at 650°C	Annealed at 750°C	GaAs
Peak Current Density (A/cm^2)	88	74	33	45
Peak Voltage (mV)	140	270	240	136
Specific Resistivity (Ωcm^2)	1.0×10^{-3}	2.9×10^{-3}	4.6×10^{-3}	2.0×10^{-3}
Voltage Drop at 20 A/cm^2 (mV)	21	58	100	37

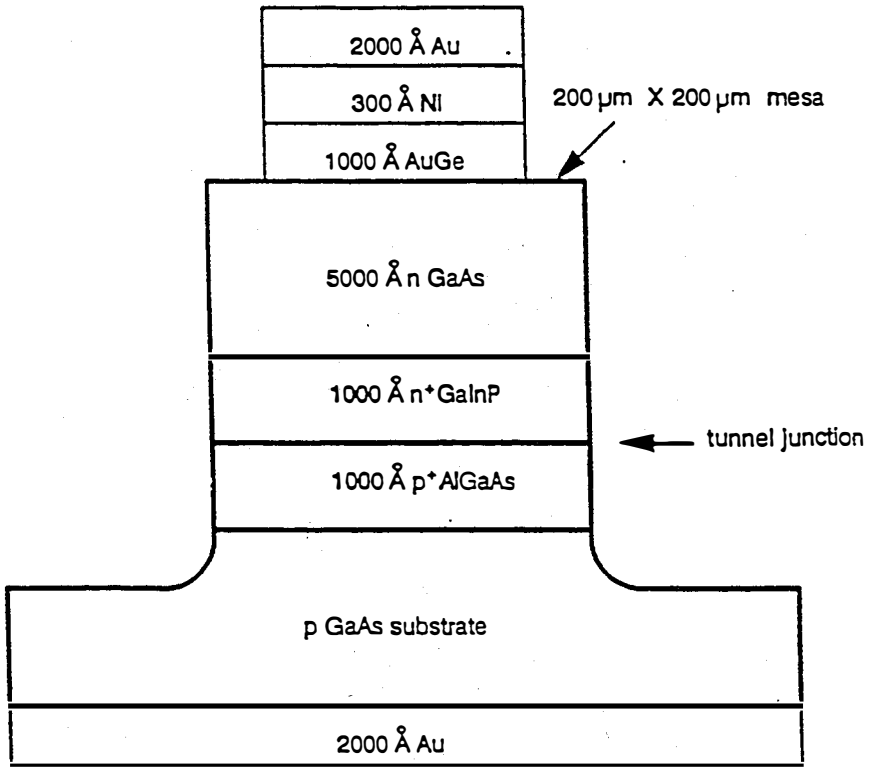

Figure 6.1 Structure of the p^+-AlGaAs/n^+-GaInP heterojunction tunnel diode.

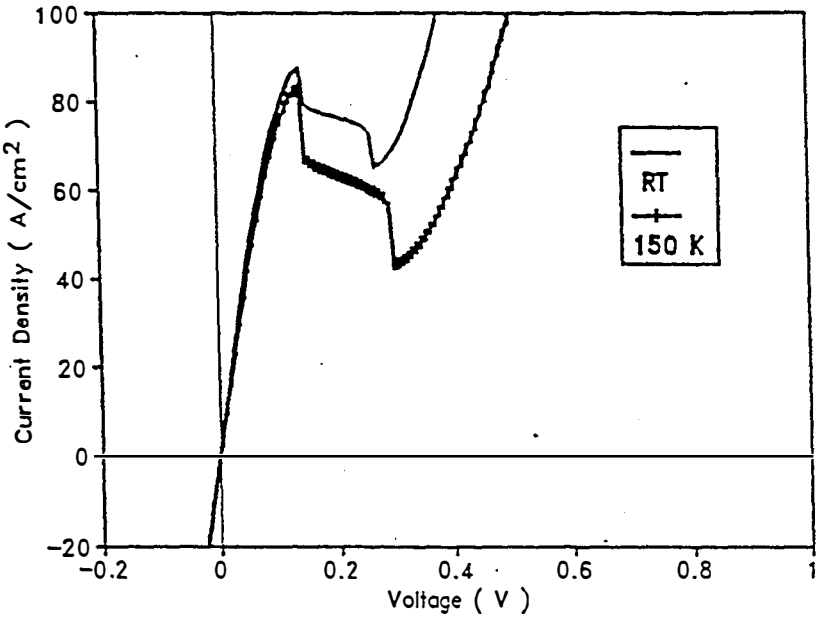

Figure 6.2 J-V characteristics of the as-grown heterojunction tunnel diode at room temperature and at 150 °K. The diode is oscillating in the negative differential resistance region.

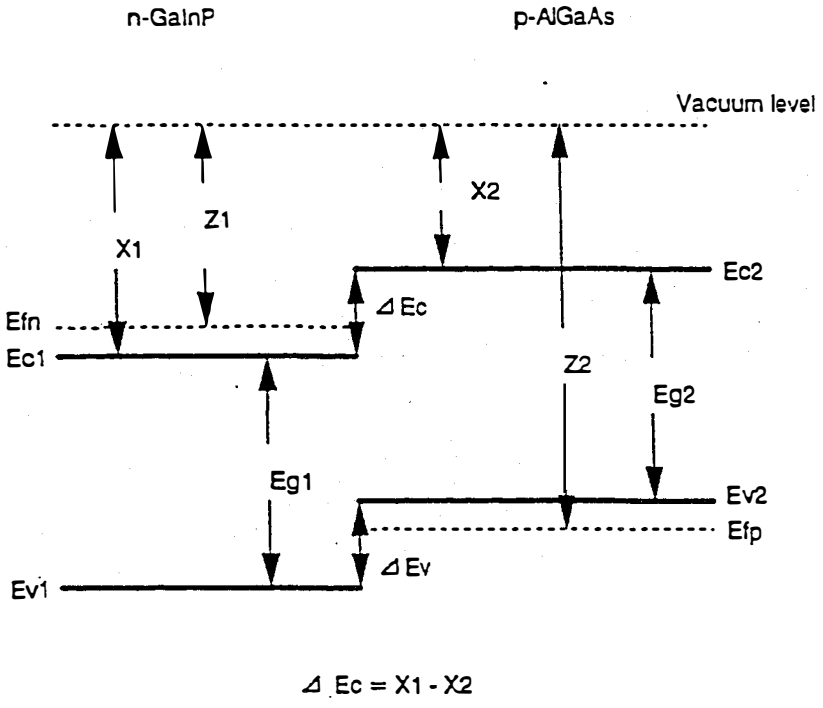

(a)

Figure 6.3 Energy band diagram of isolated p^+-AlGaAs and n^+-GaInP (a) and the expected band line-up when these two materials are brought together (b).

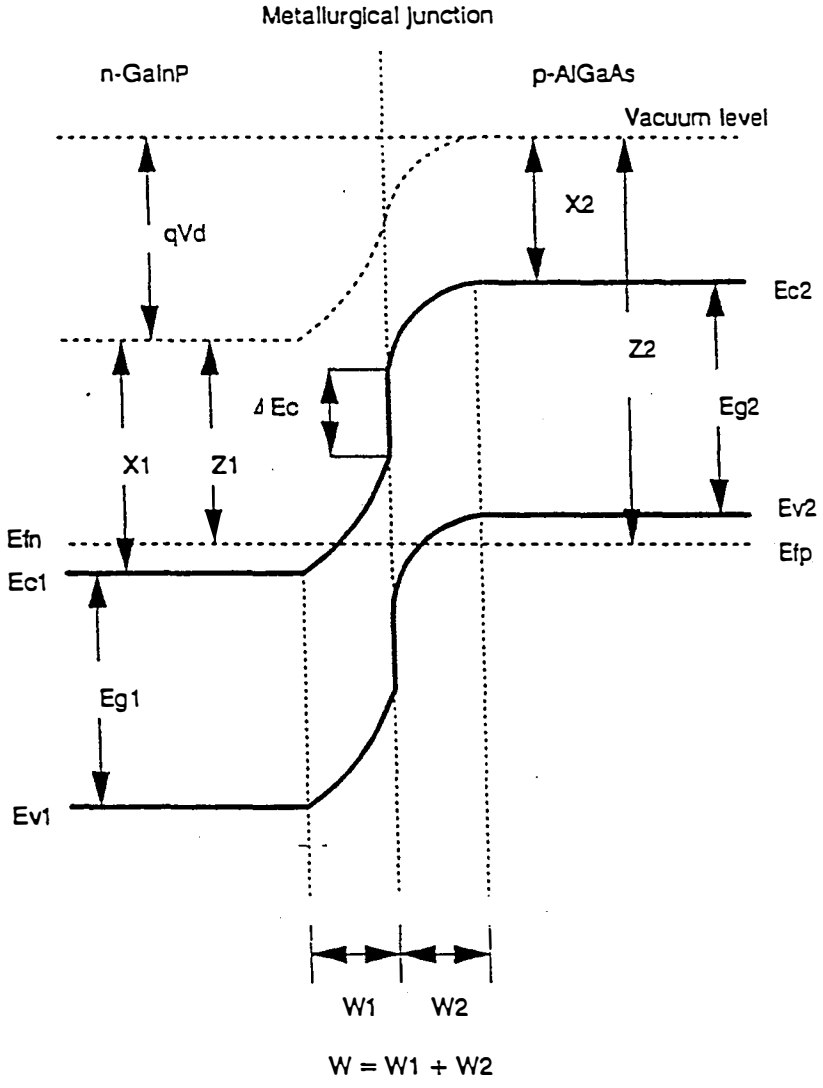
Metallurgical junction
n-GaInP
p-AlGaAs
Vacuum level
qVd
X2
Ec2
Z2
Eg2
Δ Ec
X1
Z1
Ev2
Efn
Efp
Ec1
Eg1
Ev1
W1
W2
W = W1 + W2

(b)

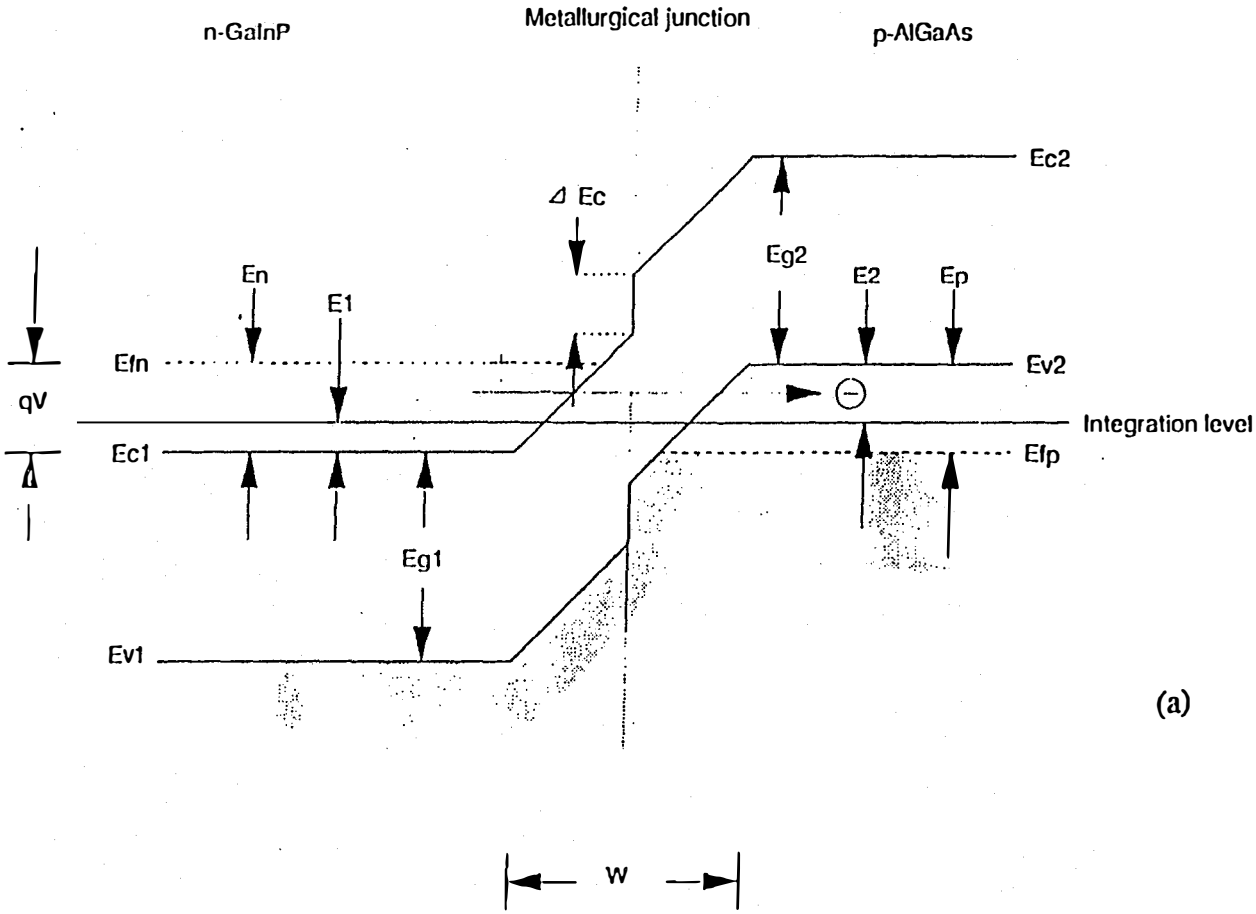

Figure 6.4 The band line-up of the p^+-AlGaAs/n^+-GaInP heterojunction at forward bias (a) and at reverse bias (b). The electron tunneling through the barrier is shown.

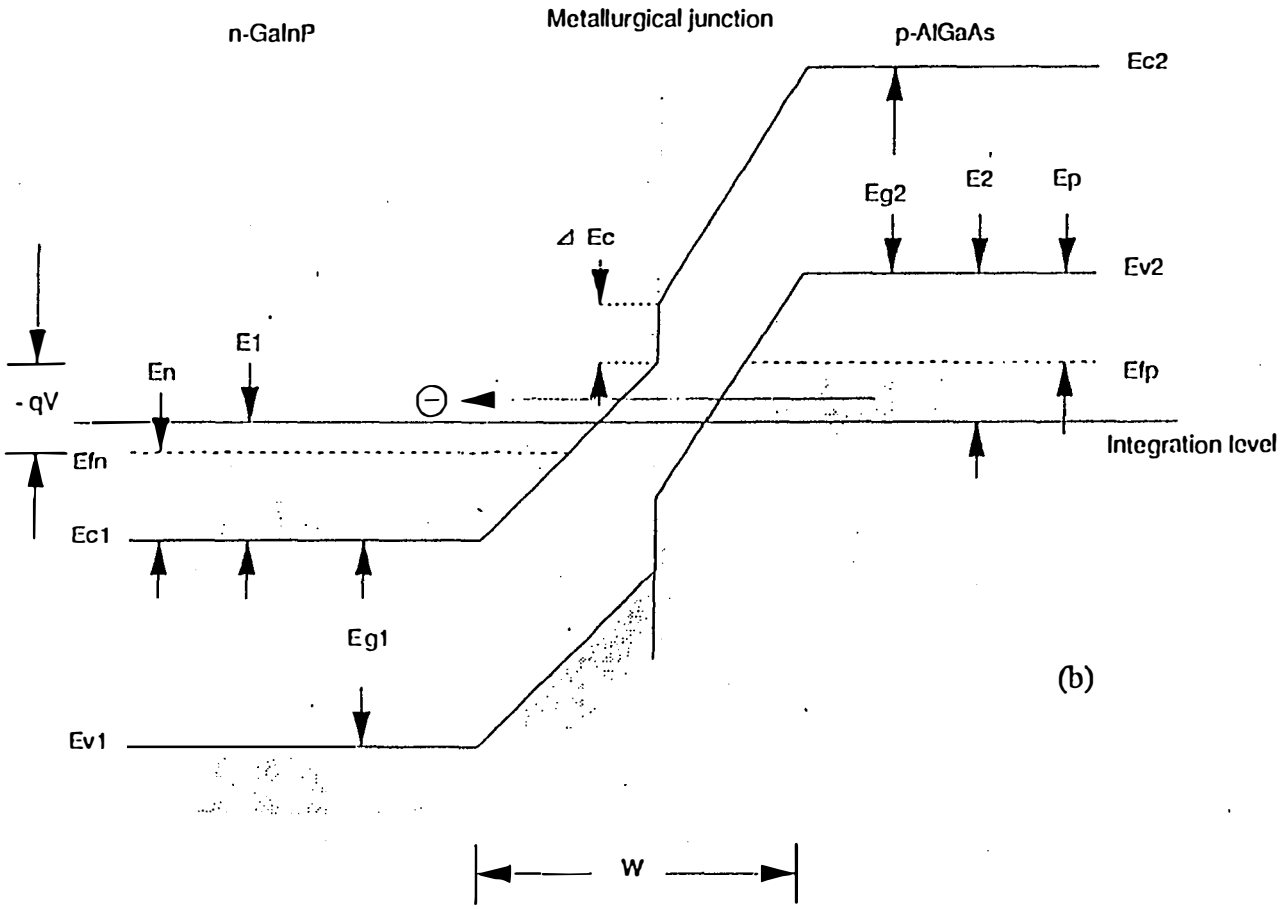
n-GaInP
Metallurgical junction
p-AlGaAs
Ec2
Eg2
E2
Ep
Δ Ec
Ev2
E1
En
Efp
- qV
Integration level
Efn
Ec1
Eg1
(b)
Ev1
W

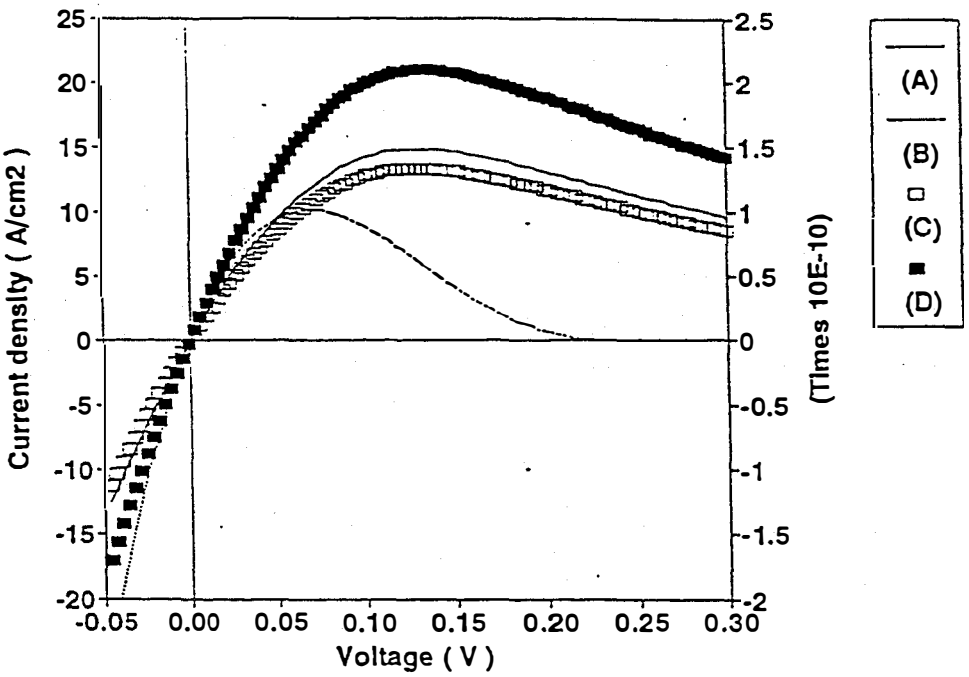

(a)

Figure 6.5 The calculated J-V curves for four different tunnel diodes at room temperature (a) and at 150 °K (b). See text for the specification of diodes (A), (B), (C), and (D).

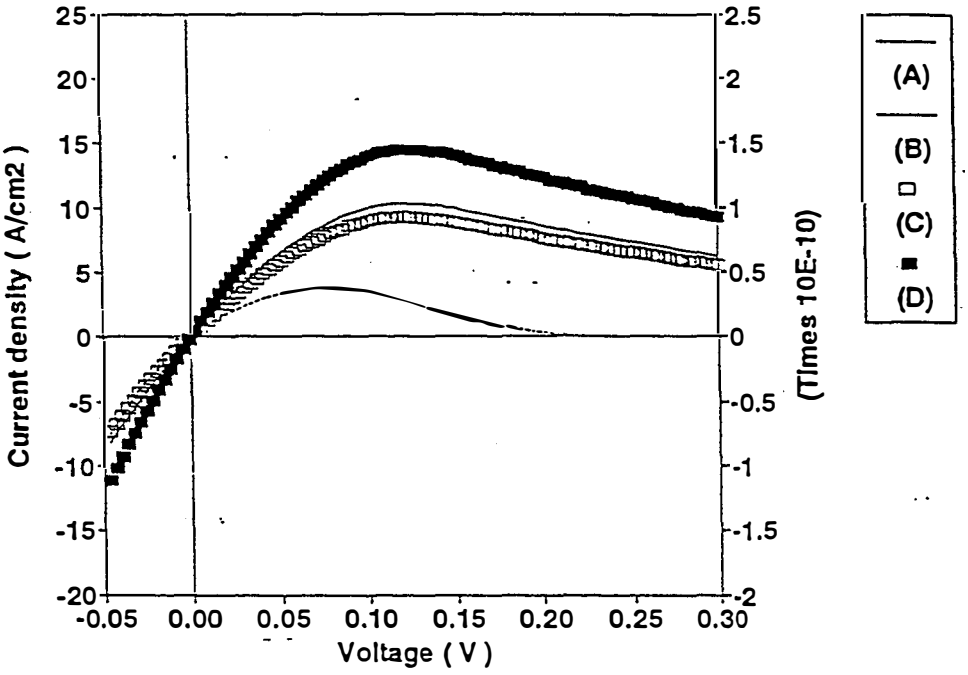
Current density (A/cm2)
Voltage (V)
(Times 10E-10)
(A)
(B)
(C)
(D)
25
20
15
10
5
0
-5
-10
-15
-20
2.5
2
1.5
1
0.5
0
-0.5
-1
-1.5
-2
-0.05
0.00
0.05
0.10
0.15
0.20
0.25
0.30

(b)

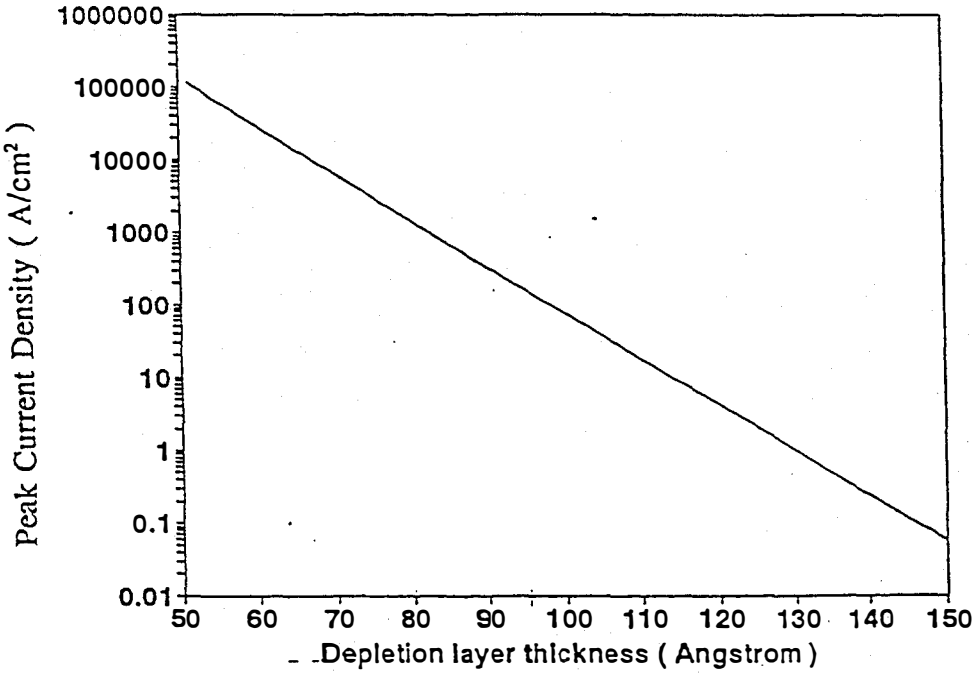

(a)

Figure 6.6 Variation of the peak tunnel current density J_p with the depletion layer thickness W (a) and W as a function of the doping level in the n-side of the p^+-AlGaAs/n^+-GaInP heterojunction (b). In (b), the doping level of the p^+-side of the junction is fixed at 1×10^{20} cm^{-3}.

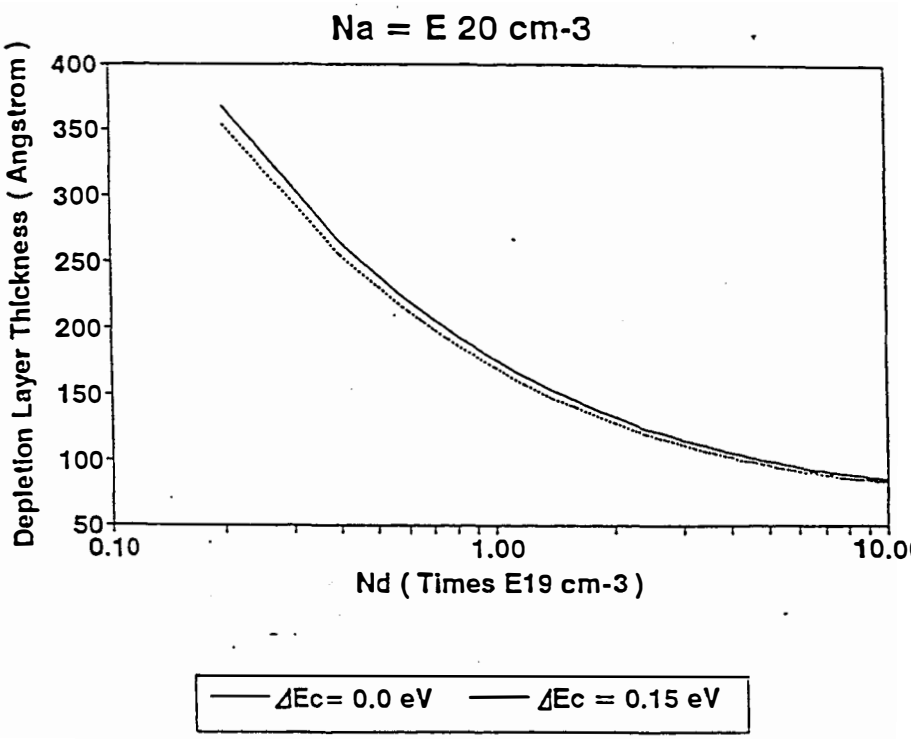
Na = E 20 cm-3
Depletion Layer Thickness (Angstrom)
400
350
300
250
200
150
100
50
0.10
1.00
10.00
Nd (Times E19 cm-3)
ΔEc= 0.0 eV
ΔEc = 0.15 eV

(b)

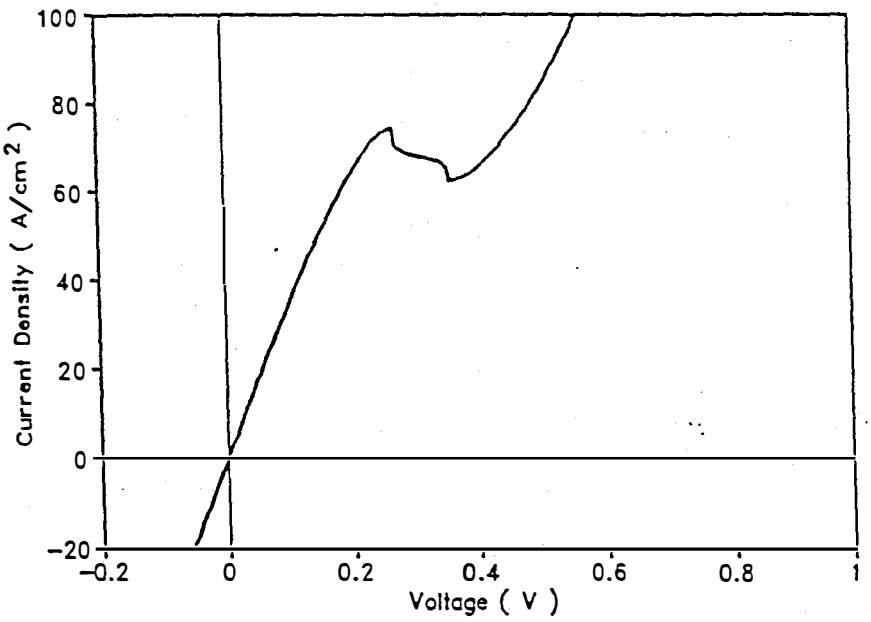

(a)

Figure 6.7 J-V characteristics of the samples annealed at 650 °C (a) and at 750 °C (b) for 30 minutes. The measurements were performed at room temperature. The diodes are oscillating

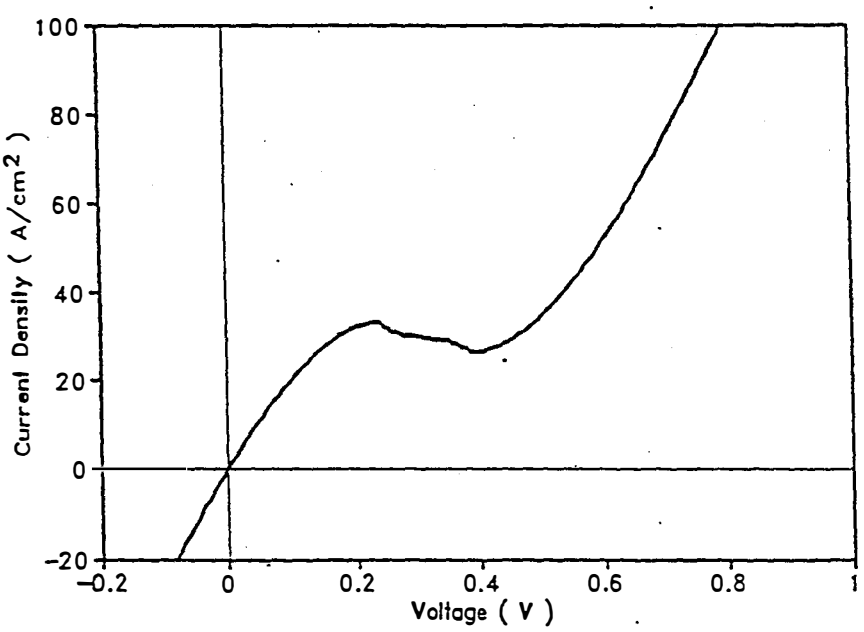
100
80
60
40
20
0
-20
Current Density (A/cm2)
-0.2
0
0.2
0.4
0.6
0.8
1
Voltage (V)

(b)

REPORT DOCUMENTATION PAGE

Form Approved
OMB NO. 0704-0188

1. AGENCY USE ONLY (Leave blank)	2. REPORT DATE	3. REPORT TYPE AND DATES COVERED
	December 1997	Final Report

4. TITLE AND SUBTITLE

New Approaches for High-Efficiency Solar Cells; Final Report

5. FUNDING NUMBERS

C: XDA-3-12114-5
TA: PV802804

6. AUTHOR(S)

S.M. Bedair and N.A. El-Masry

7. PERFORMING ORGANIZATION NAME(S) AND ADDRESS(ES)

North Carolina State University
Raleigh, North Carolina 27695-7911

8. PERFORMING ORGANIZATION REPORT NUMBER

9. SPONSORING/MONITORING AGENCY NAME(S) AND ADDRESS(ES)

National Renewable Energy Laboratory
1617 Cole Blvd.
Golden, CO 80401-3393

10. SPONSORING/MONITORING AGENCY REPORT NUMBER

SR-520-23266

11. SUPPLEMENTARY NOTES

NREL Technical Monitor: R. McConnell

12a. DISTRIBUTION/AVAILABILITY STATEMENT

12b. DISTRIBUTION CODE

UC-1260

13. ABSTRACT *(Maximum 200 words)*

This report summarizes the activities carried out in this subcontract. These activities cover growing GaAs, AlGaAs, and InGaP by atomic-layer epitaxy (ALE) at fairly low growth temperatures; using ALE to achieve high levels of doping both n-type and p-type required for tunnel junctions in the cascade solar cell structures; and studying the properties of AlGaAs/InGaP and AlGaAs/GaAs tunnel junctions in stacked solar cell structures. The effect of these tunnel junctions on the performance of stacked solar cells was studied at different temperatures and different solar fluences. Researchers also studied the effect of different types of back-surface fields, both p/n and n/p GaInP solar cell structures, and their potential for window-layer applications. Parts of these activities were carried out in close cooperation with Dr. Mike Timmons of the Research Triangle Institute.

14. TERMS

photovoltaics ; high-efficiency solar cells ; atomic-layer epitaxy ; window-layer applications ; tunnel junctions ; back-surface fields

15. NUMBER OF PAGES
121

16. PRICE CODE

17. SECURITY CLASSIFICATION OF REPORT	18. SECURITY CLASSIFICATION OF THIS PAGE	19. SECURITY CLASSIFICATION OF ABSTRACT	20. LIMITATION OF ABSTRACT
Unclassified	Unclassified	Unclassified	UL